New approach to the analysis of ribbing in coil coating

Eddy Szczurek

N° d'ordre : 07/13

Thèse présentée à l'université de Valenciennes et du Hainaut Cambrésis en vue de l'obtention du doctorat en Génie Mécanique et Energétique

Par
Eddy SZCZUREK

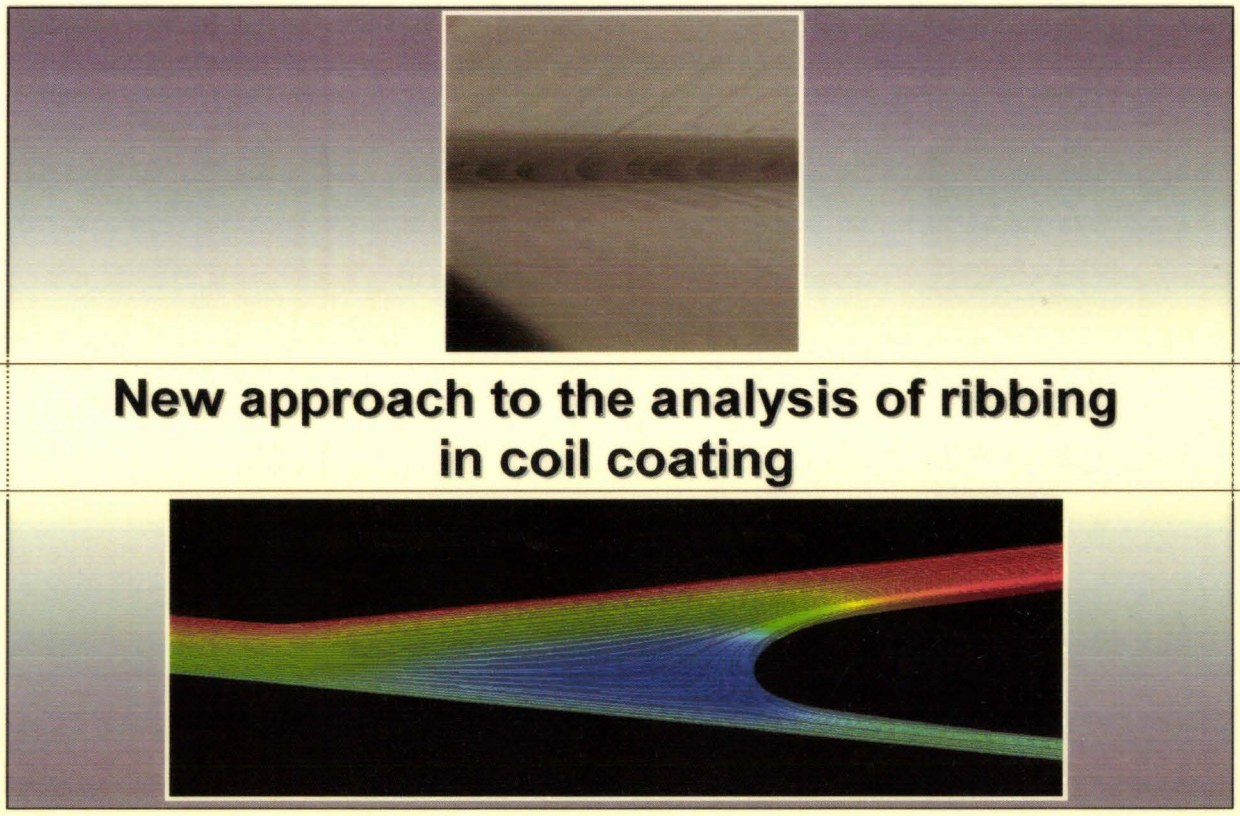

New approach to the analysis of ribbing in coil coating

Le 11 mai 2007

Devant le jury composé de :

Rapporteurs :
P. MONTMITONNET, *Directeur de Recherches CNRS, Ecole des Mines de Paris, CEMEF*
A.M. HABRAKEN-WERA, *Directrice de Recherches FNRS, Université de Liège*
Examinateurs :
C. TOURNIER, *Professeur, Université de Valenciennes, LME*
L. DUBAR, *Professeur, Université de Valenciennes, LAMIH, Directeur de thèse*
A. DUBOIS, *Professeur, Université de Valenciennes, LAMIH*
J. P. NAYLOR, *Directeur Général de MYRIAD groupe CORUS*
Invités :
L.VIELLARD, *Responsable du service Développement industriel de MYRIAD groupe CORUS*

N° d'ordre : 07/13
Thèse présentée à l'université de Valenciennes et du Hainaut Cambrésis en vue de l'obtention du doctorat en Génie Mécanique et Energétique
Par
Eddy SZCZUREK

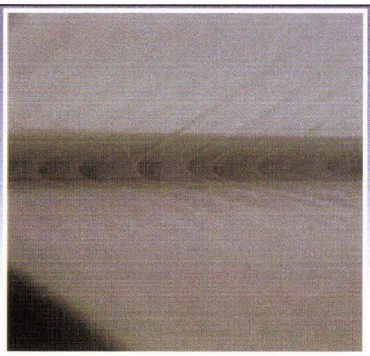

New approach to the analysis of ribbing in coil coating

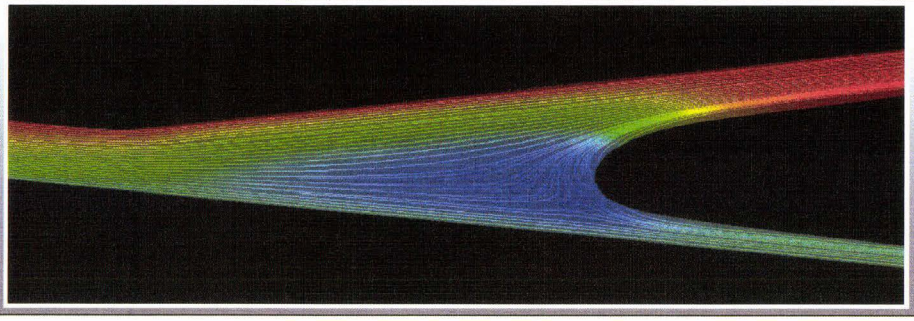

Le 11 mai 2007

Devant le jury composé de :

Rapporteurs :
P. MONTMITONNET, *Directeur de Recherches CNRS, Ecole des Mines de Paris, CEMEF*
A.M. HABRAKEN-WERA, *Directrice de Recherches FNRS, Université de Liège*
Examinateurs :
C. TOURNIER, *Professeur, Université de Valenciennes, LME*
L. DUBAR, *Professeur, Université de Valenciennes, LAMIH, Directeur de thèse*
A. DUBOIS, *Professeur, Université de Valenciennes, LAMIH*
J. P. NAYLOR, *Directeur Général de MYRIAD groupe CORUS*
Invités :
L.VIELLARD, *Responsable du service Développement industriel de MYRIAD groupe CORUS*

La science consiste à passer d'un étonnement à un autre.

Aristote

Acknowledgments

The present research work has been supported by MYRIAD - CORUS group in relation with the LAMIH: Laboratory for Automation, Mechanical engineering, Information sciences and Human-machine systems, the CNRS, the European Community, the Association Nationale de la Recherche Technique, the Conseil Régional du Nord Pas de Calais. I gratefully acknowledge the support of these institutions.

I would like to express profound gratitude to my advisors, Professor Laurent DUBAR and Dr Laurence VIELLARD for their support, encouragement, supervision and useful suggestions throughout this research work. Their moral support and continuous guidance enabled me to complete my work successfully. I am also highly thankful to Mirentxu DUBAR, associate Professor for her corrections of my English and her support for scientific publication. Thank you especially to Raphael DELTOMBE who help me during laboratory testing and Professor André DUBOIS for his valuable suggestions throughout this study.

I am grateful for MYRIAD company and especially Dr James Peter NAYLOR, Acting General Manager, and Hervé DUVAL, Technical manager, for their entrust to me. I would like to acknowledge, Daniel Michel GOSSET, Line 2 Manager, for his collaboration during my experimental investigation. I wish to thank Dr Franck DELAVENTE, project leader in CORUS STC, for his collaboration throughout this work.

My sincere thanks go to my friends Olivier PENIGUET, Kevin LOUAISIL, Sébastien HUART, Frédéric WATERLOT, Alexandre BARNES, Aurélien DUBOIS for their support and wonderful company.

A special thanks to the people of the Industrial Development of MYRIAD for their help and sympathy.

Thanks are due to my mother, Marie-Edith SZCZUREK for her love and support throughout my life. I also wish to thank my family for their support and encouragement.

My deepest appreciation goes to my girlfriend, Caroline DEVIENNE, who has been extremely patient and understanding throughout.

Eddy SZCZUREK

Abstract

The deformable roll coating is extensively used in the coil coating industry. The aim of the roll coating is to apply a thin liquid film on a moving substrate. The roll coating permits a high continuous speed and less defects application in theory. In reality, a transverse defect appears. This defect is commonly called "ribbing" and is characterized by periodic ribs parallel to the moving direction of the substrate. The wet thickness applied on the strip is adjusted by different gaps between rolls. The applied speeds and loads on the rolls modify the final film thickness and film stability. The elastomeric roll cover is used to avoid clashing between rolls, to permit thinner film application and to delay the onset of ribbing instability. The applied wet thickness on the moving substrate is a function of the speed ratio between rolls in contact, roll radius, elastomeric roll cover properties, fluid properties, exterior load applied, roll roughness and thickness of the elastomeric roll cover.

In this work, the flow between the applicator roll and the pick-up roll is presented for a deformable roll coating in negative gap mode. The aim of the study is an optimisation of the application in real industrial conditions by a good mastering of the contact parameters at the strip / roll cover interface. Compared to previous published studies, the presented work will take into account the elastomer cover behaviour used in industrial environments. A specific cyclic compression test is developed to analyse the elastomer behaviour as a function of representative solicitation and chemical environment. A modification of the Young Modulus and relaxation time of the elastomer is observed for different environments. A Prony series is identified with the compression test results and will be used in the numerical modelling. The finite element simulation of the process is proposed through a solid-fluid interaction. The solid part of the model predicts the mechanical pressure in the gap as a function of the elastomer behaviour and roll coater adjustment. The fluid part gets the associated wet thickness and free surface position.

Moreover, an experimental investigation is performed to correlate the numerical result and the industrial process. For each adjustment a ribbing defect macrophotography is performed. A specific image analysis tool is developed to evaluate the ribbing wavelength. The ribbing wavelength evaluation permits to link the bidimensional free surface position of the finite element simulation with the three dimensional instability for the different roll coater adjustments.

Résumé

L'enduction par rouleaux déformables est largement utilisée dans l'industrie du pré laquage d'acier galvanisé. Le but du pré laquage est d'appliquer une fine épaisseur de peinture liquide sur un support en mouvement. Ce procédé permet une application en continu et sans défaut en théorie. En réalité, un défaut nommé "cordage" apparaît et se caractérise par des rides de peinture parallèles au sens de défilement de la bande. L'épaisseur humide appliquée sur la bande est réglée au travers de différents passage entre les rouleaux. L'épaisseur finale et la stabilité de l'application sont modifiées par les vitesses de rouleaux et les efforts de serrage. Le revêtement d'élastomère qui recouvre certains rouleaux permet une application de peinture plus fine, d'éviter l'usure des rouleaux et de retarder l'apparition du défaut de cordage. L'épaisseur humide appliquée sur la bande est fonction du ratio de vitesse entre les rouleaux en contact, le rayon des rouleaux, les propriétés matériaux de l'élastomère, les propriétés du fluide, l'effort de serrage appliqué entre rouleaux, la rugosité des rouleaux et l'épaisseur du revêtement d'élastomère.

Dans cette étude, l'écoulement entre le rouleau applicateur et le rouleau preneur est présenté pour un serrage dit « négatif ». Le but de cette étude est l'optimisation de l'application pour des conditions industrielles, et cela à travers la maîtrise des paramètres de contact à l'interface bande / rouleau. L'originalité de cette étude par rapport aux travaux déjà publiés est la prise en compte des revêtements d'élastomère et de l'environnement industriel. Pour ce faire, un test spécifique de compression est développé pour analyser le comportement de l'élastomère face aux sollicitations et ambiance chimique industrielles. Des modifications du module d'Young et du temps de relaxation sont observés en fonction de l'environnement chimique. A partir des résultats de compression cyclique, des séries de Prony sont identifiées et sont utilisées pour modéliser le comportement viscoélastique de l'élastomère dans la simulation. Une modélisation par éléments finis du procédé est réalisée via une architecture de simulation solide-fluide. La première simulation solide permet d'évaluer la pression dans le contact en fonction des paramètres de réglages et des propriétés de l'élastomère. La seconde permet d'obtenir l'épaisseur humide et la position de la surface libre.

Afin de corréler ces résultats numériques au procédé industriel, une approche expérimentale est réalisée sur une tête d'enduction industrielle. Une base de donnée complète est créée et pour chaque réglage une macrophotographie du défaut est prise. Un outil spécifique de traitement d'image est développé pour évaluer la période du cordage sur ces photographies. Cette évaluation de période du défaut permet de relier les positions de surface libre numériques en 2D à l'instabilité en 3D pour différents réglages machine.

Contents

Introduction

Industrial context

MYRIAD is a coil coating company and a part of CORUS group. The productivity coupled with the quality of the galvanized steel product are the two conditions to be competitive in the current world. The final product of coil coating feeds the building, the coolers and the luminary industries.

MYRIAD is one of the continuous galvanized and prepainted lines around the Europe. This particularity requires a high level of process control to guaranty quality along the production. The less defect through the production process involves a loss of quality on the final product and then, an increase of production cost for the company. The different steps of process to manage the quality are defined as follows:

- Hot rolled steel quality control at the receipt.
- Pickling and cold rolling mastering to obtain a clean and less defect steel strip with the targeted thickness.
- Cold rolled steel degreasing and recristallization annealing to recover its mechanical properties.
- Thickness of galvanisation check to have an homogenous anticorrosion behaviour.
- Skin-pass mastering to obtain a good surface roughness before painting.
- Paint application and curing control to obtain the final visual aspect, mechanical properties of coating, gloss, and colour.

The operation defined by the paint application is one of the most important in the process. This operation involves the management of many resin families and colours. Moreover, the applied paint thickness can be different from a strip to another, according to the desired final product. The paint application is performed with a three deformable roll coater. The advantage of the deformable roll coater is a thinner film and less defect application in theory. In reality, a transverse defect appears. This defect is commonly called "ribbing" and is characterized by periodic ribs parallel to the moving direction of the substrate. The ribbing causes a poor quality on the final product and limits the commercial application.

The wet thickness of paint applied on the steel strip is adjusted by different gaps between rolls. The applied speeds and loads on the rolls modify the final film thickness and film stability. The studied industrial three rolls coater has two rolls with elastomeric roll cover called "applicator-roll" and "metering-roll". The last one is a steel roll called "pick-up roll". The applied wet thickness on the moving substrate is a function of the speed ratio between "applicator-roll" and "pick-up roll", roll radius, elastomeric roll cover properties, fluid properties, external load applied between rolls, roll roughness and thickness of the elastomeric roll cover.

Industrial aim

The industrial aim is defined by a product quality and productivity improvement. The deformable roll coater is used in MYRIAD for galvanized steel coating but it is also used for aluminium coating, paper or glue in other industries. The knowledge on the paint application will permit to improve many processes. Moreover, environmental restriction imposed new passivating surface treatment before paint coating. This surface treatment is obtained by deformable roll coating as the current chromatic passivation. In a near future, benefits of this paint application study could be applied to the chrome free passivation.

In order to reach these goals, MYRIAD needs to understand the paint application by deformable roll coater. This understanding will be obtained through the analysis of roll coater adjustment parameters and materials (fluid, elastomer of the roll cover).

Scientific aim

The aim of this study is to develop knowledge of the roll-coater process. To improve the product quality for the real application speed, an accurate understanding of the roll coating is essential. This understanding is based on the determination of one or more criterion based on the roll coater characteristics for limiting the ribbing instability.

With this accurate scientific learning of the flow rate in the deformable contact, it will be possible to improve productivity by short time adjustment of the roll-coater process to production variations (line speed, different resins and colours).

Recent studies on the evaluation of the wet thickness have been led. Different authors have established power law to predict the film wet thickness as a function of the contact parameters. These laws are interesting to have an approximate estimation of the wet thickness for the real application, but the evolution of the elastomer behaviour as a function of time has not been taken into account. Actually, the elastomer behaviour during the application is a very important parameter to master, because the mechanical pressure in the contact

is a function of the behaviour law. The pressure in the contact modifies the flow rate and the stability of the meniscus where the film split occurs. Concerning the ribbing instability, the position of the meniscus and the link with the ribs has been discussed. Models coming from literature to study the flow rate between deformable rolls are based on the lubrication theory coupled with a one dimensional elastic model for the roll cover deformation. The predicted critical capillary number and wavelengths of the ribbing are compared with the obtained experimental values, showing a good correlation.

In this work, the proposed approach is different from the recent studies. It is based on the numerical simulation of an industrial roll-coater in order to be as representative as possible of the real contact conditions. The introduced parameters such as line speed, roll speeds, and loads between rolls come from the production line adjustments. Compared to previous published studies, the presented work will take into account the elastomer roll cover behaviour used in industrial environments. The viscoelasticity of the elastomer gets modified with the environment. In the industrial process the used coil coating paints are very different in composition to obtain different colors and mechanical properties. A modification of the Young Modulus and relaxation time of the elastomer is observed for different environments. The elastomer and resins used for the characterization of the behaviour laws are also taken on the production line. This methodology of work is mainly oriented to get a better optimisation of the process by numerical simulation coupled to an industrial experimental roll coater. The final aim is to improve the quality and the productivity of the production line.

The first part is a literature review on the roll coating. The different experimental works, theoritical models and finite element modelling are exposed and compared. This part will help us to understand the free surface flow rate during roll coating and to define our research ways.

The second part deals with the testing stand selection. A list of available possibilities to perform the experimental investigation is suggested. After a description of the selection criterion and a comparison between testing stand, the results of the experimental investigation on the selected testing stand are summed-up. This part will help us to determine and highlight the key parameters acting on the ribbing defect and wet thickness adjustment.

The third part details the numerical modelling of the process. The goal is to understand the physical mechanisms acting on the flow rate in the deformable contact. After a presentation of the roll coater study and the used methodology, the first point is the characterization of the elastomer behaviour law for different environments. The elastomer roll cover is studied with a specific cyclic compression test to reproduce inline solicitation with the chemical environment. Finally, a Prony series is identified. It models the viscoelastic behaviour of the

elastomer in the numerical simulation. Next, the deformable finite element model is detailed. This model evaluates the mechanical pressure in the contact for different elastomer behaviour laws. The last point of this part is the fluid numerical simulation at the interface taking into account the mechanical contact pressure determined during the previous part. The influence of the contact pressure and speed ratio between rolls on the free surface position is discussed.

Chapter 1

The deformable roll coating in industrial process

1. Presentation of the industrial process

1.1 Overview of the coil coating

MYRIAD is a coil coating company and is part of CORUS group. It produces around 400KT of organic coated product per year. The principal customers are building envelope, cold room, lighting and general industry.

Myriad has two organic coating lines combined with hot dip galvanizing. Their special features are continuous lines, induction curing and vertical coating.

Figure 1-1 illustrates the industrial coil coating process. First, suppliers deliver hot rolled coils with a thickness between 2 and 3.5mm. Several operations are performed to prepare the coil for the production line. Pickling eliminates oxides on the hot rolled coil and edging adjusts the width of the strip. During the recoiling, a thin oil deposition on the strip prevents corrosion. A SENDZIMIR cold rolling mill permits a strip thickness reduction and length increasing by plastic strain. The final strip thickness is between 0.3 and 2mm.

The next steps are the degreasing and the recristallization annealing of the strip. The strip dips in a hot zinc bath around 450°C. It is the galvanizing operation. The galvanized strip is skin passed to print roughness and increase surface aspect. Then, a chemical surface treatment permits a good primer coating adhesion on the strip. The finish coat applied on the primer coat confers the final aspect and protection characteristics of the product. This coating section will be detailed in the next paragraph. The primer coat and finish coat are liquid paints including solvent in their composition. The induction curing evaporates solvent to obtain a cross-linking coating. After recoiling, the galvanized steel coil is packaged and delivered to the customers.

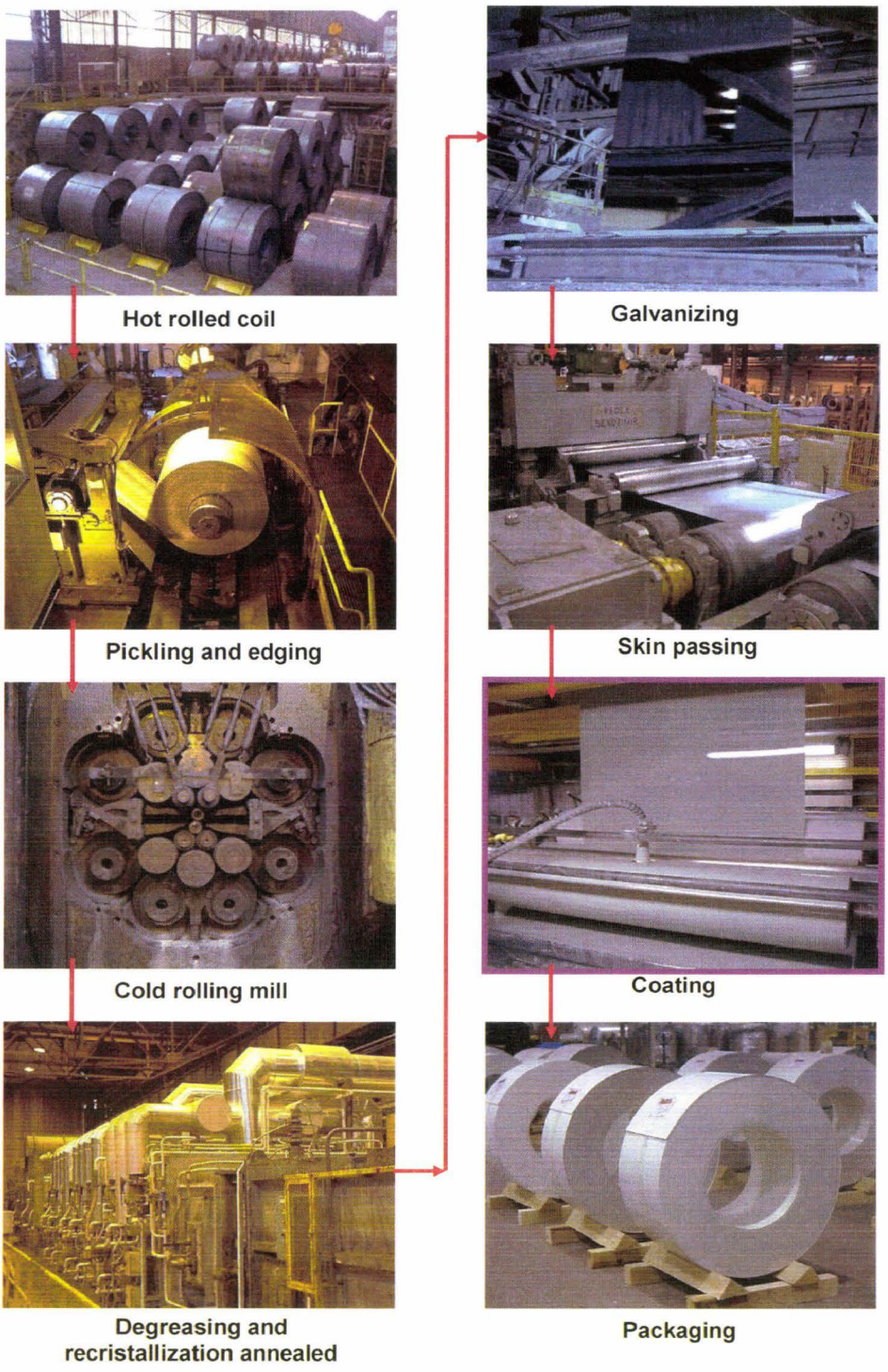

Figure 1-1: Presentation of the industrial process with the coating section

This complex industrial process is composed of different parts: cold rolling, galvanizing, prepainting and curing. To obtain the target quality of the product, each section must be mastered. Deltombe [1] studied the cold rolling mill to optimise the number of passes for a best productivity. Huart [2] analysed the

skin-pass operation to improve the surface aspect before coating and decrease the associated pollution. In order to complete the knowledge, the present work is focused on the paint application section to increase the roll coater mastering and decrease the aspect defects.

1.2 Deformable roll coating: principles and defects

A vertical galvanized strip with primer coat moves upwards. The line speed can reach 120m/min. Two roll coaters squeeze the vertical strip to avoid vibrations. The deformable roll in contact with the strip is called "applicator roll". The next rigid roll in contact with the "applicator roll" is "the pick-up roll". Finally, the deformable roll in contact with "the pick-up roll" is "the metering roll". The applicator roll deposits the liquid paint on the galvanized substrate. The radius of the applicator roll including the deformable cover can be in the range [120-135mm]. The deformable layer thickness evolves because of wear and surface finishing in the range [25-40mm]. The elastomer is polyurethane with high chemical and mechanical resistance. Table 1-2 sums-up the supplier polyurethane properties. The elastomeric roll cover is used to avoid clashing between rolls, to permit thinner film application and to delay the onset of ribbing instability (Figure 1-2) [3].

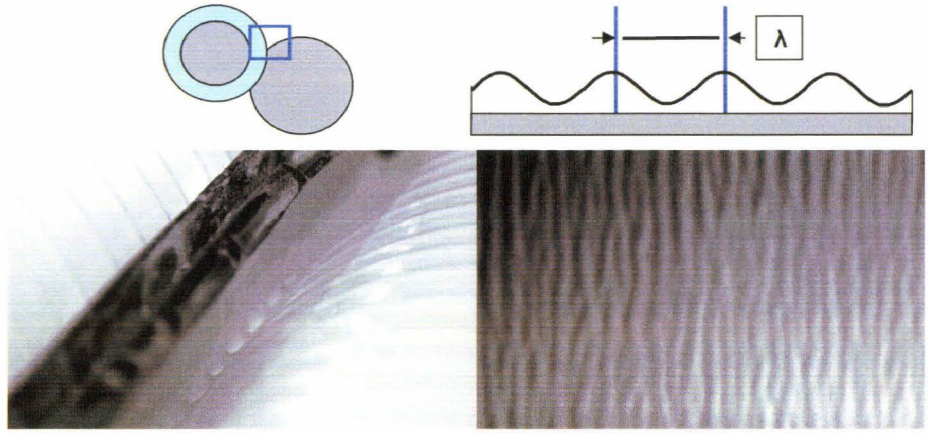

Figure 1-2: Ribbing instability between rolls (left), on the strip (right)

The ribbing causes a poor quality on the final product and limits the commercial application. When the wet thickness is adjusted between the applicator and the pick-up rolls, the ribbing is present at the contact output and is transferred to the substrate. The last contact between the strip and the applicator roll permits a levelling of the defect, but it still remains on the substrate. The wavelength (λ) characterises the ribbing defect in this study. This wavelength is in general between 1mm and 3mm. Figure 1-3 presents the standard roll coater used in the MYRIAD painting section.

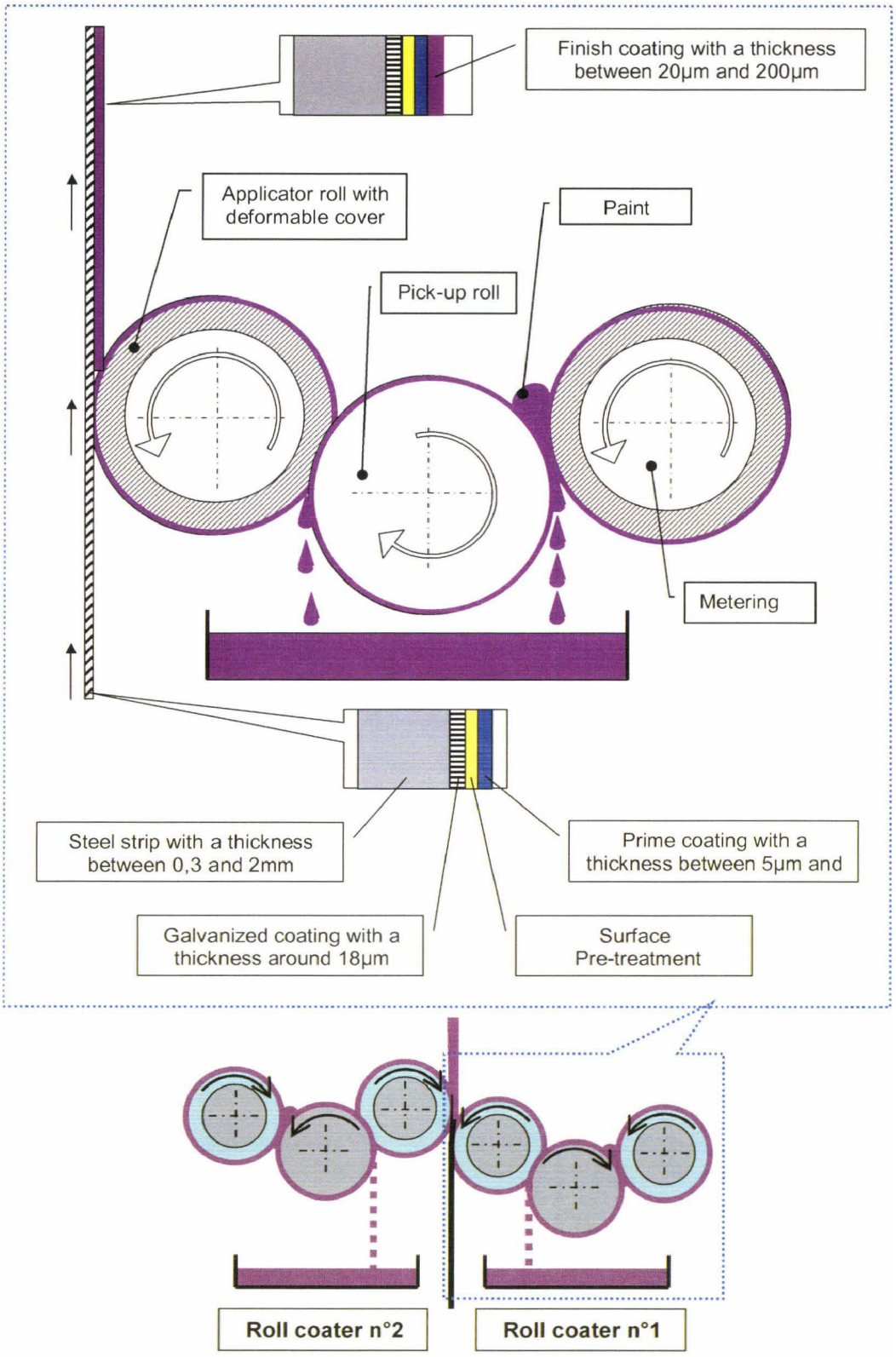

Figure 1-3: Focus on roll coater n°1 (top)

Two roll coaters during application on vertical strip (bottom)

The applicator roll has a reverse direction of rotation regarding the strip direction. Its peripheral speed of rotation is ranging between 101% and 120% of the strip speed. The pick-up roll has a 145mm radius and an inverse direction of rotation compared to the applicator roll. It is steel or ceramic made for Myriad plant. Its peripheral speed of rotation is ranging between 20 and 50% of the strip speed. The last roll in contact with the pick-up roll is "the metering roll". Its speed is around 20% of the line speed. It presets flow rate of paint. Table 1-1 sums-up the roll coater speeds.

Table 1-1: Roll coater speeds

Ls(m/min)	Strip speed	Until 120
Va (% of Ls)	Applicator speed	101 to 120
Vp (% of Ls)	Pick-up speed	30 to 50
Vm(% of Ls)	Metering speed	20

Coil coating industry uses different paint compositions. The resin families are mostly polyester (SP), Polyvinylidene Fluoride (PVDF), Polyvinyl chloride (PVC), and polyurethane (PU). Inline, operators modify the pick-up roll position to increase or decrease the paint wet thickness on the strip. They modify the roll speeds to act on the application defects and especially on the ribbing. Table 1-2 sums-up the elastomer polyurethane properties of the applicator roll cover.

Table 1-2: Polyurethane properties

Properties	**Value**	**Unity**
Hardness	45-60	Shore A
Density	1370	Kg/m3
Rm	17	Mpa
Ultimate elongation	403	%
Young Modulus (E1)	3,2	MPa
Surface energy (γsl)	53	mN/m

The surface energy acts on the wet thickness. The wettability of a liquid is defined as the contact angle between a droplet of the liquid in thermal equilibrium on an horizontal surface. Depending on the type of surface (polyurethane), and liquid (coil coating paint) the droplet may take a variety of shapes as illustrated in Figure 1-4.

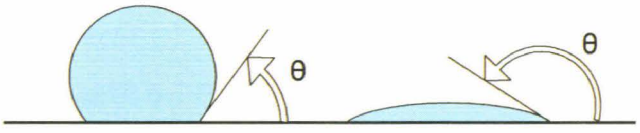

Figure 1-4: Surface wettability: non-wetting fluid (left), wetting fluid (right)

The wetting angle θ is given by the angle between the interface of the droplet and the horizontal surface. The liquid seems wetting when 90< θ <180 degrees and non-wetting when 0< θ <90. θ =0 or 180 degrees correspond to perfect wetting and the drop spreads forming a film on the surface. Actually, the wetting angle θ is a thermodynamic variable which depends on the interfacial tensions of the surfaces. Let γ_{lg} denotes the interfacial tension due to the liquid-gas surface, γ_{sl} refers to the interfacial tension due to the solid-liquid surface and γ_{sg} indicates the interfacial tension of the solid-gas interface. In thermodynamic equilibrium the wetting angle θ is given by Young's law (1-1):

$$\gamma_{sg} = \gamma_{sl} + \gamma_{lg} \cos \theta \qquad (1\text{-}1)$$

The goal of this study is to develop a better understanding of the ribbing defect in the deformable contact, in order to improve the roll coating in MYRIAD. The next paragraph focuses on the contact between the applicator roll and the pick-up roll since the ribbing defect occurs between these two rolls.

1.3 Contact zone between applicator and pick-up rolls

The roll coating permits a continuous wet film deposition on a moving substrate. The number of rolls used depends on the final product required. In fact, each film split between rolls decreases the final wet thickness. For the myriad coating, three rolls by roll coater allow a good wet thickness and quality aspect adjustment. The basis of the study is a three rolls coater system with two deformable rolls. The deformable rolls are the "applicator" and the "metering". The roll coater works in negative gap mode. For two rolls in contact (a deformable and a rigid one), if the sum of initial rolls radius is less than the center to center distance, this is "the negative gap mode". On the opposite, it is "the positive gap mode".

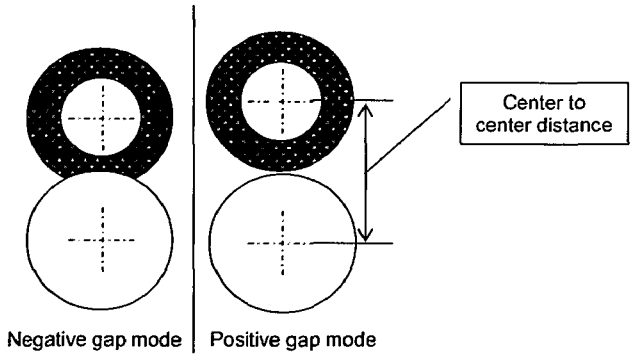

Figure 1-5: Negative gap mode and positive gap mode between two rolls

The paint is flowing through a rigid roll and a deformable one. Figure 1-6 presents the parameters used to describe deformable roll coater in general way. The rolls speed "Va, Vp" and Negative gap or initial upsetting imposed "Ng" modify the flow rate performance in the channel between rolls. The channel height or distance between roll surfaces is commonly called the gap and identified by"H0". The gap corresponds to the paint thickness which separates the two roll surfaces. At the exit, the meniscus of fluid occurs. Figure 1-7 focuses on the gap exit. The free surface (ie, the meniscus) is split in two unequal wet thicknesses on each roll.

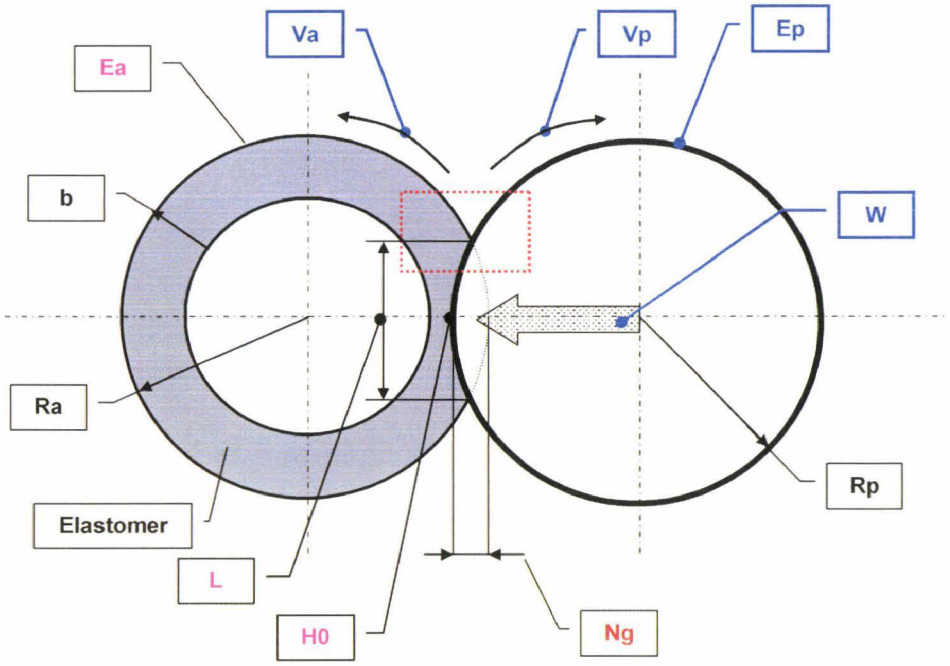

Figure 1-6: Contact parameters describing deformable roll coater used in literature and industrial plant

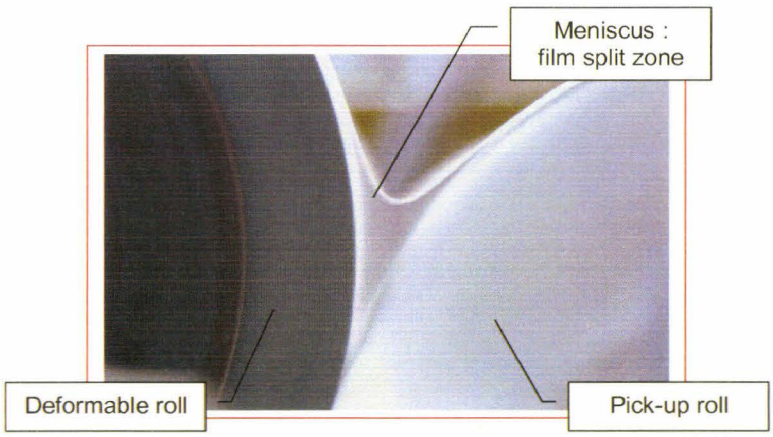

Figure 1-7: Focus on the fluid meniscus (film split zone) between two rolls

The paint film on the deformable roll "Ea" is transferred on the substrate. The wet film on the rigid roll "Ep" returns back to the paint reservoir.

The corresponding parameters that describe the contact between rolls are summed in Table 1-3. A colour code is used to distinguish the different parameters. In industrial plant, only the pick-up wet thickness and rolls speeds are measured during application. Operators adjust the wet thickness with a negative gap (red colour). The blue colour highlights parameters that will evolve in our experimental investigation. A load measurement will be performed, with the different roll speeds and the pick-up wet thickness. This is the goal of the experimental chapter. Finally, the pink colour is used for the parameters found in the literature. These last ones will be used in our numerical chapter.

Table 1-3: Description of the contact parameters and unity

	Parameters	Description	Unity
Pick-up	Rp	Pick-up radius	mm
	Vp	**Pick-up speed**	**m/s**
	Ep	**Pick-up wet thickness**	**µm**
Applicator	Ra	Applicator radius	mm
	b	Elastomer thickness	mm
	Va	**Applicator Speed**	**m/s**
	Ea	**Applicator wet thickness**	**µm**
Contact	**Ng**	**Negative gap imposed (crushing)**	**mm**
	W	**External load**	**N/m**
	L	**Contact length**	**mm**
	H0	**gap or channel thickness between rolls**	**µm**

The paint and contact geometry variation in industrial environment involves a load modification for a same negative gap "Ng". This load modification acts on the flow rate in the contact. Then, the wet thickness and the ribbing instability evolve in the time. Figure 1-8 focuses on the elastohydrodynamic action between the two rolls. In the contact, there are two principal actors: the fluid and the elastomer. The fluid is defined by its rheology: dynamic viscosity, surface tension and density. The elastomer is characterised by its viscoelastic properties: density, dynamic Young modulus, relaxation time. During application, these two materials evolve to reach an equilibrium state for a given roll coater configuration. The final wet thickness is the result of the equilibrium between three forces in the gap: the hydrodynamic viscous force induced by the fluid, the viscoelastic response of elastomer resulting from the roll cover deformations, and the external load resisting to roll deformation [4], [5]. The fluid flows through the rolls as a function of the geometry of the channel. This

geometry is the result of the coupled interaction between paint and elastomer. For small external load, the paint properties control the flow rate. The surface tension of the fluid acts on the ribbing defect by a modification of the film splitting and of the time levelling before curing [6]. For high external load, the wet thickness is very small and the elastomer properties control the flow rate.

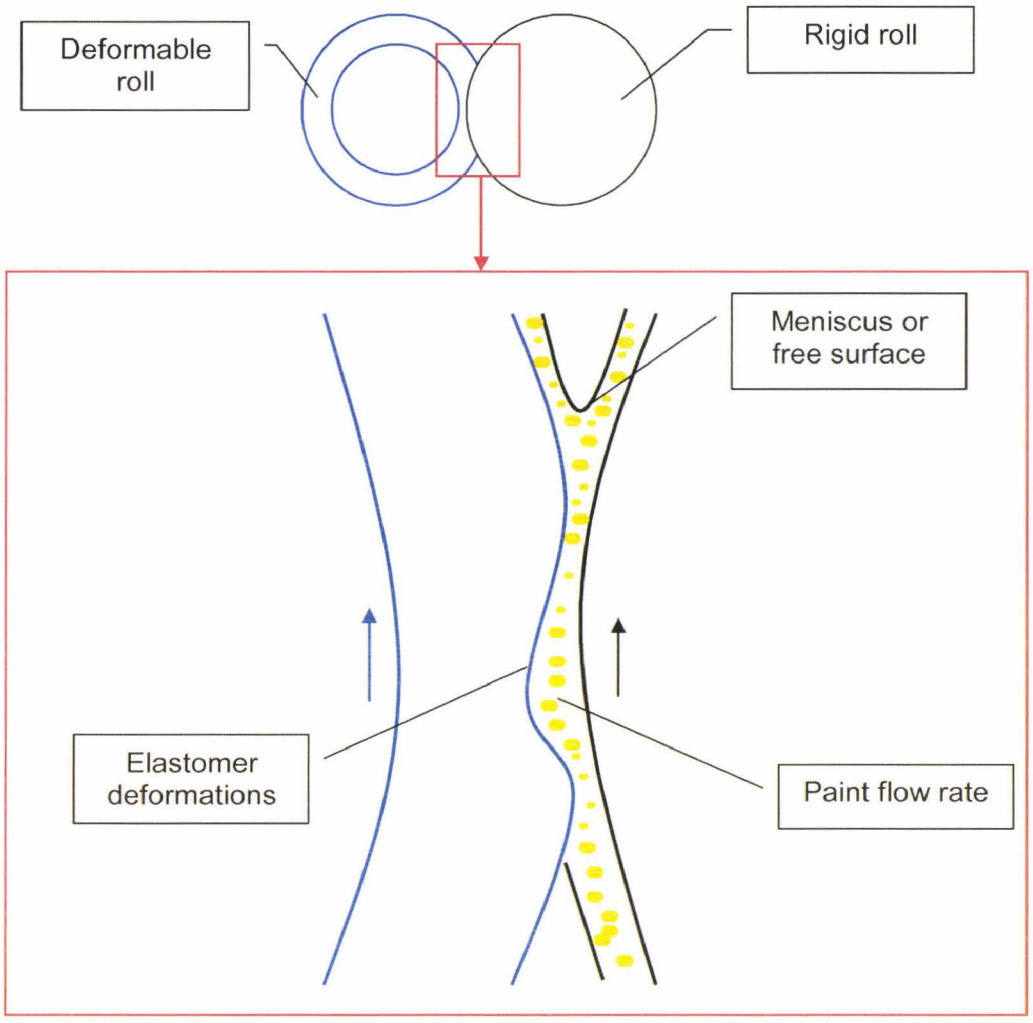

Figure 1-8: Nip deformation, equilibrium between viscous and elastic forces

We have seen the deformable contact geometry and associated parameters. In order to complete the coil coating presentation and the mechanisms governing the flow rate in the gap, a literature review is exposed. The gap performance and ribbing studies will be focused on deformable roll in negative gap mode.

2. Roll coating literature

The aim of this literature review is to highlight existing knowledge on roll coating. Several authors worked on the roll coating application. These studies were for rigid and deformable gap between rolls, roll-plate contact, both forward and reverse application.

Greener [4], [7] exposed one of the first roll coating study for viscous and viscoelastic fluids. A wet thickness prediction model is proposed for Newtonian fluid and an empirical model for non-Newtonian viscoelastic fluid. He proposed an instability criterion through a ribbing study between rolls and Newtonian fluid [8]. Babchin [9] experimentally analysed a rigid pair of rolls in forward and reverse mode. He defined different defects range as a function of the wet thickness and speed ratio. Benkreira [10], [11], [12] studied rigid roll contact between rolls in forward mode. He proposed numerical and experimental approaches. His conclusions show the inlet feeding importance on the flow rate stability in a rigid contact.

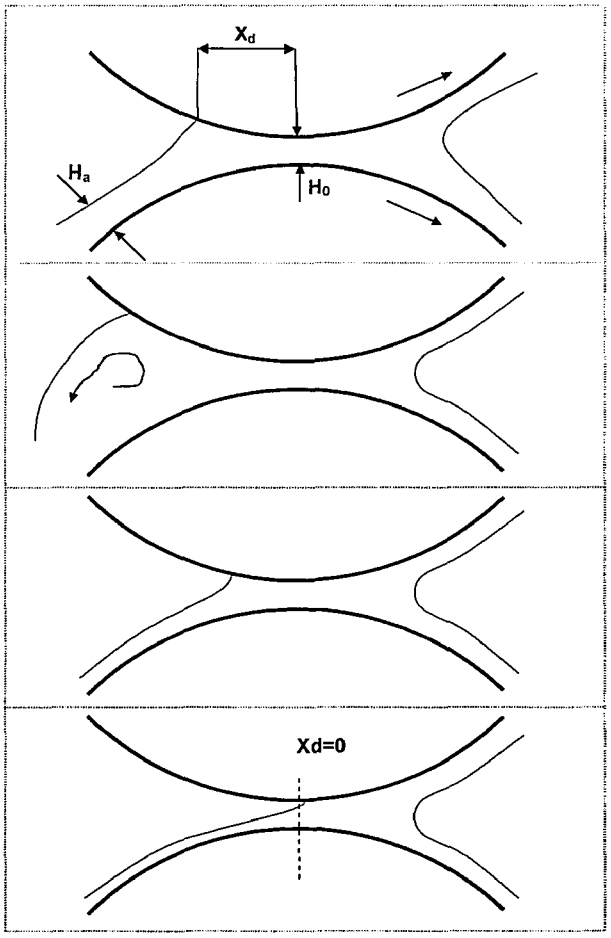

Figure 1-9: Focus on rigid gap by Benkreira [10], [11]

The dynamic wetting line position is defined by Xd in his study. Application defect is observed if the wetting line passes the middle of the contact, i.e. Xd=0. Thompson [13] proposed a fed-reservoir of a roll coater analysis. The study shows the fluid recirculation inside the reservoir as a function of roll speed. This study can be linked to the Benkreira analysis.

Savage [14], [15], [16], [17] proposed mathematical models and experimental investigation to predict wet thickness and onset of ribbing between a rigid roll and plate. Finally, Ruschak [21] overviewed the coating techniques and understanding progress. These works are not detailed in this review, because they cannot focus on the deformable problem and inline production speed.

The flow between rolls has been extensively studied by both experiments and theory. The first authors were Pearson [18], Pitt's & Greiller [19], Mill & south [20] in the fifties and sixties. They have developed many stability criteria with regards to the ribbing instability and have contributed to the mathematical model development. They observed the ribbing instability occurrence for critical capillary numbers and geometrical factor (Figure 1-10). The capillary number represents the relative effect of viscous forces and surface tension acting across an interface between a liquid and a gas, or between two immiscible liquids. The capillary number is defined by equation (1-2):

$$Ca = \frac{\mu V}{\gamma \lg} \tag{1-2}$$

With μ : dynamic fluid viscosity (Pa.s), V : mean peripheral roll speed (m/s) (1-3), $\gamma \lg$: fluid surface tension (N/m).

$$V = \frac{(V_a + V_p)}{2} \tag{1-3}$$

With Va : applicator roll speed (m/s), Vp : pick-up roll speed (m/s)

The geometrical factor is defined by equation (1-4) as follows:

$$\alpha = \frac{H0}{R} \tag{1-4}$$

With $H0$: gap between rolls (m), R : equivalent roll radius (m)(1-5)

Equation (1-5) gives the equivalent roll radius R :

$$\frac{1}{R} = \frac{1}{R_a} + \frac{1}{R_p} \tag{1-5}$$

With R_a : deformable roll radius (m), R_p : rigid roll radius (m)

For the coil coating process, α is in the range [10^{-4}; 10^{-3}] and Ca is in the range [1; 10]. For these two ranges, the ribbing defect is always present. Our experimental investigation exposed in next chapter will be in this defined ranges.

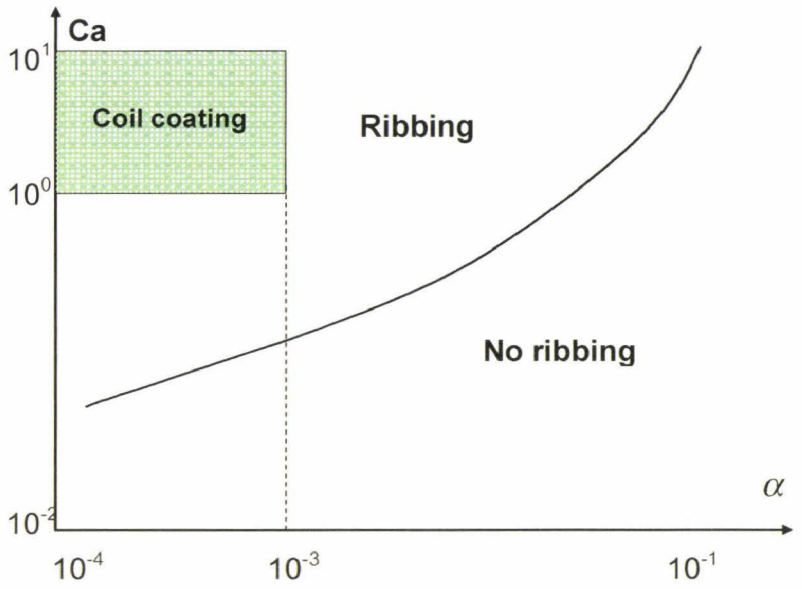

Figure 1-10: Coil coating process: diagram of stability [14], [19], [21]

This literature review is limited to the deformable contact in negative mode. The deformable roll coating literature can be separated in two-research axis:

The first axis is the theoritical approach essentially based on model development: to predict the wet thickness as a function of roll coater parameters; to study the roll coater parameters influence on the ribbing defect. The flow rate is essentially modelled by hydrodynamic lubrication theory with different free surface conditions. Moreover, different authors used the complete Navier-stokes equation to model accurately the flow rate. The elastomeric roll cover was studied from simple semi-infinite elastic domain [22], [23] to complex finite element models [3], [24].

The second axis is the experimental investigation to validate theoritical predictions. Some authors worked on experimental approaches closed to our ribbing instability problem but did not work on the deformable roll coating. The different apparatus are roll-plate, deformable roll - rigid roll or industrial roll coater. In all cases, the gap performance by wet thickness prediction as a function of the testing stand parameters and the ribbing instability occurrence will be exposed.

2.1 Theoritical works

2.1.1 Wet thickness prediction

Herrebrugh [22] solved the first elastohydrodynamic problem closed to the deformable roll contact problem. It is a lubrication problem with line contact. This author approximates the wet thickness e by equation (1-6) as a function of the deformable contact parameters.

$$e \approx 0.99 R^{0.6} (\mu V)^{0.6} E^{-0.4} W^{-0.2} \tag{1-6}$$

With,

- R : equivalent roll radius (m)
- μ : dynamic fluid viscosity (Pa.s)
- V :mean peripheral roll speed (m/s)
- E : Equivalent Young modulus (Pa)
- W : external load (N)

The equivalent Young modulus E is computed with equation (1-7) as follows:

$$E = \frac{1-\upsilon_a}{(E_1)} + \frac{1-\upsilon_p}{(E_2)} \tag{1-7}$$

With,

- E_1: Young modulus of deformable roll cover (Pa)

- υ_a : Poisson coefficient of deformable roll cover
- E_2 :Young modulus of rigid roll material (Pa)
- υ_p :Poisson coefficient of rigid roll material

Hall & Savage [23] obtained similar results that Herrebrugh for their thickness prediction.

Herrebrugh, Savage & Hall worked with a semi-infinite deformable roll hypothesis. In deformable roll coating, a finite elastomer layer defines the deformable part of the applicator roll. The elastomer layer thickness has an importance on the elastomer stiffness and influence on the flow rate.

Coyle [25] treats the problem by a coupled model. The elastomer behaviour is modelled by an Hookean spring model with linear response. The elastomer is a finite layer thickness. The fluid flow rate modelling is obtained by the lubrication theory. Equation (1-8) defines the power law computed from numerical results of his model.

$$e \approx R^{0.7}(\mu V)^{0.6} E^{-0.3} W^{-0.3} \tag{1-8}$$

Hooke [26] exposes the elastomeric layer influence on the wet thickness prediction. The layer thickness "b" has a slight influence on the wet thickness, if the half contact length "$\frac{L}{2}$" is less than the layer thickness "b".

In order to complete the analysis, Coyle used a bidimensional finite element approach [24]. The model leads to the following expression (1-9):

$$e \approx 3.12(\mu V)^{0.6} R^{0.7} E^{-0.3} W^{-0.3} \tag{1-9}$$

More recent studies have been led on the wet thickness evaluation. Carvalho [3] developed a theoretical model with non-linear elastic behaviour for the deformable cover (Mooney-Rivlin) and Navier-Stokes equations for the flow rate. The predictions show that the roll cover considerably affects the flow rate. A more complex model with single relaxation time for viscoelastic behaviour permits to predict the flow rate for thin and thick elastomer layer [27]. He

obtained two equations for thin layer $\frac{b}{R}$<0.1 and thick layer $\frac{b}{R}$>0.1, (1-10), (1-11).

$$(\frac{Q}{2VR})_{thin} = 0.67(\frac{\mu V}{ER})^{0.6}(\frac{b}{R})^{0.29}(\frac{W}{ER})^{-0.31} \quad (1\text{-}10)$$

$$(\frac{Q}{2VR})_{thick} = 0.34(\frac{\mu V}{ER})^{0.6}(\frac{W}{ER})^{-0.31} \quad (1\text{-}11)$$

With Q: flow rate (m^3/s).

Equation (1-11) is close to Coyle's equation from his finite element model (1-8). Moreover, the results are in good agreement with the experimental measurements of Cohu [28]. These laws are interesting to have an approximate estimation of the wet thickness for the real application, but the evolution of the elastomer behaviour as a function of time has not been taken into account. The elastomer behaviour during the application is a very important parameter to master, because the mechanical pressure in the contact is a function of the behaviour law. The pressure in the contact modifies both flow rate and the stability of the meniscus where the film split occurs.

The next paragraph exposes the ribbing instability defect and associated literature.

2.1.2 Ribbing instability study

Figure 1-11 illustrates the different zones of the fluid meniscus and the ribbing defect occurence.

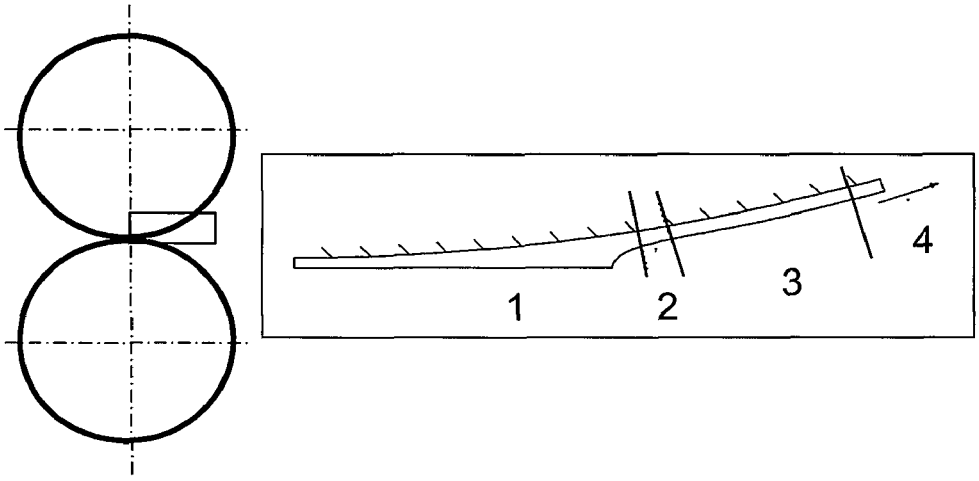

Figure 1-11: Film splitting, details of the four states

The four zones are defined as follows:

Zone 1: the pressure in the contact involves a rib occurrence and development. The meniscus position evolves.

Zone 2: the pressure gradient is not sufficient to act on the meniscus position. The viscous forces and the surface tension are in equilibrium in the fluid.

Zone 3: the viscous forces do not govern the fluid stability. The surface tension is dominant and permits the ribs levelling.

Zone 4: the wet film reaches its stable state.

Carvalho & Scriven [29] developed a theoritical model to study the flow rate between deformable rolls based on the lubrication theory coupled with a one-dimensional elastic model for the roll cover deformation. The principal result is the prediction of higher Ca for a deformable nip than for a rigid nip. In fact, he proposed a comparison between a rigid gap and a deformable one. The deformable contact permits to obtain a stable flow rate when the ribbing defect occurs in the rigid one. An important remark is the decreasing of the ribbing wavelength with an increasing of the load.

Gostling [30] studied a deformable negative gap mode for equal roll speed and Newtonian fluid. His finite strip model coupled with the lubrication theory shows a different behaviour of the gap for higher external load. The fluid separation restabilizes at large negative gap. The wet thickness in this case increases on the deformable roll when the pick-up wet thickness decreases. When the external load increases, a thinner elastomer layer increases the film stability. This last work is very interesting because it shows the transition between low load and high load importance on the roll coater mastering. In fact, the roll

coater requires different adjustments as a function of the imposed load and elastomeric layer thickness for a same-targeted wet thickness.

The above theoritical power laws to predict the wet thickness and the parameters acting on the ribbing wavelength need to be validated. This is the goal of the experimental works.

2.2 Experimental works

In order to validate numerical and theoritical prediction, several experimental approaches have been performed and exposed in the literature.

2.2.1 Wet thickness prediction

Several authors have reported experiments with deformable contact and Newtonian fluid. Smith & Maloney [31] established a power law with 700 data points defined by equation (1-12):

$$e \approx 4(\mu V)^{0.64} R^{0.58} E^{-0.35} W^{-0.34} \quad (1\text{-}12)$$

Coyle obtained a power law defined by equation (1-13) with 200 data points on a rigid roll-deformable roll testing stand.

$$e \approx 4.1 R^{0.42} (\mu V)^{0.49} E^{-0.41} W^{-0.43} \quad (1\text{-}13)$$

Coyle did not get a good correlation between experimental(1-13) and theoritical results (1-8). He explained these discrepancies by the viscoelastic properties of the roll cover. In fact, his mathematical model is built on elastic roll cover response. The real elastomer is a viscoelastic material with relaxation time.

Cohu [28] performed experimental measurements on industrial three rolls coater. This is a similar industrial roll coater as the one used in Myriad. The roll cover is viscoelastic and the fluid is coil coating paint. The final power law obtained is described by equation (1-14):

$$e \approx 0.4 R^{0.7} (\mu V)^{0.6} E^{-0.3} W^{-0.3} \quad (1\text{-}14)$$

Equation (1-14) is in good agreement with equation (1-8) obtained by finite elements approach of Coyle. The maximum error encountered between

experimental and power law is around 25% for the experimental studied parameters of Cohu.

Figure 1-12 sums-up the different power laws of the literature for a specific configuration. On one hand, wet thickness predictions are closed for Cohu [28], Coyle [25] and Herrebrugh [22]. Cohu performed measurements on industrial roll coater and his results will be our reference. On the other hand, for Coyle [24] and Smith & Maloney [31] wet thickness predictions are higher. These two last results seem to be too far from reality with regards to the deformable roll coating process.

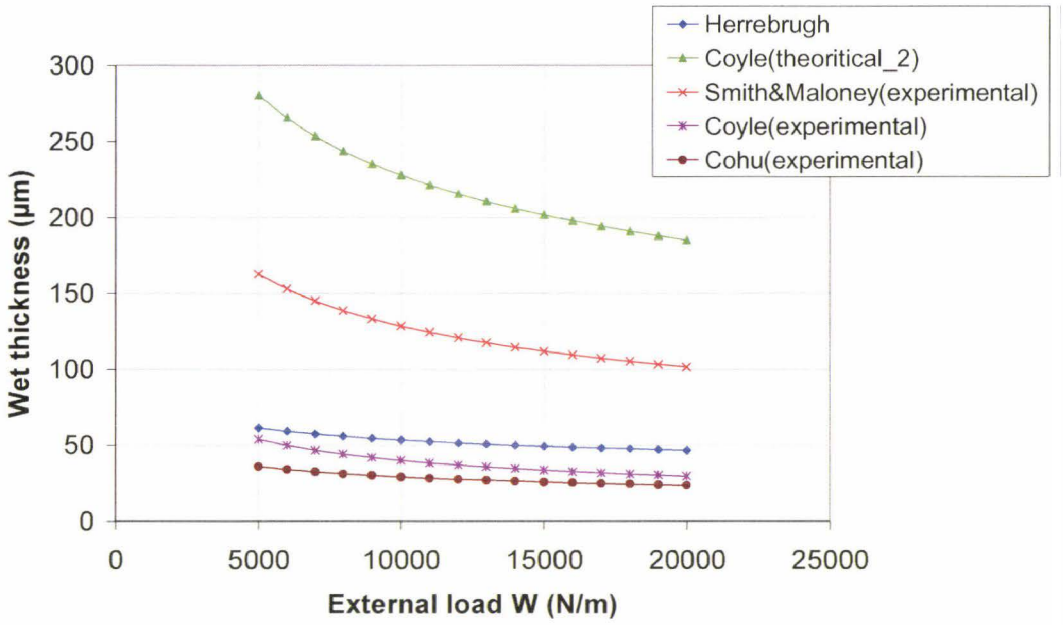

Figure 1-12: Wet thickness prediction as a function of the external load,

(Viscosity =0,5Pa.s, V=1m/s, R=0,069, E=3MPa)

2.2.2 Ribbing instability study

Adachi [32] studied the ribbing instability for a rigid roll-plate apparatus. The ribbing wavelength was evaluated for different oils and speeds. The position of the meniscus and the relation with the ribs were discussed. Figure 1-13 illustrates the free surface position observation and influence on the ribbing wavelength.

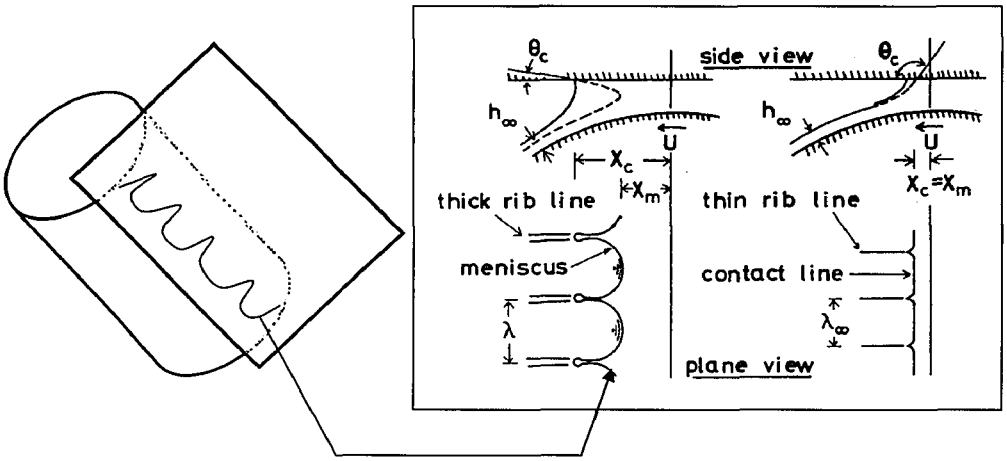

Figure 1-13: Ribbing wavelength between roll and rigid plate [32]

The ribbing defect amplitude increases when the angle with the plate θ_c decreases. On the opposite, the ribbing amplitude decreases when θ_c increases and comes in the contact between roll and plate. In addition, the ribbing wavelength decreases with the amplitude and inversely. It is a rigid roll-plate contact but the experimental observations are very interesting to understand the ribbing defect variations. Moreover, these observations found to be good with the below study of Carvalho.

Carvalho & Scriven [33] studied the stability of the flow in the transverse direction of a deformable contact. The two rolls are partially immerged in a liquid. The liquid composed of water and glycerine is Newtonian with a viscosity in the range [0.092; 0.115Pa.s]. The ribbing wavelength observation is obtained through a flexible and transparent film fixed on the rigid roll. They show that the critical capillary number is delayed at smaller gap compared to rigid roll.

Chong [34] observed the same phenomenon for a negative gap mode with deformable contact. The ribbing instability wavelength decreases on the two rolls when the external load between rolls increases. In the same time, the wet thickness on the rigid roll decreases. The viscoelastic effect of the rubber involves a wet thickness increasing on the deformable roll. This phenomenon appears for high imposed external load or negative gap. Figure 1-14 exposes his results. The fluid used is not coil coating paint and the maximum speed is 64m/min. There are no coating problems at this line speed on industrial line. These results are very interesting but come from a testing stand and are not representative of an industrial environment. The industrial environment exposes the roll coater to temperature variation, different paint temperature and viscosity, vibrations.

Tiu [35] studied a non-Newtonian flow between reverse roll and negative gap mode. He exposed the influence of fluid viscoelasticity and the increasing of the

free surface stability in reverse mode. The viscoelastic fluid produces a thicker film than a high viscous Newtonian one. In fact, the viscoelasticity of fluid has a great importance for large meniscus. This type of meniscus is observed between rigid roll.

Finally, Zevallos [36] proposed a non-Newtonian fluid approach between rigid rolls in forward mode. The conclusions are closed to Tiu's ones. The viscoelasticity destabilizes the flow in forward mode and implies a low critical capillary number. The ribbing defect appears faster with non-newtonian fluid than with Newtonian fluid.

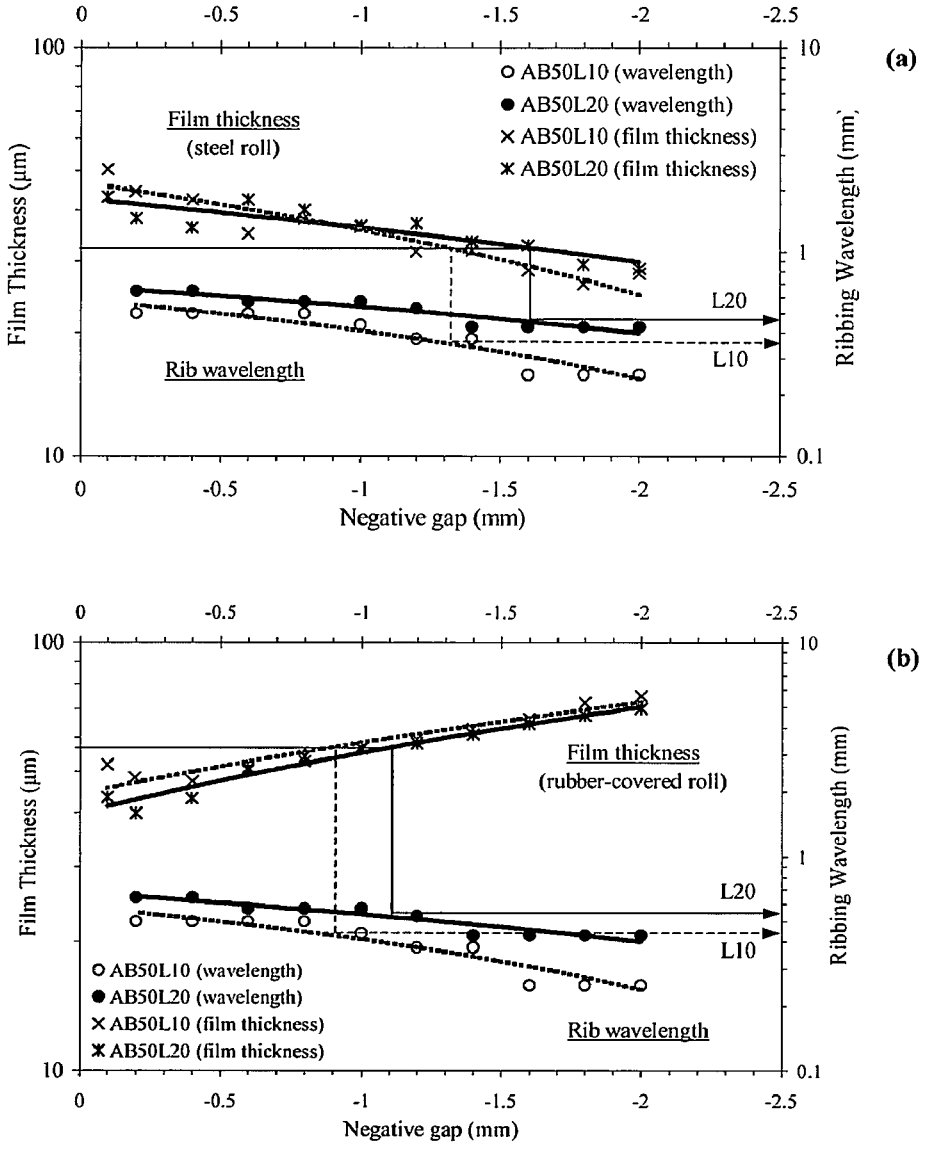

Figure 1-14: Film thickness and ribbing wavelength on the rigid roll (a) and deformable roll (b) [34]

3. Additional works

We reviewed the contact between two rolls in literature. Two authors investigated the contact between roll and strip. The two approaches are based on a numerical approach by finite elements.

Carvalho [27] proposed a finite element model to analyse the elastohydrodynamic of tensioned web roll coating process. He studied the angle and speed between roll and strip influence. The results showed an influence of these two parameters on the film stability.

Chandio [37] studied a similar contact between strip and roll with finite element modelling. His study showed the strip vibration occurrence in specific conditions and the influence on the fluid stability. A pressure is occurred between strip and roll as a function of the speed ratio between both. This is this pressure variation, which involves strip vibration and modification of the free surface position.

4. Thesis scope

In this study, the proposed approach is different from the above presented recent studies. It is based on the numerical simulation of an industrial roll-coater in order to be as representative as possible of the real contact conditions. The introduced parameters such as line speed, roll speeds, and loads between rolls come from the production line adjustments. The elastomer and resins used for the characterization of the behaviour laws are also taken on the production line. This methodology of work is mainly oriented to get a better optimisation of the process by numerical simulation and correlation with an industrial experimental roll coater. The final aim is to improve the quality and the productivity of the production line by a better roll coater mastering.

The study will be led in three steps. An experimental approach, a numerical analysis of the process with accurate behaviour laws and an optimisation transfer to the production line.

First, inline investigation permits to select many interesting configurations and materials to study the ribbing defect. After a testing stand selection, a complete experimental investigation is performed on industrial roll coater. The experimental results are analysed. It permits us to establish the key parameters on the roll coater efficiency.

From this experimental investigation, a numerical approach is proposed to understand the process. This numerical simulation of the process is based on a structure interaction on the fluid. The influence of the elastomeric roll cover on the flow rate and free surface position is proposed. We need elastomer and

paint behaviour law to feed the simulation. The elastomer is characterized by a specific cyclic test in industrial environment developed at the LAMIH. From this test, a complete identification methodology is used to define the behaviour law parameters. Prony series are used to model the elastomer behaviour in the numerical simulation. The paint is a simple Newtonian fluid model in the numerical simulation. The numerical results are correlated to the experimental ones.

Final step, a knowledge transfer to the production line will be performed. This transfer acts on the roll coater adjustment optimisation and operator understanding of the paint application with deformable rolls.

Chapter 2

Key parameters on roll coater efficiency

Introduction

To optimize the industrial deformable roll coating application, we need to analyze the ribbing defect and the key parameters acting on it. Experimental investigation is the best way to understand this phenomenon in a real environment and to fix the industrial roll coater limits. It will allow us to identify the key operating parameters to study. The operator experience brings knowledge on the inline parameters influence. The speed line is one of the most important parameter on the defect occurrence but not the only one. The operators adjust the roll speeds by a percentage of the line speed. For example, 101% of the line speed for the applicator roll and 30% of the line speed for the pick-up roll. In these conditions, the paint and roll cover behaviours are very different for a line speed increasing. There is no defect on the product for 60m.min-1 line speed and there is ribbing at 100m/min.

Chapter 1 described the process and especially the paint application. The usual approach for the LAMIH (Laboratoire d'Automatique, de Mécanique et d'Informatique industrielles et Humaines) would have been a complete testing stand development to reproduce the studied process [1], [2]. In our context, high speed, industrial coil coating paints and industrial solvents involve many safety problems. Moreover, a set of two testing stands is available in MYRIAD.

A criterion for the selection of the testing stand is first presented. The selected testing stand and the associated measurement equipment are first detailled. Finally, the complete set of experiments is performed. The main conclusion permits to highlight key parameters for industrial roll coater efficiency.

1. Definition of the criterion and testing stand selection

This part deals with the selection of the testing stands. Two testing stands are available to perform experimental investigations. As previously said the design of a specific prototype is impossible in the laboratory regards to the safety and environmental standards. To select the best testing stand between the different available possibilities, we define a selection criterion called "Cs". A simple ratio (G/T) characterizes this criterion. A good item (G) corresponds to the possible reproduction of a given industrial parameter on a testing stand. A total item (T) corresponds to the sum of available item. Table 2-1 sums-up the different parameters which are taken into account for the selection criterion.

Table 2-1: Parameters selected for the selection criterion, industrial line reference

Parameters	Reference: Industrial line
Dimensions	
Applicator diameter(mm)	210 to 270
Pick-up diameter(mm)	290
Roll width(mm)	1470 to 1680
Strip width(mm)	until 1504
Strip thickness(mm)	until 2mm
Speed	
Line(m/min)	100
Applicator(% of line speed)	200
Pick-up(% of line speed)	150
Other	
Curing	induction
Industrial paint	yes
Strip sample	yes
Using facility	no
Measurement equipment	
Load cell	Available
Ribbing evaluation by camera	-
Wet thickness measure	Available
Viscosity measure	Available
Criterion selection	
Good item	14
Total item	16
G/T	0,875

In fact, the best testing stand would be the industrial line. Of course, this possibility is not conceivable and the significant reason is the cost due to the lost of productivity involved by trial (lost of raw material and unproductivity for customers). The Cs computed for the reference line is 0.875.

In order to complete the above presentation, the two testing stands in relation with the industrial process are described. For each of them, the advantages and disadvantages are exposed and finally the selected experimental stand will be faced to the authors' approach.

- Industrial roll coater as a testing stand

The industrial process exploits up to four roll coaters during coating (Figure 2-1). It permits a fast colour changing. During roll coating, two roll coaters coat and two others are available. One of them will be used to perform trials. This testing stand is then a part of the production line. We define a work hypothesis to perform trials and face some production line problems. The ribbing defect appears between rolls and it must be reduced before the contact with the strip to optimize the coating and its levelling [38].Then, the contact with the strip and the induction curing are not considered in experiments. If an optimization is determined, it will be possible to connect the roll coater to the line. It permits an industrial coating with final product correlation and analysis.

With this industrial roll coater, all the industrial conditions are present to have a good view of the key parameters and to correlate the results with the future numerical simulations. The industrial parameters are coil coating paints (Table 2-2), elastomeric roll cover properties (Table 2-2), standard diameters (210mm until 270mm), gap imposed between rolls, real line speed (until 100m/min), temperature in the room, and line vibrations. This industrial environment ensures the good reproduction of the defects and especially of the ribbing or flow line defect.

Table 2-2: Designation, description and selected material for paint and elastomeric roll cover for this experimental study

Industrial coil coating paint family		
SP	**Polyester resin**	**BC,TC1,TC2**
PVDF	Polyvinylidiene fluoride	-
PVC	polyvinyl chloride	-
PU	Polyurethane	-
Industrial elastomeric roll cover		
PU	**Polyurethane**	PU
EPDM	Ethylen polyden diene	-
NI	Nitrile	-

In the same time, the industrial environment presents disadvantage and in particular the using facility problem. During the inline production, the selected roll coater usually applies the back coat paint as BC. We can use this roll coater between two planned products. The roll coater is available between 1 hour and 5 hours. During this time, we must clean the testing stand to start with our selected paint (BC, TC1, TC2), work out, perform the trial and still clean the roll

coater for the production needs. The contact parameters measurement is another difficulty. In fact, we measure the load between rolls by a load cell, the pick-up wet thickness by an eccentric roll, and the ribbing defect by a macrophotography. For each parameter modification, these three values must be measured in a minimum of time. All trials and therefore line speed depend on the production planning (paint, strip width and thickness). A simple modification for the lower problem in the production involves new parameters measurements. The control of the trial is much more difficult in this unfriendly environment than in a laboratory. The Cs computed for this testing stand is 0.63. In the final step of experiments, the experimental roll coater device is added to the line and Cs reaches 0.875 (Table 2-3).

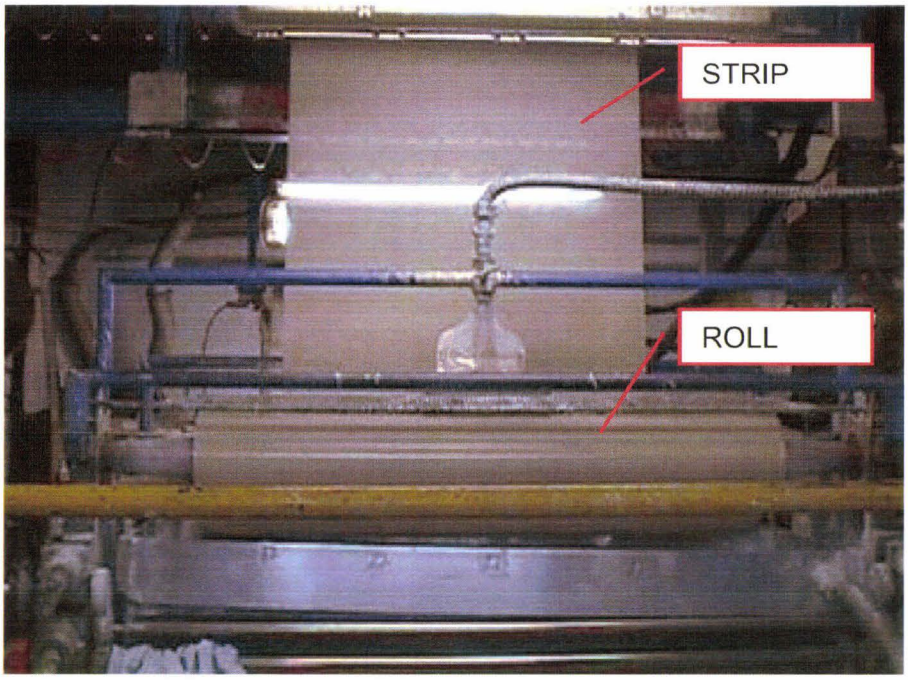

Figure 2-1: industrial roll coater

- MYRIAD "Research and development pilot line"

This reduced scale line is an accurate tool to reproduce the induction baking cycle of the coil coating paint. "MYRIAD" uses this line to validate the new paint composition for the curing problem like the boiling. This line is a good tool for this kind of study, because we have a lot of time to work out and perform trials. Specific roll coater adjustments allow the ribbing defect occurrence but no correlations with the industrial line are possible. There are three rolls like the production line and the same materials for elastomeric roll cover properties (PU) and paints (SP, PU, PVDF, PVC). The roll diameters are 40% smaller than the production line (167mm until 185mm) and one fifth smaller width (295mm). The baking apparatus is an induction oven. Table 2-3 describes the roll coater dimensions. However, an important disadvantage exists. The line and rolls

speed are very low. The maximum line speed is about 20m/min. It is five to six times slower than the real line speed. In these conditions, dynamic behaviour of the fluid is not the same. In theory, a fluid similarity approach can be done to reproduce the defect.

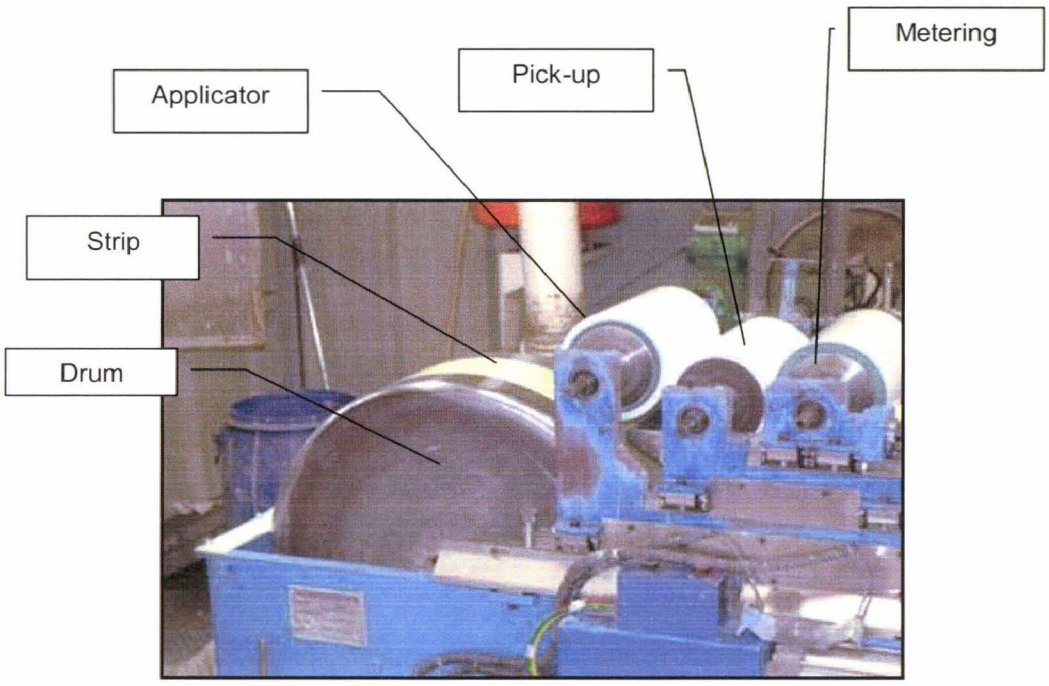

Figure 2-2: R&D Pilot line roll coater

The strategy to obtain the same dimensionless number defined by the capillary number and the Reynolds number, between the real process and the pilot line is a fluid properties modification. This modification involves many problems for the baking cycle because the solvent quantity in the paint is not the same.

Figure 2-2 presents the roll coater of the pilot line. The Cs computed for this testing stand is 0.375 (Table 2-3). Table 2-3 sums-up the two possibilities for the experimental investigation with the associated criterion of selection. The testing stand selected for the experimental investigation is the industrial roll coater. The Cs is greater than the Myriad R&D pilot line and the speed is too important in the defect reproduction to be neglected.

Table 2-3: Testing stand parameters and associated selection criterion

Parameters	Reference: Industrial line	Roll coater device	R&D pilot line
Dimensions			
Applicator diameter(mm)	210 to 270	210 to 270	167 to 185
Pick-up diameter(mm)	290	290	180
Roll width(mm)	1470 to 1680	1470 to 1680	295
Strip width(mm)	until 1504	No strip*	140
Strip thickness(mm)	until 2mm	No strip*	until 2mm
Speed			
Line(m/min)	100	100	21
Applicator(% of line speed)	200	200	200
Pick-up(% of line speed)	150	150	150
Other			
Curing	induction	no*	induction
Industrial paint	yes	yes	yes but modified
Strip sample	yes	no*	yes
Using facility	no	no	yes
Measurement equipment			
Load cell	Available	Available	To buy
Ribbing evaluation by camera	-	To buy	To buy
Wet thickness measure	Available	Available	Available
Viscosity measure	Available	Available	Available
Criterion selection			
Good item	14	10	6
Total item	16	16	16
G/T	0,875	**0,63**	0,375
*During trial, but possibility to perform an industrial application			

To complete the presentation of the testing stands a review of the authors 'experimental approach is exposed. Cohu [28] uses an industrial roll coater. In his configuration, a big drum is used to simulate the contact with the strip but no real coatings are performed during trials. Cohu measures the wet thickness by eccentric roll and scraping. The scrapping method permits measurements on the deformable roll. In his experimental investigations, the ribbing defect was slightly studied. The final product is evaluated by a roughness measurement on dry product for the paint used in his trials. The result of his investigation is a power law to establish the wet thickness as a function of the roll coater parameters with an accuracy of 25% compared to his industrial measurements. Jones [39] and Chong [34] use a complete laboratory-testing stand with a contact between deformable and rigid rolls but their testing stand has no baking cycle and thus no final product comparison. The disadvantage for Jones and Chong is the miss of connection with a real process. Many authors have performed experimental approaches to determine wet thickness power law as a function of the contact parameters [40], [32], [24]. In reality, each process has a particular power law for a range of parameters.

The selected experimental device is the industrial roll coater. The measurement equipment to evaluate the wet thickness and ribbing defect wavelength will be detailed in the following part.

2. Industrial roll coater as experimental device : measurement strategy

The aim of this paragraph is to detail the measurement equipment used during our trials to evaluate wet thickness and ribbing defect wavelength. The adjustment parameters (paint viscosity, speed, geometry and load between rolls) have been already presented. The Figure 2-3 presents the industrial roll coater and the measurement equipments.

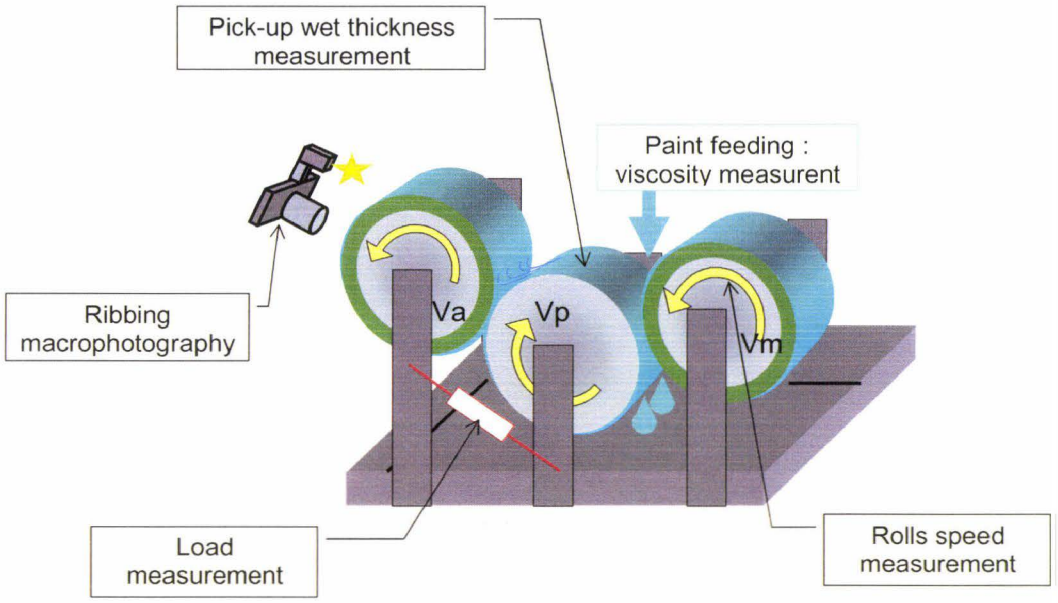

Figure 2-3: experimental roll coater and measured parameters

2.1 External load between deformable and rigid roll

The external load is a function of the roll diameter, paint viscosity, and elastomeric roll cover properties. The operator modifies the position between rolls to act on the wet thickness. This position displacement corresponds to a load response. Two load cells are placed between the applicator roll and the pick-up roll in order to measure the load response during trial. The load measurement is parallel to the rolls axis to have a direct value of the imposed load. Figure 2-4 precises the load cell position. The maximum accepted load is 20KN by load cell with 4% error on the instantaneous measurement. A load cell is placed on each side of the roll coater. The zero of the load cell is obtained when the two rolls are just in contact. As soon as the pick-up roll position is modified, the pressure on the fixed load cell increases or decreases. The continuous value of the load cannot be monitored on this device. One single value is recorded by configuration. The load measurement is in N/m in this

study to have a universal reference. In fact, the roll length is variable in Myriad and this experimental investigation is based on one specific roll length. Numerical simulation evaluates the correspondence between gap and load. The method will be detailed in the numerical chapter of the work.

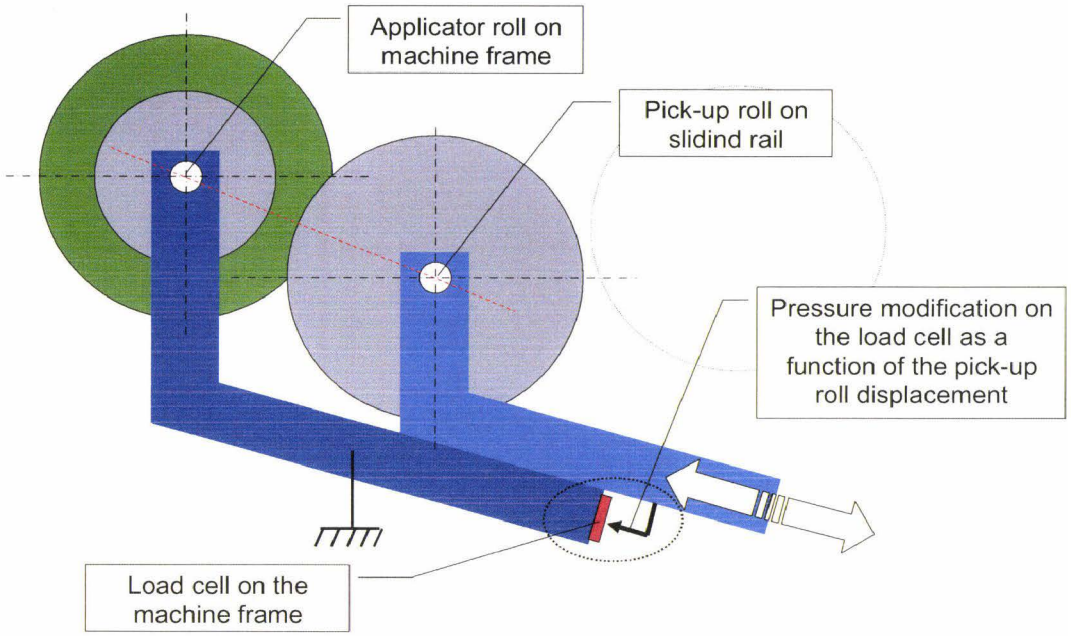

Figure 2-4: load cell position focus on the roll coater

2.2 Pick-up wet thickness

The operator adjust the roll coater with the pick-up wet thickness to reach the targeted final product thickness. He uses an eccentric roll to measure the wet thickness on the pick-up roll and we will use the same technique in our trials. Figure 2-5 illustrates the eccentric roll. It permits a fast wet thickness measurement but the reliability is not very good. The accuracy is around 5% for a 100µm total scale. The accuracy is a function of the operator, and paint viscosity. This technique is not reproducible for the deformable roll due to the elastic strain. The scrapping method used by authors [28],[34] is not conceivable to face this problem. This method is based on the paint weight measurement for a given time interval. This methodology requires too much time and manipulation to be performed in the available time of the trial.

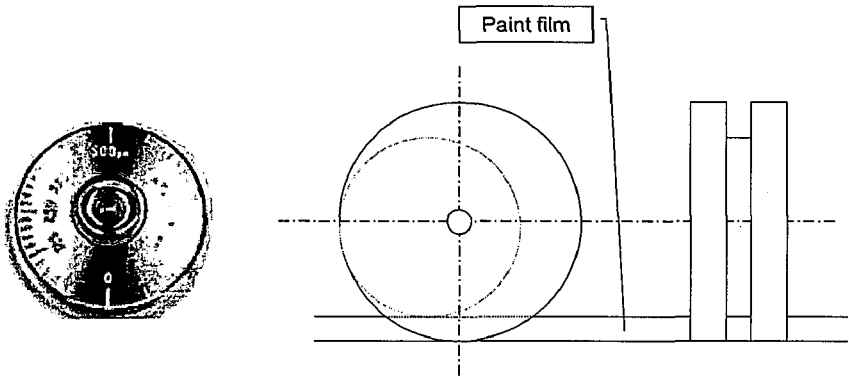

Figure 2-5: Pick-up wet thickness measurement with eccentric roll

2.3 Ribbing wavelength

In order to evaluate ribbing in their experimental investigation, Pearson [18], Pitts [19], Mill & South [20], Adachi [32], and Benkreira [12] use a photography based strategy. To evaluate the rib wavelength in our trials we use a macrophotography coupled with an image analysis processing. The digital camera is a "Nikon D70" with a 6.1 Millions Pixels resolution sense. The lens is a "Sigma" f3.2/50mm macro. A macrophotography of the ribbing defect on the applicator roll is carried out for each parameter modification. In our case, the database will be around 450 macrophotography for the ribbing defect. A specific image analysis tool has been developed to automatically process the data and evaluate the ribbing wavelength. Figure 2-6 explains the methodology.

First, we need a reference scale macrophotography (A). The program processes this macrophotography to evaluate the number of pixel corresponding to 1mm length. Then, the program processes the complete database of the ribbing defect macrophotography. This tool is based on a "Dériche filter". This filter uses grey levels photography. It highlights the grey variations in the horizontal and vertical direction. The ribbing defect is composed of vertical lines. Then, the horizontal filter is selected for the analysis. From the original macrophotography (B), the horizontal "Dériche filter" evaluates the contour of each rib. A binary search allows rib number evaluation (C) and the associated profile. The ribbing wavelength is computed with the rib number and the reference scale. The result is a rib wavelength associated with each macrophotography database (D).

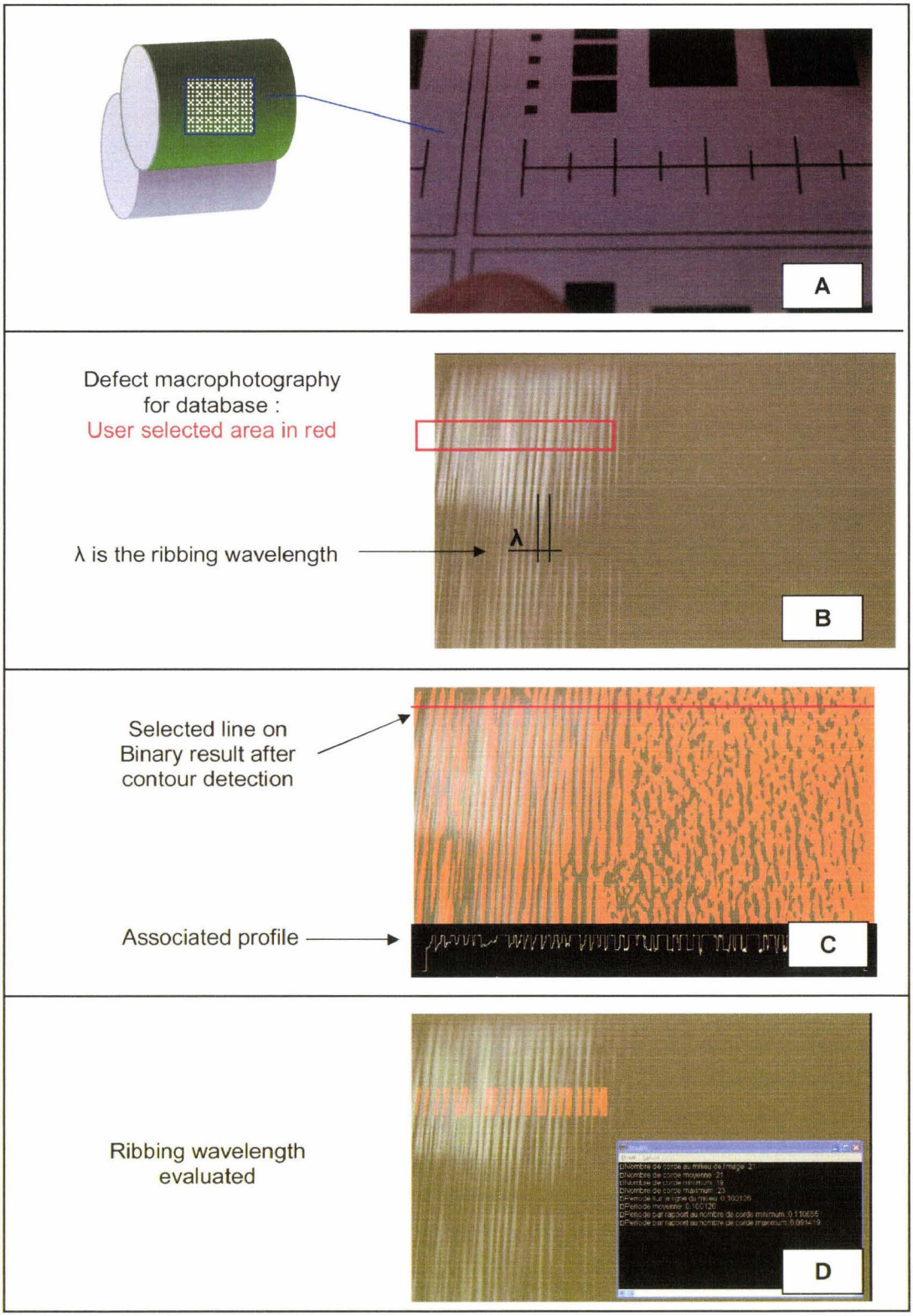

Figure 2-6: Ribbing wavelength evaluation methodology

2.4 Viscosity and temperature

The inline viscosity is measured by a standard cup(Figure 2-7). A given amount of paint flows through a 4mm diameter hole. The time to empty the cup can be linked to the paint viscosity. It is a simple inline method to evaluate the viscosity. The viscosity in "seconds" is used inline. In our case, the dynamic viscosity is needed. We use a correponding table to perform the conversion. The paint density in "kg/m^3"and the time in "seconds" permits to evaluate the dynamic viscosity in "Pa.s". We use three paints in our experimental investigation. The polyester resin family is selected because it represents an important part of the industrial production. The three studied paints are a backcoat called BC, and two white polyester top coats TC1 and TC2. Table 2-4 sums-up the paint designation and viscosity. In a near future, shear flow and elongational rheometer will be used to have an accurate viscosity measurement in relation with the inline solicitation.

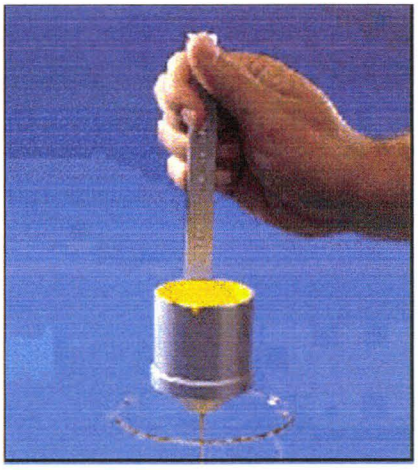

Figure 2-7: Standard cup for viscosity measurement

Table 2-4: Paints designations and properties

Designation	BC	TC1	TC2
Description	Polyester Backcoat	Polyester Topcoat	Polyester Topcoat
Inline viscosity (s)	105	105	95
inline target wet film (µm)	17	40	45
Dynamic viscosity (Pa.s)	0,51	0,51	0,59
Surface Tension (N/m)	0,035	0,035	0,035

The measurement strategy associated to the experimental roll coater has been exposed. In the next part, the research of key parameters on roll coater efficiency is presented.

3. Key parameters on roll coater efficiency : experimental measurements

The basis of the experimental investigation consists in the standard operating adjustments. Inline operators can act on two important parameters to target the good wet thickness. These two parameters are gap between rolls and speed ratio between rolls. For each selected top coat paint (TC1 and TC2), a standard adjustment is performed. The speed ratio is 0.3 with an applicator roll speed at 101% of the line speed and pick-up roll speed at 30% of the line speed. The gap corresponds to a load of 6867N/m. The gap remains the same for the two top coats since the rolls diameters and the elastomeric cover do not change during trials. For the two topcoat paints, the corresponding pick-up wet thickness is in the range [35-38µm]. From this first operator adjustment, extrapolations of the speed and load parameter around their corresponding reference values define the trials adjustments. Input data for experiments represent 150 configurations by paint (roll coater adjustment). The total number of wet thickness and ribbing wavelength measurement is around 450. The reference adjustment is based on the topcoat because it gives an added value to the product. The backcoat has no decorative use.

In order to complete the experimental overview, Table 2-5 sums-up the parameters and range. Concerning the geometrical parameters, the applicator roll diameter "Da" is 265mm and its associated elastomeric cover thickness "b" is 37.5mm. The elastomeric roll cover is polyurethane with high mechanical and chemical resistance. The polyurethane characteristics will be exposed in chapter 3. The pick-up roll diameter "Dp" is 290mm. Roll diameters are considered constant during trials. There is no contact between the applicator roll and the strip, then, the strip vibrations are not taken into account. The line speed during trials is a function of the inline production. The three trials are performed for a line speed "Ls" between 77 and 85m/min. A percentage of the line speed defines the peripheral speed of roll. The applicator roll speed "Va" is between 101% and 120% of the line speed, and the given pick-up roll speed "Vp" between 20% and 60% of the line speed. The speed ratio "S" is going from 0.16 to 0.6 for our trials. "S" is defined by equation (**2-1)** as follows :

$$S = \frac{Vp}{Va} \qquad (2\text{-}1)$$

Finally, the external load "W" is in the range [2866-16866N/m]. It corresponds to the imposed gap. Parameters range and materials used for trials are summed in Table 2-5.

Table 2-5: Experimental parameters and range

Parameters	Range	Unity	Material
Line speed, **Ls**	77-85	m/min	-
External load, $\mathbf{W_i}$	2866-16866	N/m	-
Applicator roll diameter, **Da**	265	mm	Polyurethane
Applicator roll cover thickness, **b**	37,5	mm	Polyurethane
Roll cover hardness	50	Shore A	-
Pick-up roll diameter, **Dp**	290	mm	Steel
Applicator roll speed, **Va**	101-120	% of Ls	-
Pick-up roll speed, **Vp**	20-60	% of Ls	-
Speed ratio = Vp/Va , **S**	0,16-0,6	-	-
Fluid cup viscosity at T=20°C, **μ**	0,51-0,59	Pa.s	Polyester resins

3.1 Analysis of the load influence

The first parameter studied is the external load imposed between the deformable applicator roll and the rigid pick-up roll. From now on, low load case (WL) and high load case (WH) will respectively correspond to 6867N/m and 16866N/m. Inline, to modify the wet thickness, the operator modifies the gap between these two rolls. This gap modification corresponds to a load variation due to the viscoelasticity of the applicator roll cover. The external load has a direct influence on the pick-up wet thickness (Figure 2-8) and applicator ribbing wavelength (Figure 2-10). This influence has been studied in our trials and will be discussed later.

3.1.1 Load influence on the wet thickness

Figure 2-8 shows the pick-up wet thickness evolution as a function of the imposed external load between the applicator roll and the pick-up roll. The measured wet thickness on the rigid pick-up roll is in the range [15-95μm] for WL and [10-38μm] for WH. In fact, for each load case, speed ratio variation is performed between 0.16 and 0.6. This speed ratio variation explains the range of wet thickness for a given load. For each load case, when the speed ratio "S" increases the pick-up wet thickness increases.

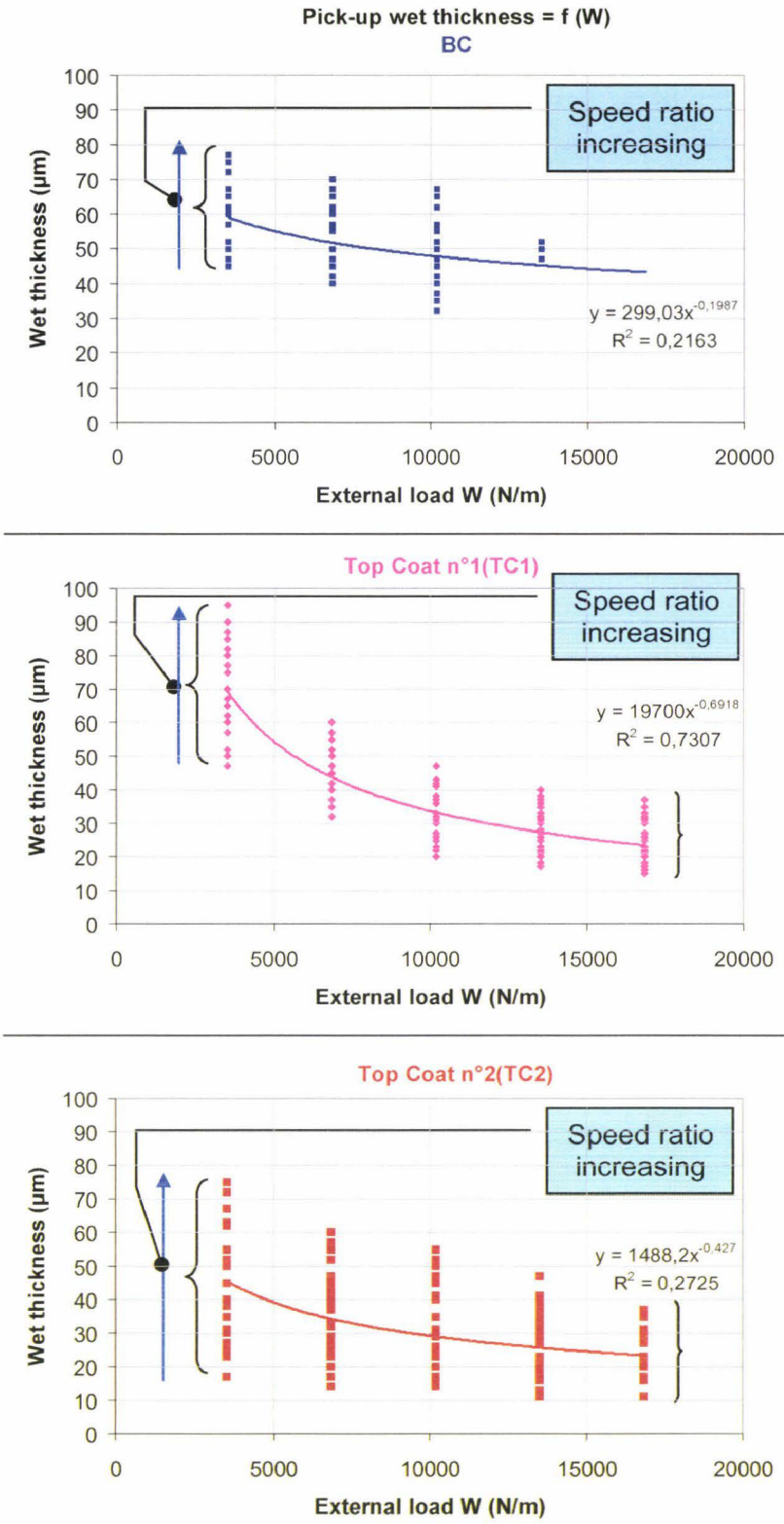

Figure 2-8: Pick-up roll wet thickness as a function of the imposed external load between rolls, three paints: BC, TC1 and TC2

The curves have the same tendency for TC2 and BC. They correspond to experimental data for a 75m/min line speed. In the case of TC1, the experimental line speed was 85m/min. For TC1 a faster wet thickness decreasing is observed than for TC2 and BC. These three curves are given to have a global tendency and we can see a bad determination coefficient (around 20% for BC and TC2). Nevertheless, a global tendency of the load influence on the pick-up wet thickness can be observed. The paint behaviour sensitivity to the line speed is highlighted.

Figure 2-9, presents the wet thickness for four speed couples. In the case of BC for its two last speed couple, Vp equals to 40% contrary to TC1 and TC2 where Vp=50%. A given speed ratio can be obtained for different speed couples. The goal is to highlight the separate speed influence on the wet thickness. This diagram underlines first the influence of the imposed external load on the pick-up wet thickness. It shows that the speed ratio has a direct influence on the wet thickness. As for an example, we study the curves corresponding to Va = 101% - Vp = 30% and Va = 101% - Vp = 50% for TC1 and TC2. These curves (◊ ♦) have the same tendency with a power law exponent of -0.9. A least square fitting gives a coefficient of correlation around 98%. The pick-up speed difference of 20% leads to an average offset between the two curves. This offset is 20µm for TC1 and 16µm for TC2. The BC paint is less sensitive with an offset of 11µm, but Vp = 40% of the line speed. When the external load between the two rolls increases, the wet thickness offset decreases. The pick-up roll speed influence on the wet thickness decreases with the external load increasing.

The deformable roll wet thickness is not measured in our trials. Elastomeric roll cover effect has an importance on the deformable wet thickness. For higher load case, CHONG [34] shows an increasing of the deformable wet thickness when the pick-up wet thickness decreases or reaches a limit. The elastomeric roll cover has an increasing influence on the wet thickness for the higher load cases just when the speed ratio influence decreases. The goal in this part is to obtain a power law to predict the wet thickness on the rolls as a function of the different parameters of the roll coater. Neverthless, each process has a particular power law, and it seems difficult to obtain a global law for all the roll coater.

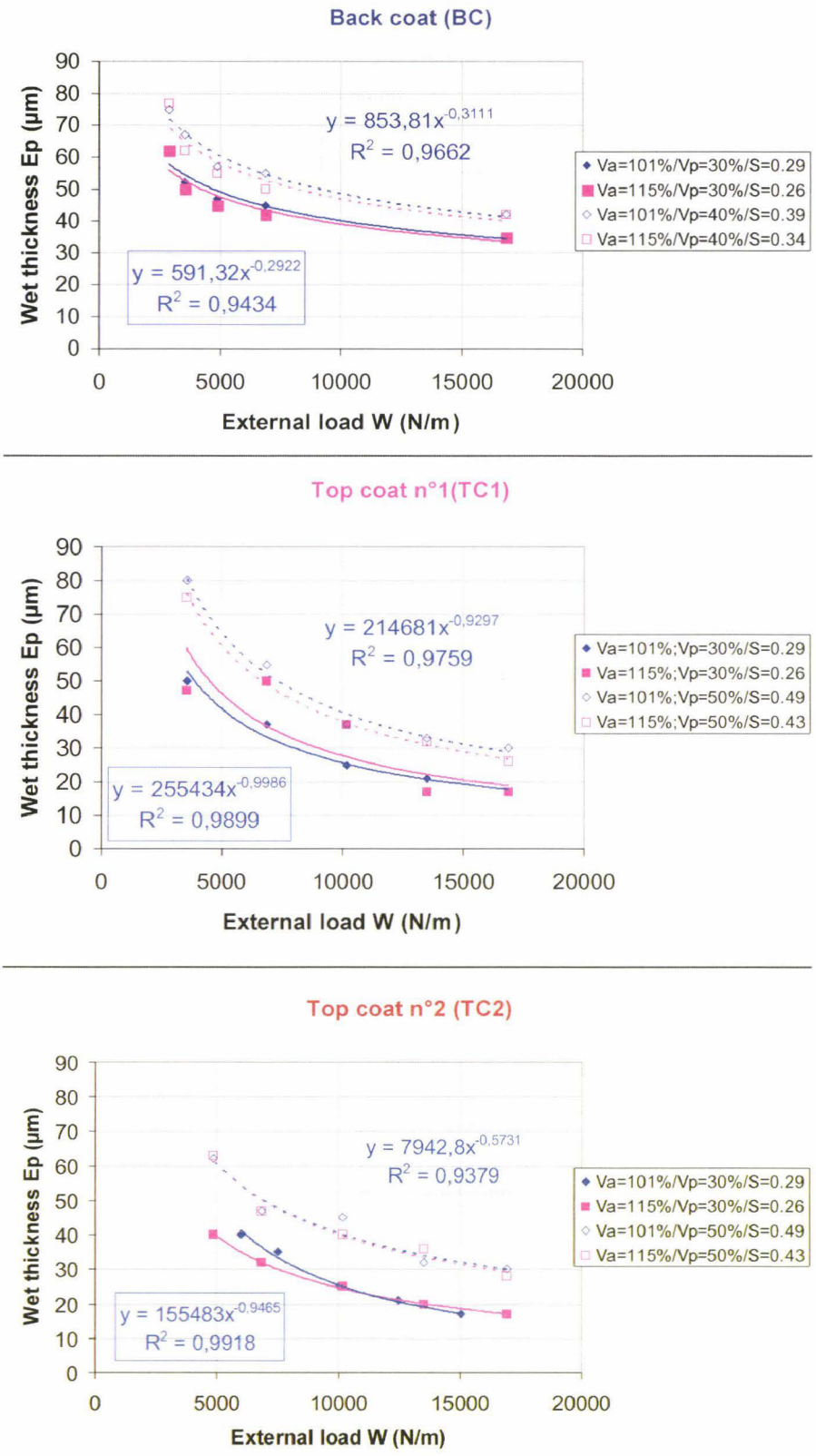

Figure 2-9: Pick-up roll wet thickness as a function of the imposed external load between rolls, four speed couples, three paints BC, TC1 and TC2

We have seen the influence of the imposed external load between rolls on the wet thickness, but it also acts on the ribbing wavelength. It is the object of the next point.

3.1.2 Load influence on the ribbing wavelength

The imposed external load has an influence on the ribbing wavelength. Figure 2-10 shows this influence. In this diagram, a mean ribbing wavelength with a standard deviation is computed for each load case. A low influence of the speed ratio on the ribbing wavelength has been observed. The least square method used to build the curves gives a good correlation coefficient between 95% and 99%. The global analysis shows that the ribbing wavelength decreases when the load increases for the three paints. The ribbing wavelength is between 1,2mm and 2,4mm. On one hand, the minimum ribbing wavelength is obtained for TC1 polyester top coat and the higher external load. On the other hand, the maximum ribbing wavelength is obtained for BC polyester back coat and the lower load. The general phenomenon is a ribbing wavelength decreasing with the increasing of the external load.

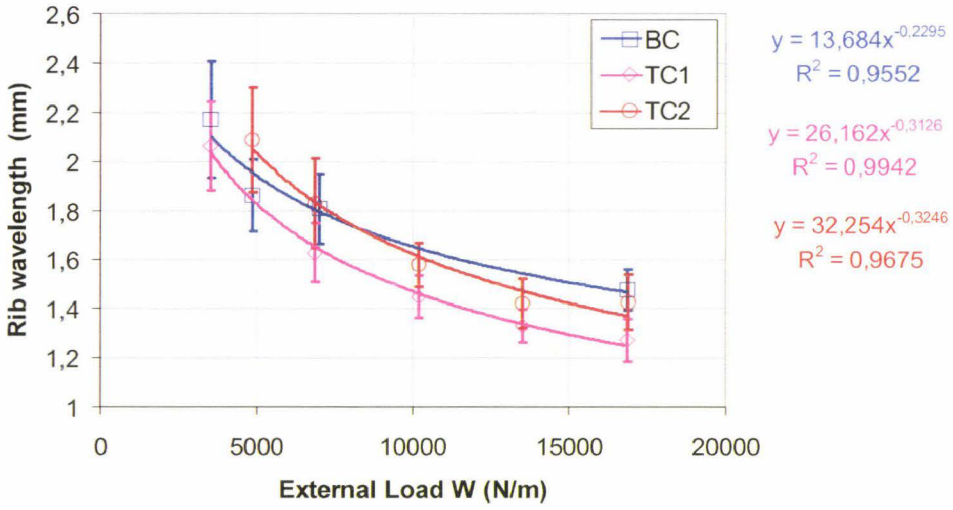

Figure 2-10: Applicator ribbing wavelength as a function of the imposed external load between rolls for the three paints BC, TC1 and TC2

Power law permits a good approximation of the load influence. For TC1 and TC2, a negative exponent of 0.3 defines the load influence on the ribbing wavelength. For BC, it is a negative exponent of 0.2, but its behaviour is different due to chemical resin composition. These three paints give global tendency of the external load influence on the ribbing wavelength. We have seen a difference of 1mm between WL and WH on the ribbing wavelength. This variation is very important for the levelling of the micrometric wet film of paint.

To have a better understanding of the load influence on the ribbing wavelength, Figure 2-11 illustrates the phenomenon. Two cases are presented and defined as follows: a lower load case corresponding to a small negative gap between rolls and a higher load case corresponding to an important negative gap. The lower load involves a long ribbing wavelength with high meniscus of fluid between rolls. The results after the application on the strip is a long period defect λ with high amplitude. Anyway, the higher load case involves a small period defect λ with small amplitude. For this example, a defect measurement has been realised on the final baked product to compare with the wet defect photography.

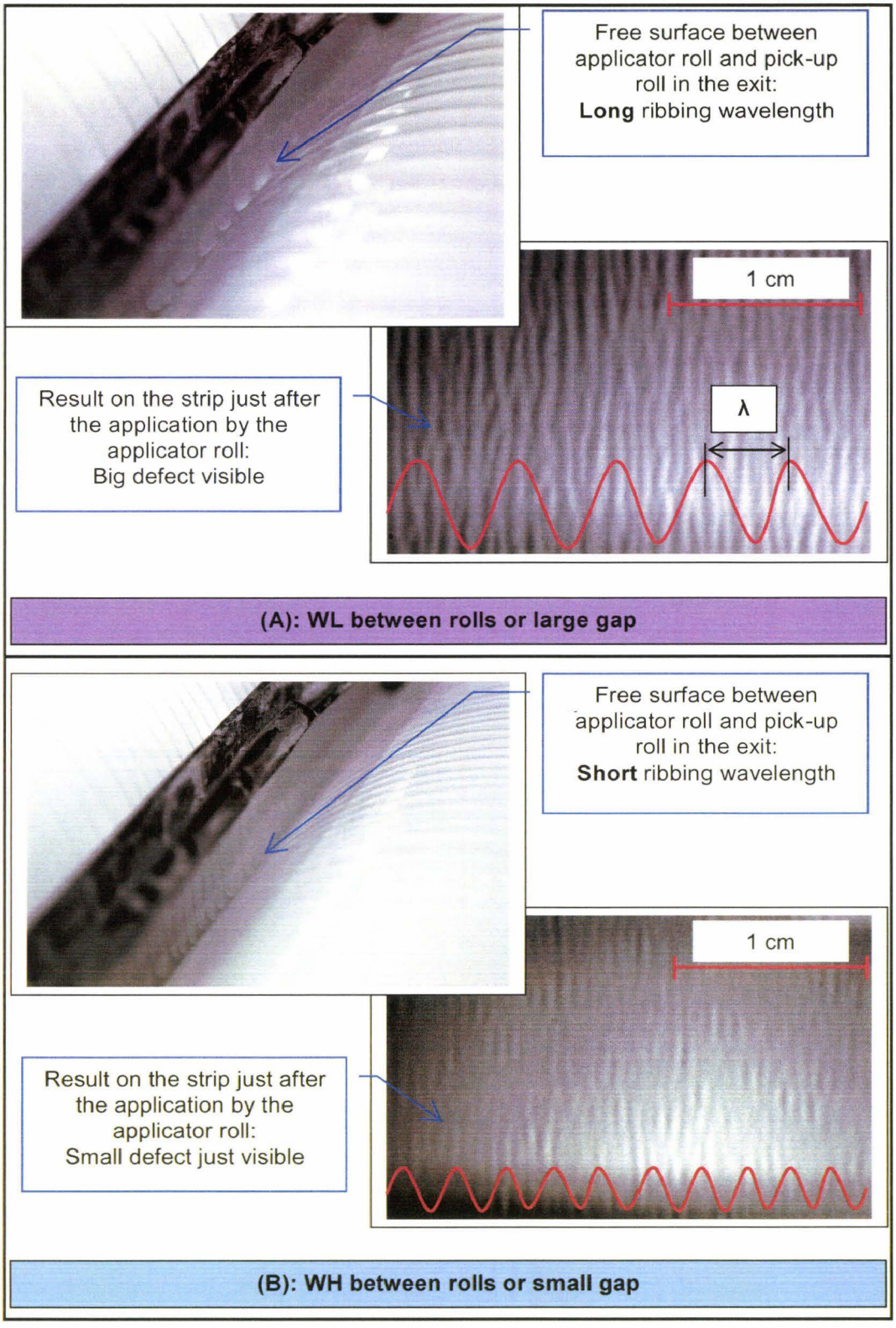

Figure 2-11: Photography of the load influence on the ribbing wavelength on the industrial roll coater

The dry measurement has been performed with a profilometer (Figure 2-12). This last one measures the wavelength and amplitude defect on the dry product.

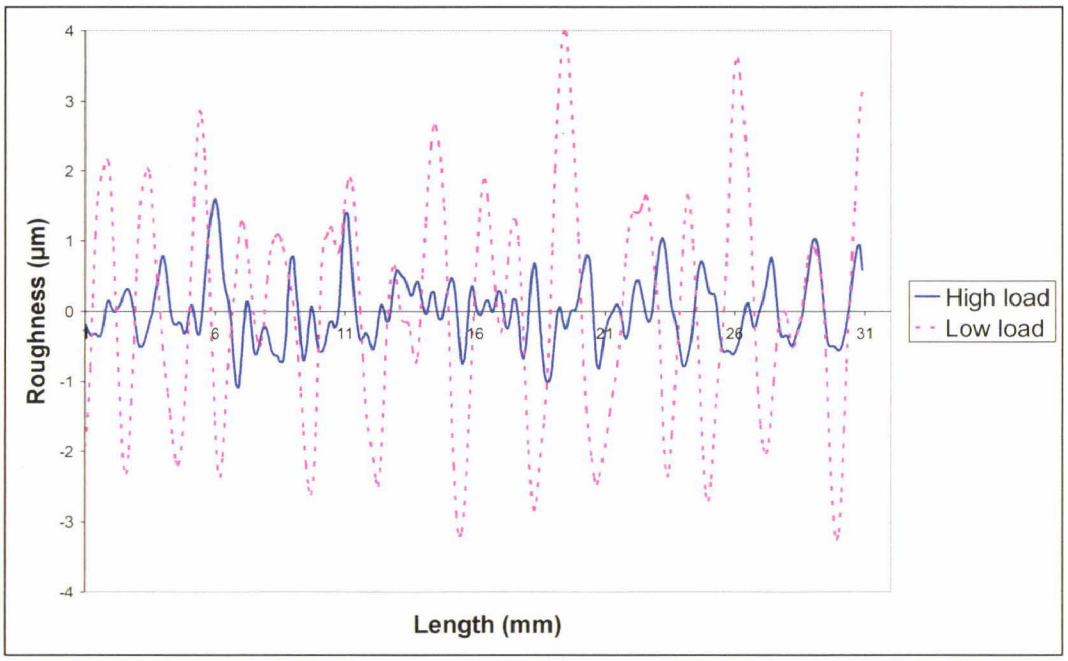

Figure 2-12: Roughness measurement with the profilometer on the dry product

The wet ribbing wavelength is compared to the dry ribbing wavelength in Table 2-6. We can see in the wet case, a smaller ribbing wavelength in the high load case than in the low one. When, we compare the dry ribbing wavelength and wet ribbing wavelength, the results have the same tendency. Concerning the dry ribbing amplitude, the difference is much more important with 4.24µm for WL and 1.41 for WH. A smaller wet ribbing wavelength involves a smaller wet amplitude. The levelling before curing is better [38] and the final product has a better surface aspect. The higher load case seems to give the better final product quality (Figure 2-11). A smaller wet wavelength and amplitude will be the goal to increase the quality inline (Table 2-6).

Table 2-6: Applicator ribbing wavelength and dry amplitude as a function of the external imposed load for the three paints

	Wet ribbing wavelength λ (mm)	Dry ribbing wavelength (mm)	Dry ribbing amplitude (µm)
Lower load case	1,97	2,41	4,24
Higher load case	1,45	2,2	1,41

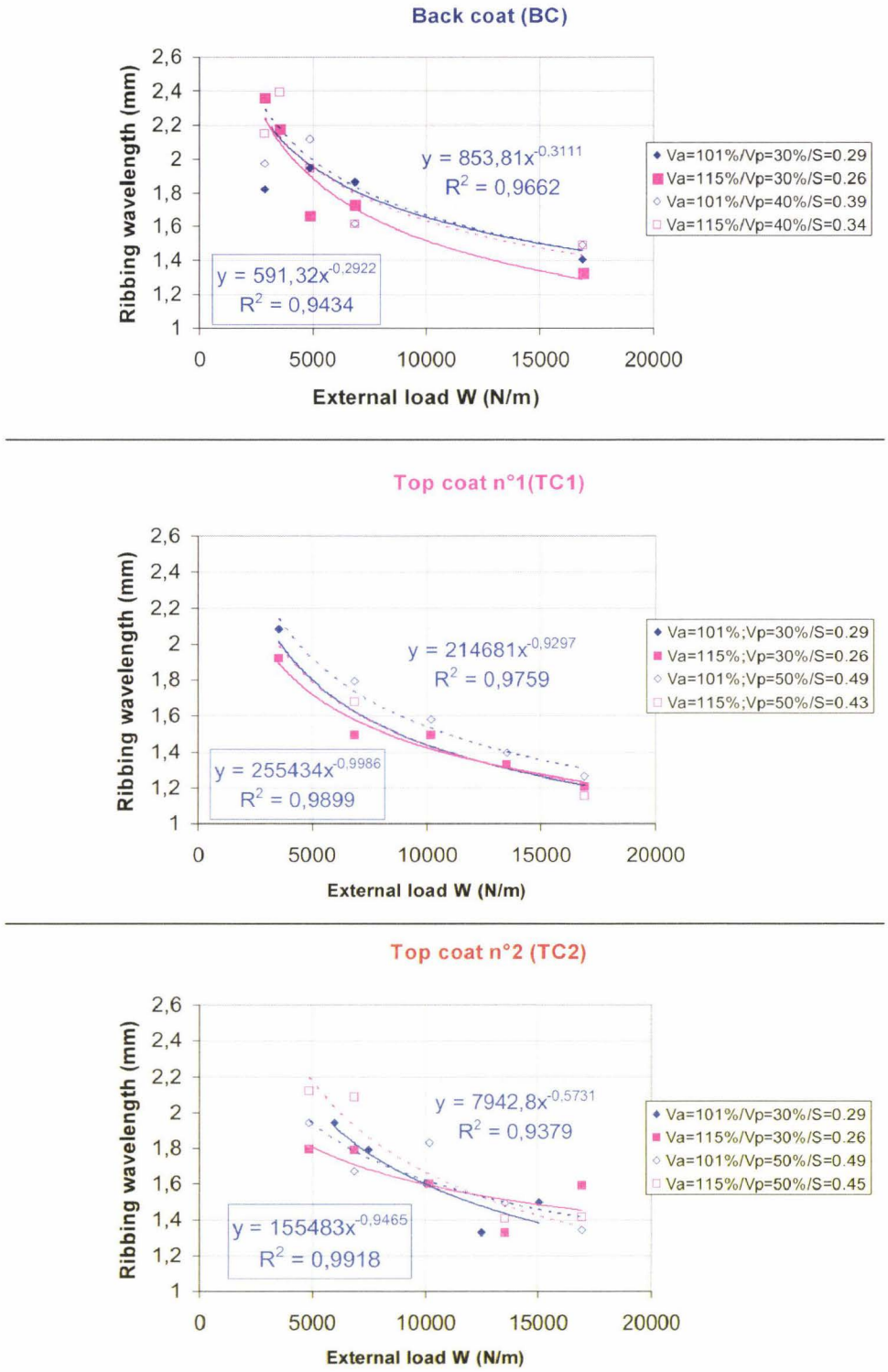

Figure 2-13: Applicator ribbing wavelength as a function of the external load four speed couples, Three paints: BC, TC1 and TC2

In order to complete the external load influence on the ribbing wavelength, Figure 2-13 shows the load influence on the ribbing wavelength for different speed couples.

The speed influence for these four speed couples on the ribbing wavelength is found to be small. The respective coefficient of correlation for Va = 101% - Vp = 30 % and Va = 101% - Vp = 50% are 98% and 97%. An offset around 0.2mm is observed between the two curves. This offset is constant from WL case to WH case. From these results, the speed of the pick-up roll has less influence on the ribbing wavelength. A first conclusion could be at this stage: the minimisation of the ribbing defect will occur when the load between rolls will be higher and when the pick-up roll speed will be lower. This conclusion leads to the loss of wet thickness when the imposed external load increases with the decreasing of the pick-up roll speed. To understand this phenomenon the next paragraph analyses the roll speed influence on the pick-up wet thickness and the applicator ribbing wavelength.

3.2 Rolls speeds influence

3.2.1 Rolls speeds influence on the pick-up wet thickness

The Figure 2-14 shows the speed ratio influence on the pick-up wet thickness. The speed ratio is ranging from 0.25 to 0.6. For each paint (BC, TC1 and TC2), the lower load case (WL) and the higher load case (WH) are presented. The general observation is an increasing of the pick-up roll wet thickness with the speed ratio. A power law is in good agreement with the experimental points. The coefficient of correlation is between 91% for BC and 97% for TC1. Between TC1 and TC2, no differences are observed in the wet thickness. The power laws are the same for the given load case. A wet thickness difference is noted with BC. The smallest wet thickness is 32µm for BC with WH and a little speed ratio S. The pick-up thickness for TC1, TC2 is around 16µm for the same adjustment. The wet thickness for top coat is thinner for a given external load and speed ratio than the back coat (Table 2-7).

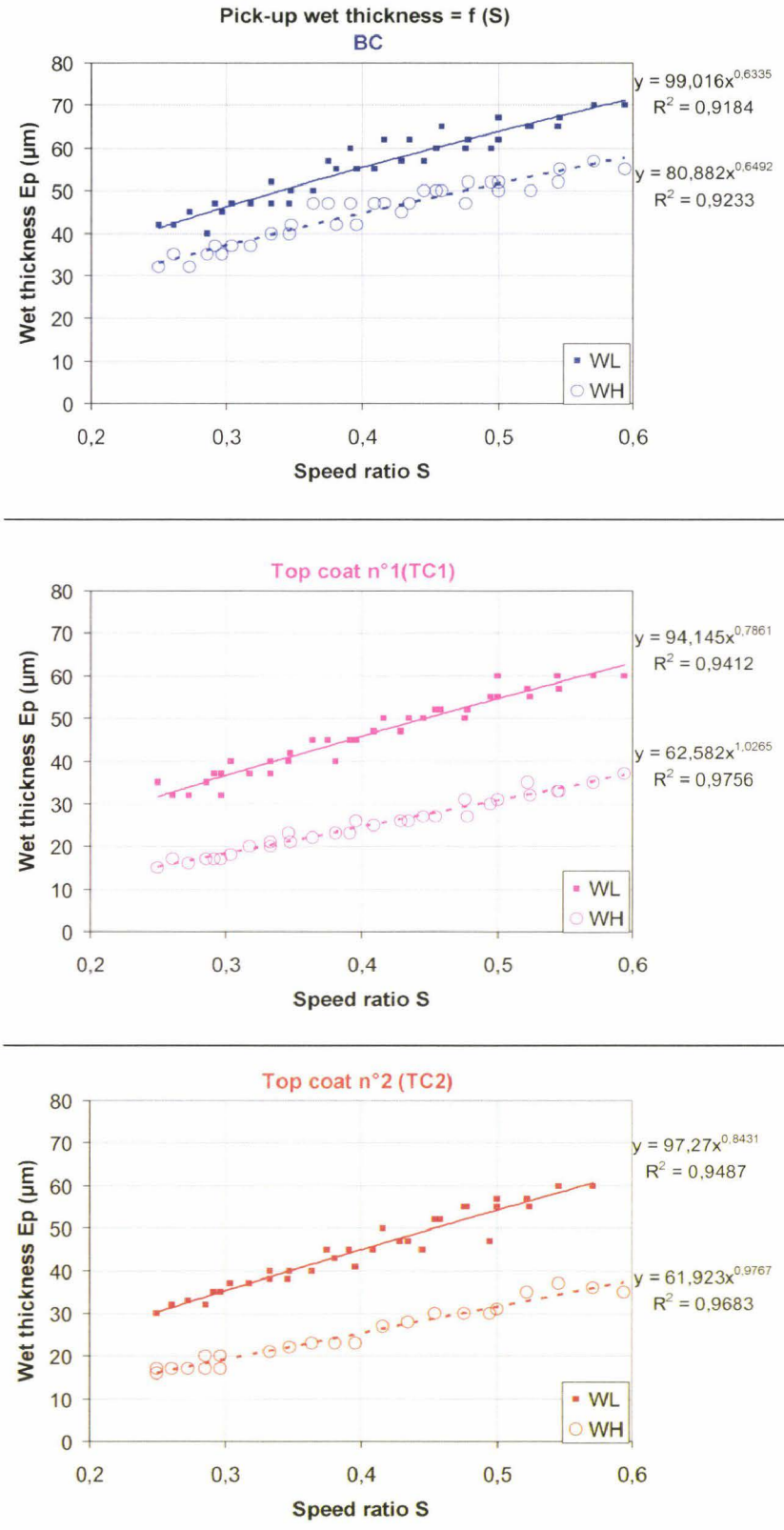

Figure 2-14: Pick-up wet thickness as a function of the speed ratio between rolls for a low load and a high load

Table 2-7: Wet thickness comparison for S=0,35 and S=0,55 and for two load WL and WH

S=0,35	Low load WL	High load WH
Polyester back coat: BC	50 µm	40µm
Polyester top coat: TC1	40µm	22µm
Polyester top coat: TC2	38µm	22µm
S=0,55	**Low load WL**	**High load WH**
Polyester back coat: BC	68µm	55µm
Polyester top coat: TC1	58µm	35µm
Polyester top coat: TC2	58µm	35µm

The difference between back coat and top coat wet thickness can be explained by the paint composition difference and by its reaction with the elastomeric roll cover. In general, authors consider the fluid by a simple viscosity [28], [24], [41], [32], [25], [21], [14], [15], [12], corresponding to the Newtonian plate for a high shear rate. Between the applicator roll and the pick-up roll, the shear rate is high and is between 10^4 and 10^6 s^{-1}. Shear rate $\dot{\gamma}$ is a gradient of velocity and defined by equation (2-2) as follows:

$$\dot{\gamma} = \frac{\partial Vx}{\partial x} = \frac{Vx}{x} \qquad (2\text{-}2)$$

In our case, the study is exclusively based on polyester resins and the paint is considered Newtonian. Myriad uses PE, PVC, PU and PVDF resins.

The speed ratio influence and in particular the roll speeds influence on the wet thickness will be an important parameter to master the roll coater. Figure 2-15 details the speed couple (Va – Vp) for BC, TC1 and TC2. Each box presents the wet thickness evolution as a function of the pick-up roll speed Vp for a corresponding constant applicator roll speed Va. In the four boxes, the pick-up wet thickness increases with the pick-up roll speed. The wet thickness is between 16µm and 57µm for WH case and between 32µm and 70µm for WL case. The greatest thicknesses are obtained for the back coat for the same load.

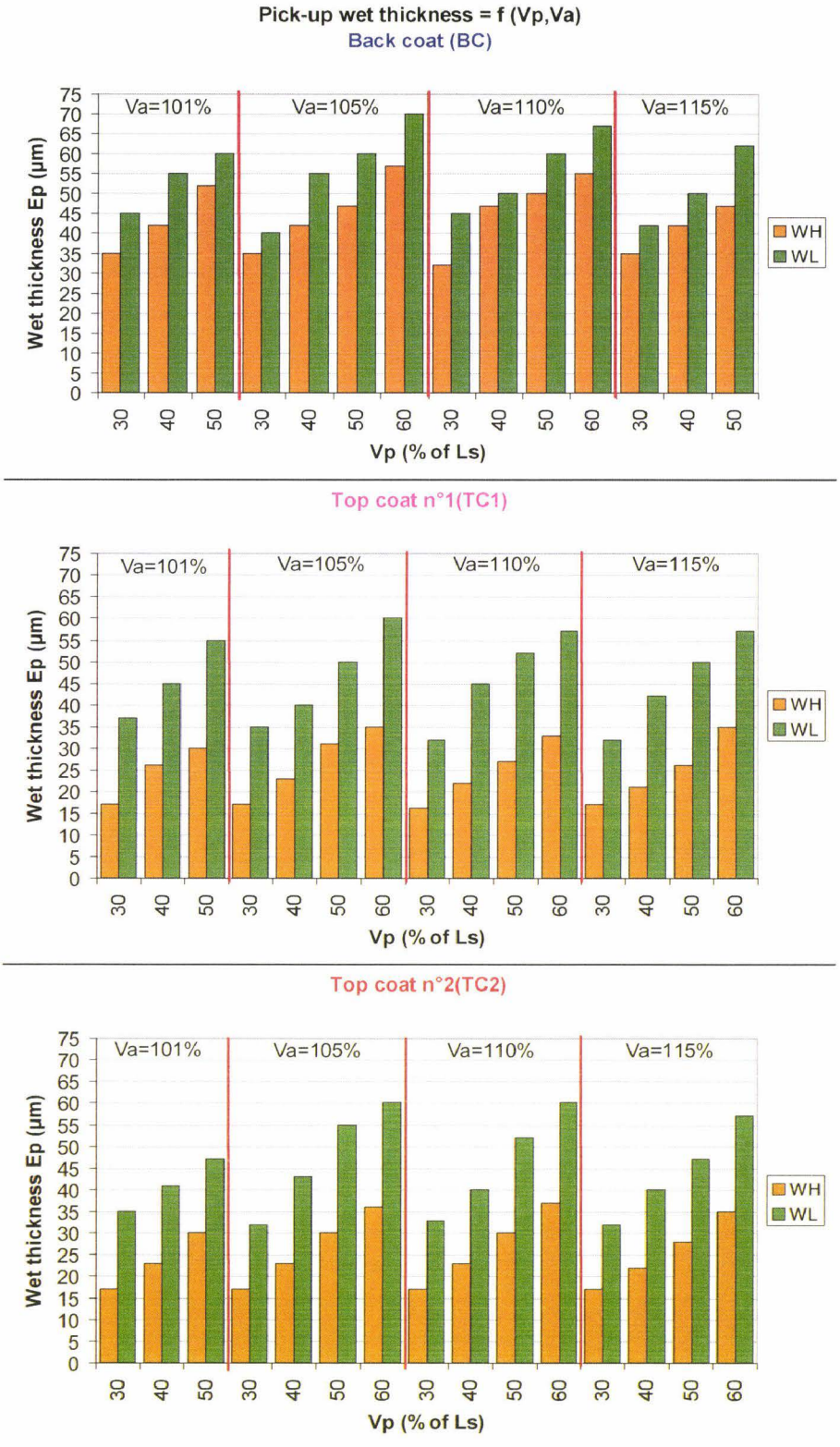

Figure 2-15: Wet thickness as a function of the roll speed couples, two load cases, three paints : BC, TC1 and TC2

An offset on the wet thickness is observed between the lower load case WL and the higher load case WH. For standard line adjustment Va = 101% - Vp = 30%, the offset is around 10µm for BC, 20µm for TC1 and 18µm for TC2. For Va = 101% - Vp= 50%, the offset is around 8µm for BC, 25µm for TC1 and 17µm for TC2. The roll speed affects the pick-up wet thickness evolution but the offset seems to be constant when external load decreases. A mean offset δ with a standard deviation σ are computed for the three paints. Table 2-8 sums-up the results.

Table 2-8: Wet thickness offset between WL and WH,

Three paints: BC, TC1 and TC2

	Mean offset δ	Standard deviation σ
BC	10,07	3,26
TC1	20,92	3,59
TC2	19,35	3,13

We can obtain the same pick-up wet thickness for many configurations of the roll coater but the increase of imposed external load decreases the range and the sensibility of the adjustment.

3.2.2 Rolls speeds influence on the ribbing wavelength

Figure 2-16 shows the rolls speeds influence on the ribbing defect. The ribbing wavelength is evaluated for two external loads WL and WH. The applicator roll speeds are between 101% and 115% of the line speed. The pick-up roll speed is ranging from 20% to 60% of the line speed. From these results it is not possible to extract an objective conclusion. For the three tested paints, the curves are very scattered and no accurate fitting is possible. The applied external load gives an initial ribbing wavelength. The ribbing wavelength has a stochastic evolution with speed. The minimum ribbing wavelength is 1.15mm for TC1 and WH. The maximum ribbing wavelength is 2.20mm for BC and WL. Table 2-9 sum-up the mean ribbing wavelengths "mrw" and standard deviation "σ" for each case.

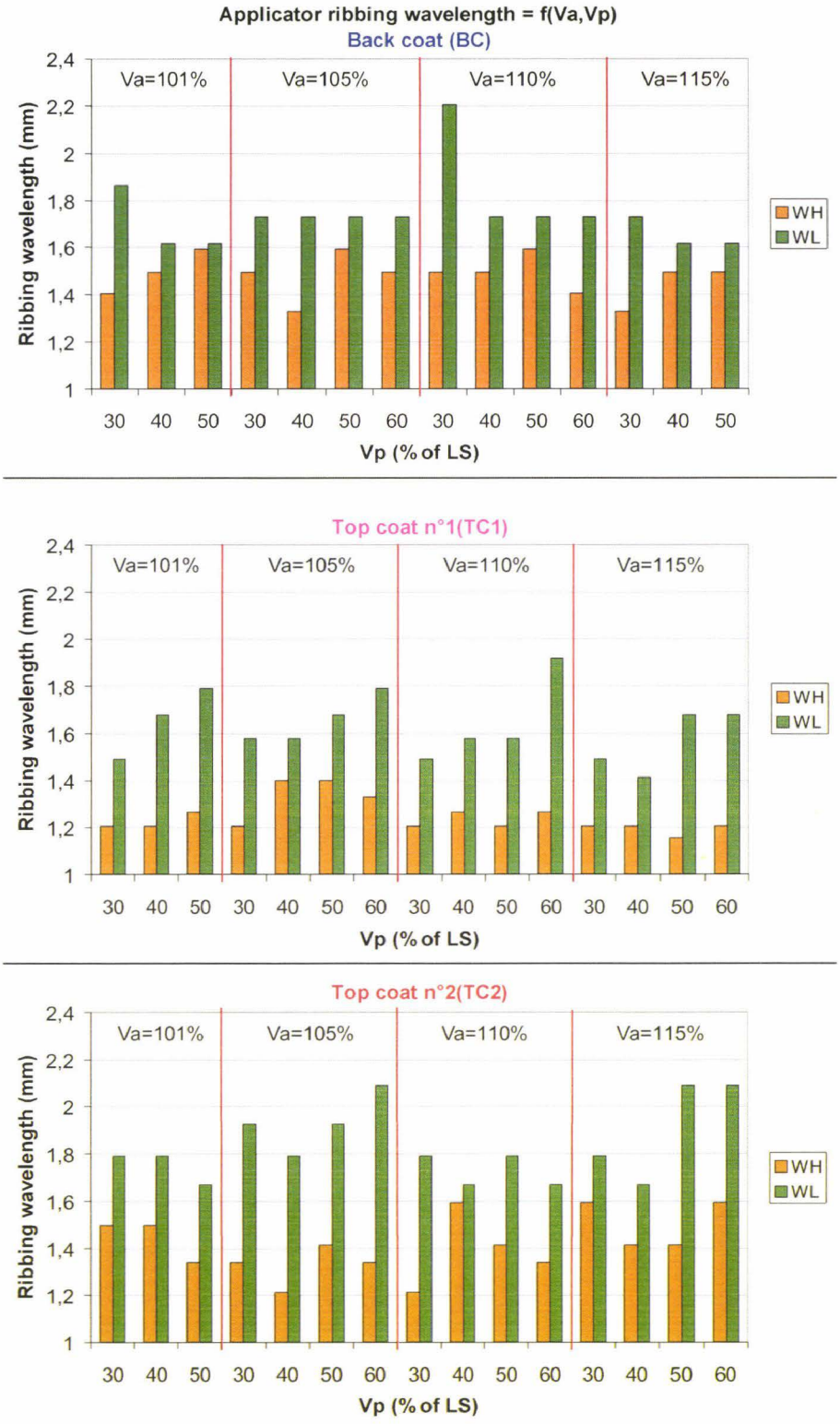

Figure 2-16: Ribbing wavelength as a function of rolls speeds,

Two load cases, three paints: BC, TC1 and TC2

Table 2-9: Mean ribbing wavelength with standard deviation,

Two load cases, three paints: BC, TC1, TC2

		WH	WL
BC	mrw (mm)	1,47	1,74
	σ	0,08	0,14
TC1	mrw (mm)	1,24	1,63
	σ	0,07	0,13
TC2	mrw (mm)	1,41	1,83
	σ	0,12	0,15

The mean ribbing wavelength is ranging from 1,24mm to 1,47mm for the high external load. It is ranging from 1,63mm to 1,83mm for the low external load. The minimum ribbing wavelength for WL is bigger than the maximum ribbing wavelength for WH. Rolls speeds have a low influence on the ribbing defect wavelength for each tested paint. The most important parameter acting on the wavelength is the imposed external load between rolls. For a given external load, it is possible to establish a ribbing wavelength border between high load and low load. A value of 1,54mm seems to be correct. Ribbing wavelength never exceeds this value for WH. It is difficult to establish a link between the roll speed and the ribbing wavelength with regards to the external load influence.

We have seen that the external load has an influence on the wet thickness and on the ribbing wavelength. In the same time, we have seen that the speed ratio has a great influence on the pick-up wet thickness, but not on the ribbing wavelength. That remains to be checked because Carvalho [29] have seen a ribbing wavelength decreasing when the roll speed increases. To complete this experimental investigation, a coupled approach of these parameters is proposed in the next part.

3.3 Coupled parameters

Figure 2-17 presents the ribbing wavelength as a function of the scalar product: speed ratio S by applied load W. The ribbing wavelength measurement and display are not very accurate for the small ribbing wavelength variation. It is sufficient to evaluate the ribbing wavelength for a comparison between a high load and a low load. Two distinct areas are visible. A vertical area is on the left for WL and a horizontal one is on the right for WH. The ribbing wavelength is between 1.4mm and 2.3mm for WL and between 1.1mm and 1.6mm for WH. The increasing of the external load decreases the ribbing wavelength range. For the low and high load cases, many set-ups give a ribbing wavelength lower than 1.5mm. To highlight the aim of an external load increasing, Table 2-10 presents the percentage of the ribbing wavelength less than 1,5mm for the low load case and the high load case. This criterion is a good value to obtain a good quality

product. In Table 2-6 we have seen the final dry product for a given wet application.

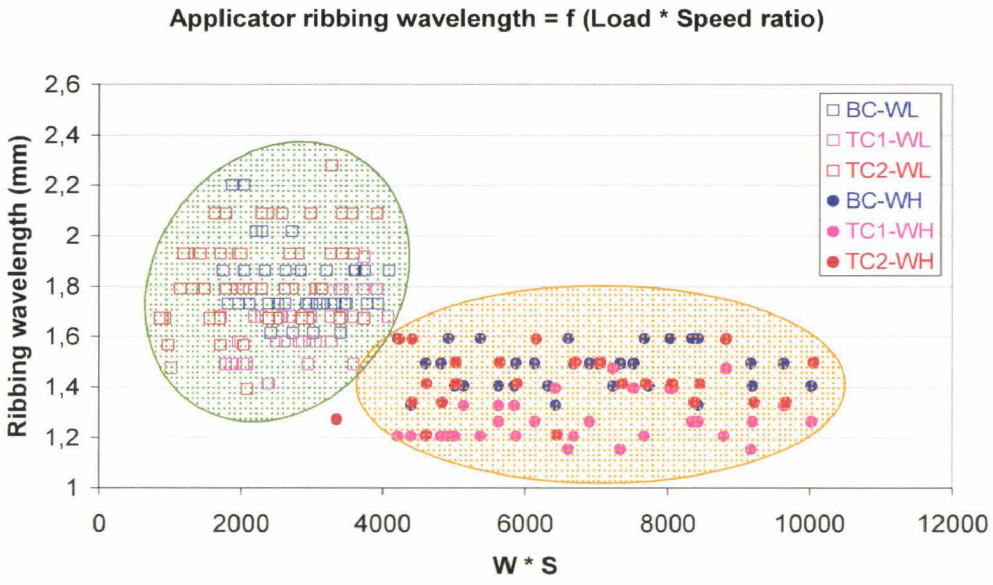

Figure 2-17: Ribbing wavelength as a function of the scalar product of (External load * speed ratio)

The dry ribbing wavelength and corresponding amplitude are smaller for the high load case. The wet ribbing wavelengths are less than 1.5mm in this case.

Table 2-10: Number of measurements and associated percentage to the total with a ribbing wavelength less than 1.5mm, two load cases

	WL	WH
	Total by load	
TC2	33	26
TC1	36	31
BC	35	34
	104	**91**
	Number for λ<1,5mm	
TC2	2	22
TC1	3	31
BC	0	25
	5	**78**
	% by colour	
TC2	6,06	84,62
TC1	8,33	100,00
BC	0,00	73,53
	% total	
	4,81	**85,71**

For the low load case, the total population is 104 ribbing wavelength values. Only 4.81% of this population has a ribbing wavelength less or equal to the quality criterion. For the high load case, the total population is 91 ribbing wavelength and 85.71% of this population has a ribbing wavelength smaller than the quality criterion.

Figure 2-18 shows the wet thickness as a function of the speed ratio S by the scalar product of the applied load W. This diagram approach makes obvious the decrease of the wet thickness interval with the increasing of the external load. The wet thickness is in the range [15µm, 70µm] for WL and [10µm, 58µm] for WH. The slope of the three curves decreases when (W*S) increases.

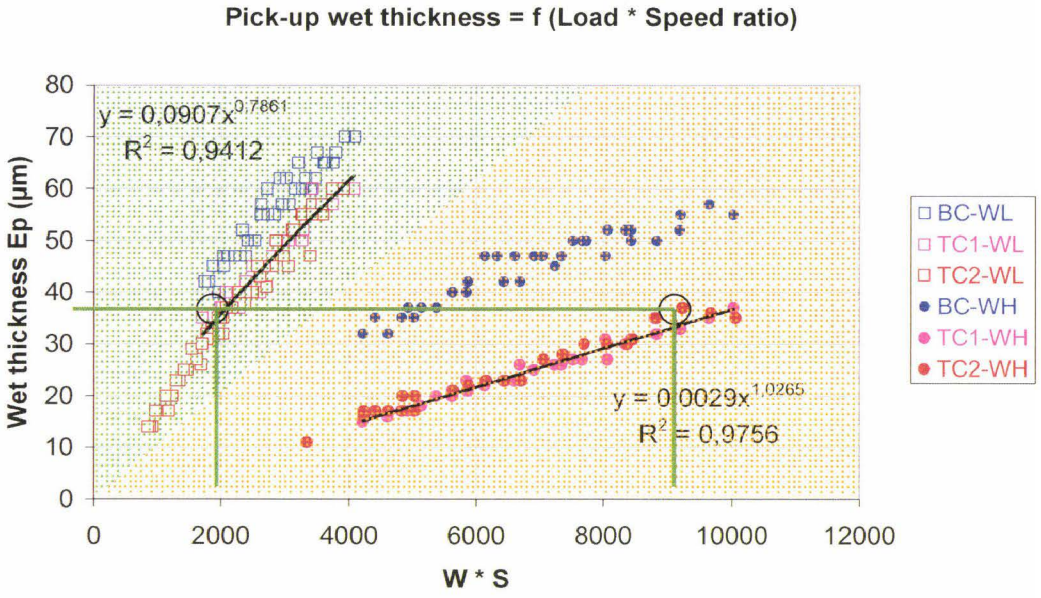

Figure 2-18: Ribbing wavelength as function of the scalar product (External load * speed ratio)

The standard pick-up wet thickness for polyester top coats is around 35µm. Usual inline adjustment gives a (W*S) of 2000 to obtain this thickness. In our trials, the ribbing defect is reduced for high load case. This (W*S) of 9000 gives the same thickness with a smaller defect. The roll speed adjustment is going from 0.2 to 0.6. For the top coat, the wet thickness variation is reduced to 28µm for WH, when it was 46µm for WL. The wet thickness adjustment by speed ratio decreases when the external load increases. The elastomeric roll cover will have a dominant influence on the wet thickness adjustment for the high load case. The goal of these two diagrams presentation is to highlight the external load influence on the ribbing wavelength decreasing. The link with the speed ratio to compensate the loss of wet thickness has been already shown.

4. Conclusion

Trough these different results, we have established the influence of the external load and speed ratio between rolls on the pick-up wet thickness and applicator ribbing wavelength. The key parameter to reduce the ribbing defect is the external load imposed between rolls. The increasing of the external load between the pick-up roll and the deformable roll permits to decrease the ribbing wavelength and amplitude of the defect. In the same time, the gap reduction involves a decreasing of the flow rate between rolls and a loss of applied wet thickness. The first way to face this problem would be a modification of the speed ratio between rolls. This operation permits a little adjustment range and reaches a limit as a function of the external load. The other way to increase the range of the speed ratio is a work on the materials and especially on the elastomeric roll cover. The behaviour of this material is varying during life because the paint environments are different and its thickness is decreasing with surface finishing. These two coupled parameters acting with the line speed effect, the pressure and the geometry in the gap involve a wet thickness and ribbing modification.

Currently the operator imposes a roll speed and modifies the negative gap between roll to have a good wet thickness. These work techniques are based on the experiment of the production plant people. It implies a modification of the ribbing wavelength for each negative gap modification. The roll coater is not mastered to improve the application quality and to limit the starting waste. The waste is due to the time of roll coater adjustment. The knowledge on the gap dynamic will help us to reduce these quality and adjustment problems.

The tool that will help us to understand the deformable roll coating process is the finite element simulation coupled with a material analysis and identification. The finite element approach permits a complete and accurate understanding on the physical mechanisms in the studied contact. The elastomeric roll cover will be analysed in laboratory by a specific technique developed at the LAMIH. The goal is an understanding of its behaviour to the speed influence and paint environment. Behaviour law identification will feed the numerical simulation to analyse its influence on the flow rate. We have seen the experimental load influence on the ribbing defect and the limit of speed ratio compensation on the wet thickness. With the numerical simulation, it will be easy to study the influence of each parameter, speed, load, elastomeric cover properties, on the flow rate. This understanding of parameters influence will bring information on the best roll coater adjustment to use. Moreover, the relation with the ribbing wavelength will be established from numerical simulation and experimental data. The final goal is to obtain many abacuses to facilitate the operators' adjustment as a function of the roll coater characteristics. On one hand to

decrease the time of roll coater adjustment and on the other hand to improve the quality of the final product.

Chapter 3

Numerical strategy for wet thickness and free surface prediction

1. Outline

In the experimental part, the flow between the applicator roll and the pick-up roll has been studied in negative gap mode. The result highlights the key parameters on roll coater efficiency. The knowledge of key parameters leads us to an optimisation of the application in real industrial conditions. A good mastering of the contact parameters facilitates this optimisation. Knowledge on key parameters influence on the contact dynamic is essential to optimise the industrial roll coater adjustments. These parameters are the imposed external load (i.e., the gap) and the speed ratio between rolls: an increase of the negative gap decreases the ribbing wavelength. The idea is to use the numerical simulation to analyze these phenomena and increase their understanding. Moreover, the implementation of a predictive plan of the coil coating can become an essential tool to reduce the adjustment time for a new paint application. A fluid solid interaction (FSI) computation plan seems an interesting way to do it. A review of existing commercial codes has been performed taking into account the free surface management. The selected code showed some limits in the management of the elastomer behaviour (no viscous behaviour consideration of the elastomer). For these reasons and some problems of convergence due to the very low thickness of fluid, the computation of parameters is divided in two parts:

1) Computation of the mechanical stress in the gap with a large deformation solver dedicated to solid mechanics.

This predictive plan is built with the solid impact on the fluid flows. First, we perform a F.E.M simulation of the deformable contact between applicator and pick-up roll without fluid between both. The viscoelasticity of the elastomer gets modified with the inline chemical environment. In the industrial process the used coil coating paints are very different in composition to obtain different colors and mechanical properties. Modifications of the Young Modulus and relaxation time of the elastomer are observed for different environments.

The elastomer behaviour is modelled by a Prony series. The parameters of this behaviour law come from a new identification methodology. A specific cyclic compression test has been developed to reproduce inline solicitation. The results of the numerical simulation are mechanical pressures in the contact as a

function of the behaviour laws, geometries of the contact and deformable layer thicknesses. The mechanical pressure will be used as boundary condition in the fluid simulation.

2) Computation of the parameters of the paint (meniscus, free surface) with a solver dedicated to fluid mechanics.

The fluid dynamic simulation is performed with a F.E.M free surface code. The used fluid model is Newtonian. There is no deformable part but the imposed mechanical pressure reproduces the elastomer influence on the flow rate. The different results are the free surface position and wet thicknesses as a function of the different elastomer behaviour laws, speeds rolls and viscosity. The free surface position can be directly associated with the ribbing wavelength. Compared to previous published studies, the presented work will take into account the elastomer cover behaviour used in industrial environments.

Figure 3-1 illustrates the strategic position of the F.E.M simulation in the complete study. This chapter deals with the part inside the red dash point box. The global view links the numerical simulations, experimental investigation and industrial process.

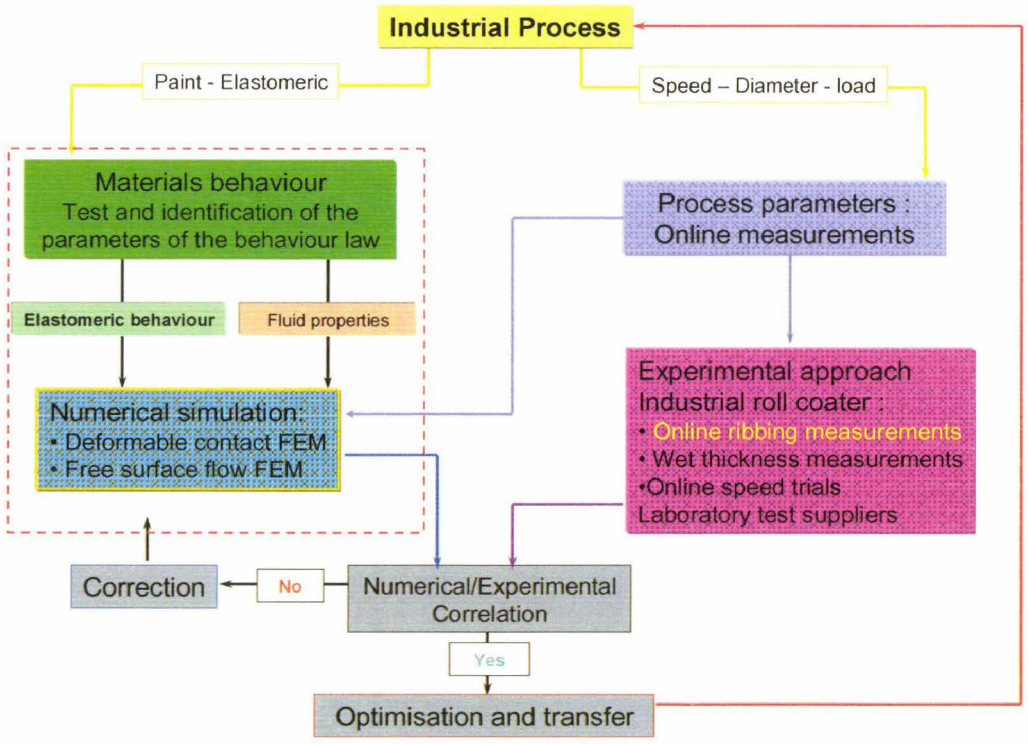

Figure 3-1: Numerical simulation coupling diagram

In the chapter 2, we have studied the industrial process by an experimental approach. The goal was to obtain a complete database with roll coater

parameters and associated ribbing macrophotography. From the result of the numerical chapter, a correlation in term of external load is performed. This load comparison allows a linking between numerical simulations and experimental measurements. A correction will be performed in the numerical simulation to obtain a good correlation if it is necessary. After that, from the obtained results in this chapter and in with the experimental approach, a transfer on the industrial roll coater will propose an optimisation of the roll coater adjustment.

The next paragraph deals with the methodology used to determine elastomer behaviour law. This behaviour law will feed the deformable contact finite element simulations.

2. Elastomeric roll cover behaviour law

This part is devoted to the determination of an accurate behaviour law for the elastomeric applicator roll cover. During the application, the elastomer undergoes cyclic compression followed by relaxation phenomenon and dips in different paints including solvent. To study the behaviour of this elastomer, a cyclic compression test with a specific device has been chosen in order to reproduce the exact process phenomenon at the same frequency, amplitude and with a solvent bath. From the cyclic compression test results, a rheological model is established. The generalized Maxwell model has been developed since it permits a simple fitting of the experimental results. When the Maxwell model is established, an analytical computation is performed to obtain the Prony series parameters. The Prony series is required for the used finite element solver. Figure 3-2 summarizes the methodology used for the elastomer behaviour law identification.

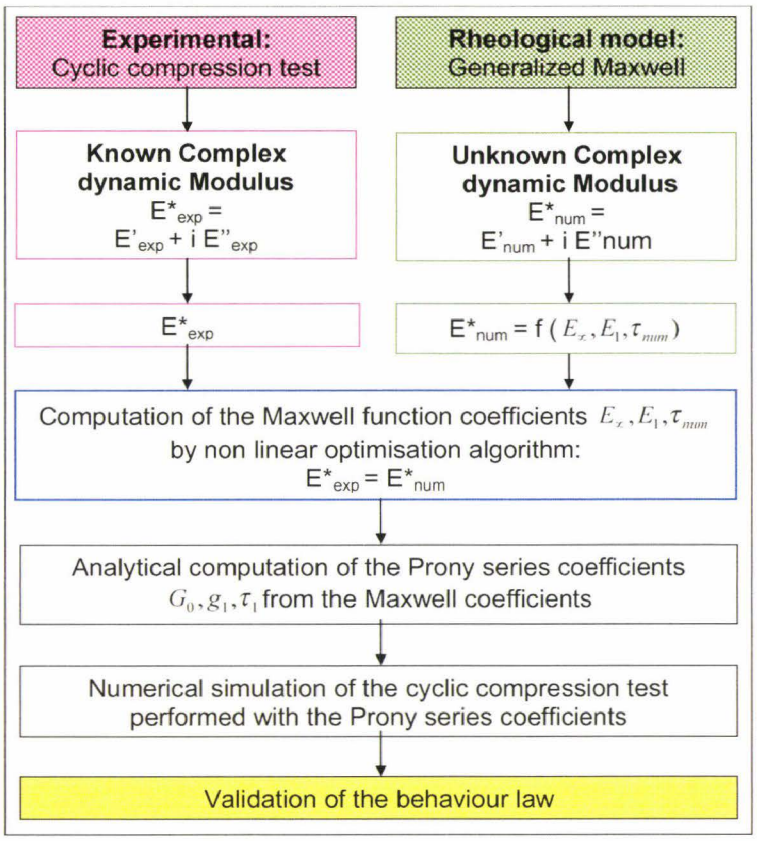

Figure 3-2: Methodology of identification of the behaviour law

The next paragraph introduces the specific device used during cyclic compression test.

2.1 Presentation of the cyclic compression test

The cyclic compression test is performed on a tensile testing machine with a hydraulic cylinder command in vertical position. The driver that commands the machine allows different configuration to pilot the displacement of the moving crosshead: sinus, square, triangle. The frequency and amplitude of displacement are adjustable. The load cell used during the test is a 6KN one. A cylindrical workpiece is moulded by the supplier. Standard cylindrical workpiece with a diameter d_0 of 29mm and height h_0 of 13mm is used.

The bottom of the workpiece is glued on the steel cylinder to ensure a permanent position. The steel cylinder is filled with solvent or paint before cycling to reproduce industrial chemical environment. The Figure 3-3 shows the stand on the testing machine. A sinusoidal displacement with a frequency (f) and an amplitude (dh_{max}) is imposed. A small initial compression on the workpiece permits to keep the contact during the cyclic compression test. The

load response is recorded every hundred cycles. This cyclic compression test brings the experimental curves to determine the coefficients of the behaviour law. The linear viscoelasticity theory is used to compute the parameters of the generalized Maxwell model and finally Prony series.

The representative frequency and amplitude of solicitation to the production line are exposed in the next paragraph.

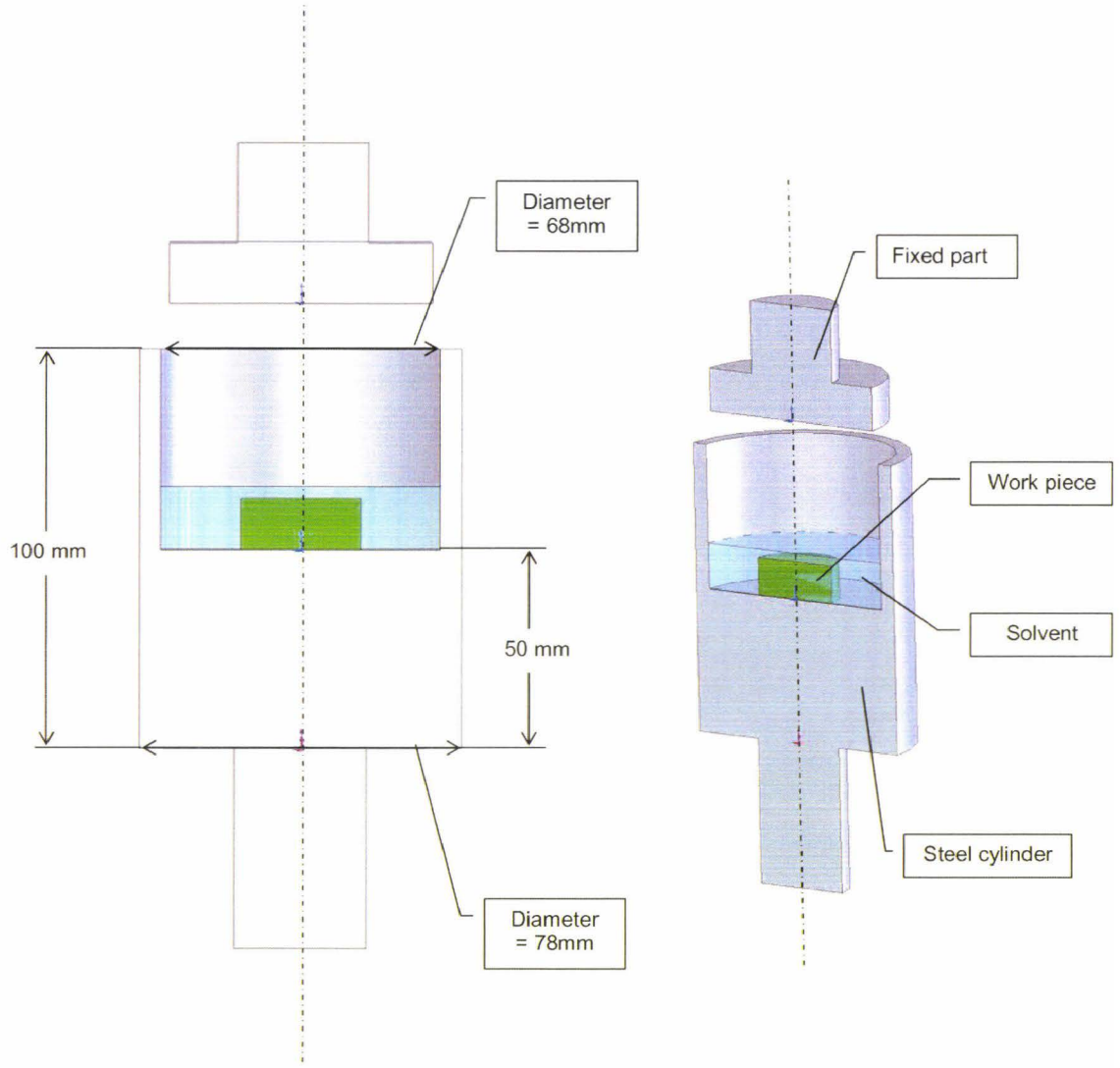

Figure 3-3: Specific device for the cyclic compression test

2.2 Cyclic compression test conditions to reproduce inline solicitations

Inline, the elastomer of the applicator roll undergoes upsetting followed by relaxation time. The elastomer is in contact with the strip and the pick-up roll

(Figure 3-4). The frequency of solicitation is a function of the line speed, roll speed and roll diameters. The goal of the cyclic compression test is a reproduction in laboratory of the solicitation undergone by elastomer on the roll coater.

The cyclic compression test is performed during 7500 cycles in different selected environments. The number of cycle corresponds to 2700m of painted strip during an inline production. The reference line speed is 85m/min with an applicator roll speed of 110%. We consider two upsetting by revolution because of the applicator/pick-up and applicator/strip contacts.

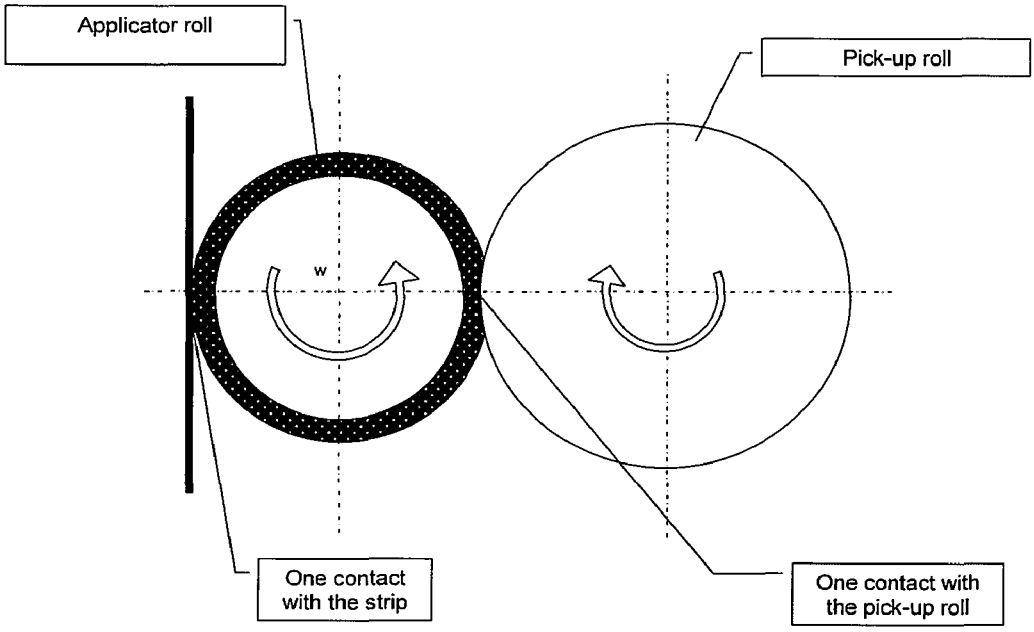

Figure 3-4: Contact localisation on the applicator roll

The computed frequency f for the cyclic compression test is the double frequency of rotation w of the applicator roll defined by equations (3-1), (3-2).

$$w = \frac{Va}{Ra} \tag{3-1}$$

$$f = 2w \tag{3-2}$$

With,

- Va the applicator roll speed (m/s)

- w the applicator roll frequency of rotation (tr/s)
- Ra the applicator roll radius (m)
- f the cyclic compression test frequency (Hz)

The calculated frequency of the cyclic compression test is f=3.8Hz. To perform the cyclic compression test, we need of the inline upsetting amplitude (Ng). Figure 3-5 illustrates the evaluation of Ng.

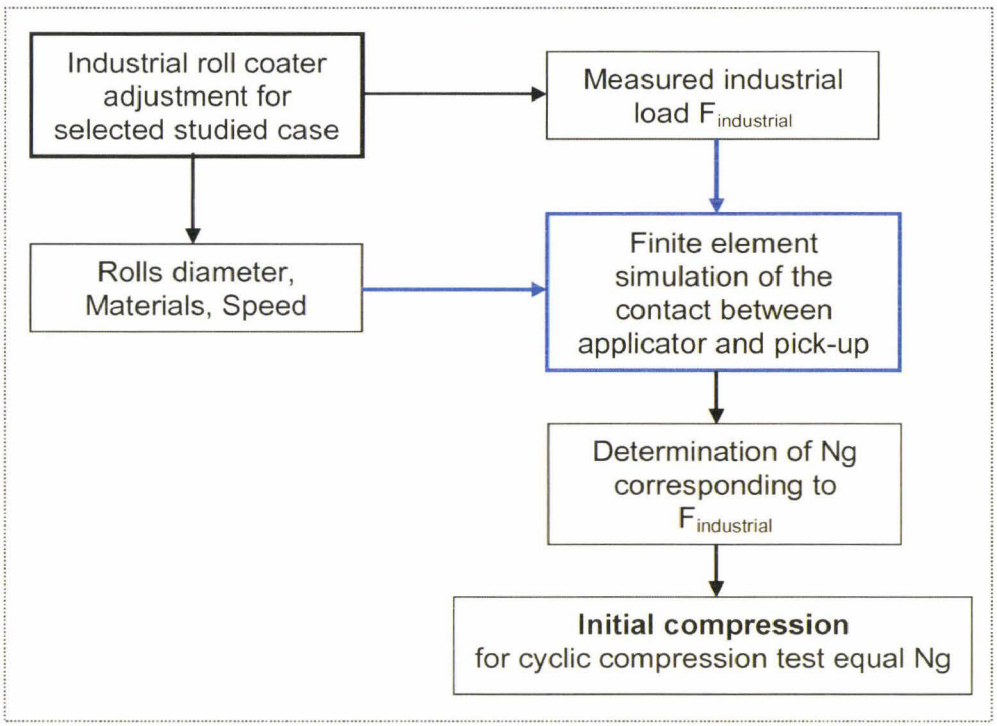

Figure 3-5: Ng evaluation for the imposed initial compression

A numerical simulation of the contact is performed to obtain a load reaction as a function of the roll coater adjustment. The evaluated Ng is around 2mm for a usual inline application with the selected roll coater configuration of the chapter 2. This value will be used as initial compression in the cyclic compression test. The amplitude of solicitation $dh\max$ is 1.5mm around this initial compression to keep the contact during test.

The next paragraph exposes the used equations and model in the methodology of identification. The final results will be the Prony series to reproduce the viscoelastic behaviour of the elastomer roll cover in finite element simulation.

2.3 Linear viscoelasticity theory

A sinusoidal displacement is applied on the workpiece and the following equivalent strain is used:

$$\varepsilon(t) = \varepsilon_0 \sin(wt) \quad with \quad \varepsilon_0 = \frac{dh_{max}}{h_0} \tag{3-3}$$

With,

- ε_0 the maximum imposed strain
- w (rad/s) the pulsation
- t (s) the time

The corresponding stress answer (3-4) computed from the load response is sinusoidal with a phase angle difference φ ranging between $[0;\frac{\pi}{2}]$.

$$\sigma(t) = \sigma_0 \sin(wt + \varphi) \quad with \quad \sigma_0 = \frac{F_{max}}{S_0} \tag{3-4}$$

With,

- σ_0 the maximum stress
- w (rad/s) the pulsation
- t (s) the time
- φ (rad) the phase angle
- $S_0(mm^2)$ the initial section

The elastomer behaviour is a function of the phase angle between strain and stress. The elastomer is completely elastic if φ=0 or completely viscous if $\varphi = \frac{\pi}{2}$. Between these two values the elastomer has a viscoelastic behaviour.

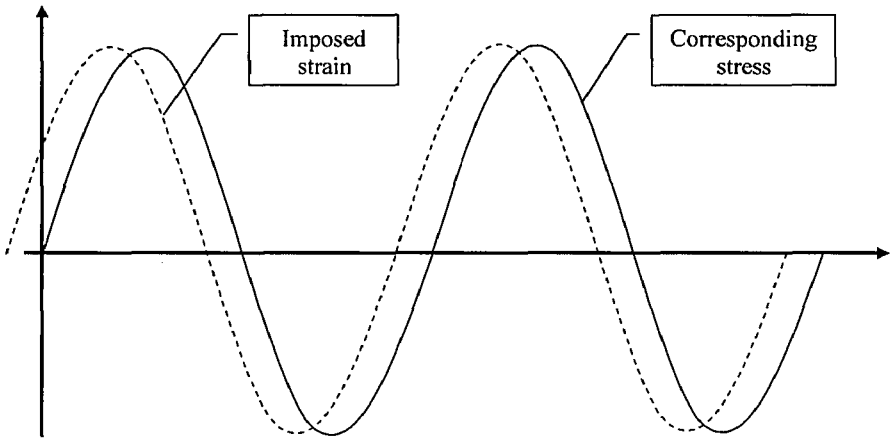

Figure 3-6: Imposed strain and corresponding stress for viscoelastic material

From the complex representation of the equations (3-3), (3-4), the corresponding complex Young modulus: $E^* = \frac{\sigma}{\varepsilon}$ (3-5) is defined as follows:

$$E^*_{exp} = \frac{\sigma_0}{\varepsilon_0} e^{i\varphi} = \frac{\sigma_0}{\varepsilon_0}(\cos\varphi + i\sin\varphi) = E' + iE'' = E'(1 + itg\varphi) \tag{3-5}$$

with ,

- $\left|E^*_{exp}\right| = \frac{\sigma_0}{\varepsilon_0}$ the dynamic Modulus
- $E'_{exp} = \left|E^*_{exp}\right|\cos\varphi$ the real part of the dynamic Modulus. It characterizes the response that is in phase with the excitation. E'_{exp} is called the « Storage Modulus ». It corresponds to the measurement of the energy stored and restored during a cycle.
- $E''_{exp} = \left|E^*_{exp}\right|\sin\varphi$ the imaginary part of the dynamic Modulus. It characterizes the response that is in quadrature with the excitation. E''_{exp} is called the « Loss Modulus ». It corresponds to the measurement of the dissipated energy during a cycle.

Figure 3-7 illustrates the dynamic modulus through the imaginary representation as described above.

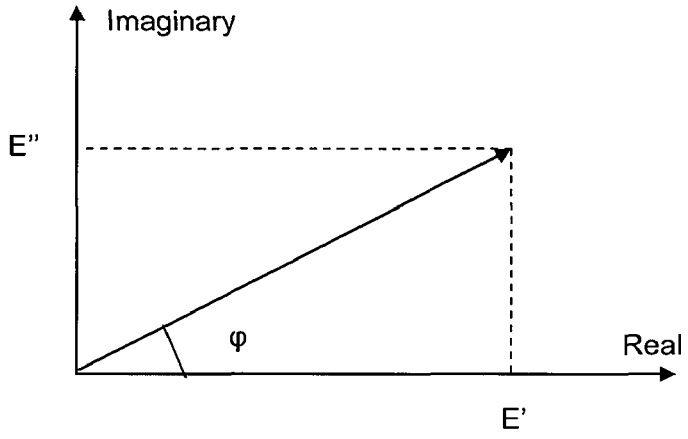

Figure 3-7: Dynamic modulus in the complex plan

Experimental test permits to compute the real part E'_{exp} and imaginary part E''_{exp} of the complex modulus. These two values will be the references for the determination of the mathematical model coefficients. The selected mathematical model is the Maxwell generalized model. It is selected to reproduce the behaviour of the Polyurethane in the numerical simulation. Finally, it will be transformed in Shear relaxation Prony series. The finite element program need this formulation to simulate the viscoelastic behaviour.

2.4 Generalized Maxwell model identification

The next step is the determination of the behaviour law coefficients. Figure 3-8 illustrates the Maxwell generalized model.

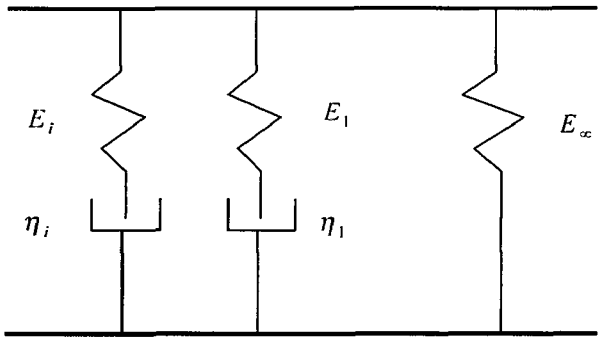

Figure 3-8: Maxwell generalized model

This model is chosen since it can model a wide range of time-dependent viscoelastic behaviour with their spring-dashpot elements in parallel. Validation of the result will show good accuracy of the model with n=1.

The elastic relaxation modulus $E(t)$ is described by equation (3-6) as follows:

$$E_{mm}(t) = E_\infty + E_1 e^{-\frac{t}{\tau_{mm}}} = E_\infty (1 + \frac{E_1}{E_\infty}) e^{-\frac{t}{\tau_{mm}}} \quad (3\text{-}6)$$

With the relaxation time coefficient (3-7),

$$\tau_{mm} = \frac{\eta_1}{E_1} \quad (3\text{-}7)$$

With,

- η_1 the dashpot coefficient
- E_1 the corresponding elastic coefficient (spring)
- E_∞ the long term elastic coefficient

For a harmonic excitation, the dynamic Modulus $E^*(w)$ is computed with the Fourier transform of the normalized Modulus (3-8):

$$Ft(w) = \int_0^\infty \frac{E_1}{E_\infty} e^{-\frac{t}{\tau_{mm}}} e^{-iwt} dt \quad (3\text{-}8)$$

The relation between the dynamic Modulus E^* and Ft is defined by (3-9),

$$E^*(w) = iw \cdot Ft(w) \quad (3\text{-}9)$$

In this case, the integration of (3-8) with the factorized form of (3-6) gives (3-10),

$$E^*(w) = E_\infty \left(1 + iw \left[\frac{E_1 . \exp^{-\left(iw + \frac{1}{\tau_{mm}}\right)t}}{E_\infty \frac{1}{\tau_{mm}} + iw} \right]_0^\infty \right) \quad (3\text{-}10)$$

And, the final expression of the dynamic Modulus E^*(3-11)

$$E^*(w) = E_\infty + \frac{iwE_1}{\frac{1}{\tau_{num}} + iw} \tag{3-11}$$

The dynamic modulus E^* can be separated in real and imaginary part as previously seen in Figure 3-7. In this case, we can write $E^* = E' + iE''$ to obtain E'_{num} and E''_{num}.

Equation (3-12) and (3-13) defines E'_{num} and E''_{num}:

$$E'_{num} = \frac{E_\infty + w^2\tau_{num}{}^2(E_\infty + E_1)}{1 + w^2\tau_{num}{}^2} \tag{3-12}$$

$$E''_{num} = \frac{E_1 w\tau_{num}}{1 + w^2\tau_{num}{}^2} \tag{3-13}$$

The real part E'_{num} and imaginary part E''_{num} expressions are known for the single term generalized Maxwell model. In the experimental part, cyclic compression test and linear viscoelasticity have been used to determine the values of E'_{exp} and E''_{exp}. The goal of this identification methodology is to compute the three coefficients E_∞, E_1, τ_{num} of the Maxwell model to fit on the experimental results. An optimization program on Matlab© software is developed to perform this curve fitting. We use optimization and curve fitting toolbox in this case. Nonlinear models are more difficult to fit than linear models since the coefficients cannot be estimated using simple matrix techniques. Instead, an iterative approach is required. Figure 3-9 illustrates the different steps of the optimisation. First, we start with an initial estimation for each coefficient. This estimation of Prony series coefficients comes from a tire study [45]. The elastomer properties used to manufacture tire are closed to our polyurethane one. Optimization program produces the fitted curve for the current set of coefficients. It adjusts the coefficients and determines whether the fit improves. The direction and magnitude of the adjustment depend on the fitting algorithm. In our case, the Trust-region method is used for non-linear minimisation [46]. The process iterates by returning to previous step until the fit

reaches the specified convergence criterion. The convergence criterion is 10^{-3}. Finally, the result is the three coefficients of the generalize Maxwell model.

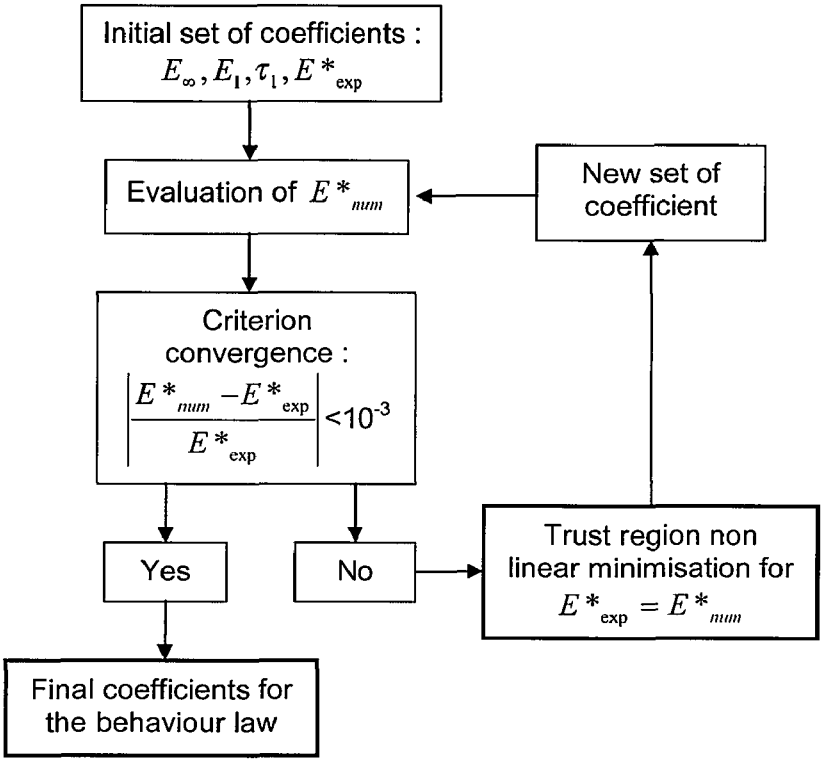

Figure 3-9: optimisation diagram

The Prony series coefficients can be evaluated from E'_{num} and E''_{num} for the finite element model.

2.5 Prony series coefficients evaluation

The finite element code uses a single term Prony series based on the Shear relaxation modulus Gr defined by (3-14).

$$Gr(t) = G_0(1 - g_1(1 - e^{-\frac{t}{\tau_1}})) \tag{3-14}$$

With,

- G_0 the instantaneous shear relaxation modulus
- τ_1 the shear relaxation time

- g_1 the Prony series spring coefficient.

We need to compute g_1, τ_1, G_0 from the single term Maxwell function. The linear viscoelasticity hypothesis are used to performed this computation. The different used relation to determine the bulk modulus K (3-15), shear modulus G (3-16) and Young Modulus E_0 (3-17) are defined as follows:

$$K = \frac{E_0}{3(1-2\upsilon)} \tag{3-15}$$

$$G = \frac{3E_\infty}{9K - E_1} \tag{3-16}$$

$$E_0 = E_\infty + E_1 \tag{3-17}$$

We know all the parameters and the final relations for the Prony series coefficients are (3-18), (3-19), (3-20) [7],

$$g_1 = 1 - \frac{G}{G_0} \tag{3-18}$$

$$\tau_1 = \frac{9K - E_\infty - E_1}{9K - E_\infty} \tau_{num} \tag{3-19}$$

$$G_0 = \frac{3K(E_\infty + E_1)}{9K - (E_\infty + E_1)} \tag{3-20}$$

The equations to determine the parameters of the behaviour law are established. The experimental results, computed coefficients and numerical validation for one example of elastomer are presented in the next part.

2.6 Validation of the behaviour law with numerical compression test

2.6.1 Geometry and boundary conditions

The numerical compression test is modelled via a rectangular mesh (Figure 3-10) 14.5mm length and 13mm height, with 100 plane stress axisymmetric elements with 4 integration points.

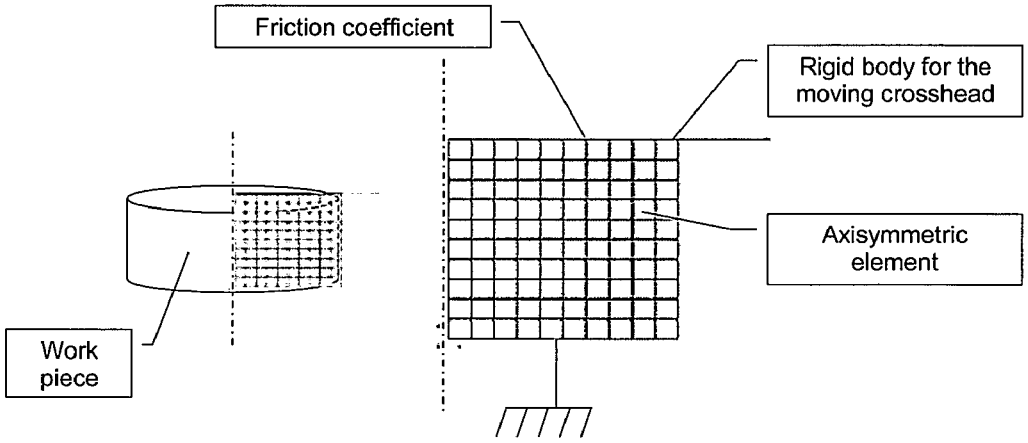

Figure 3-10: Numerical compression test, geometry and boundary conditions

Axis of revolution for the symmetry is the centre of the workpiece. The basis of the rectangular plane has a zero displacement to model the glue on the experimental test. A rigid line represents the moving crosshead. Between the rigid line and the top of the rectangular plane, a friction coefficient of 0.8 is used [47]. An initial compression is imposed by the rigid line displacement. When the rigid line is in position, a sinusoidal displacement is imposed for one cycle. The displacement comes from the experimental results for an accurate modelling. The elastomer in ambient environment (ie, without solvent or paint) is chosen for the comparison between the experimental and the numerical stress. Coefficients computed by the above methodology are summed-up in Table 3-1.

Table 3-1: Polyurethane properties without solvent from cyclic compression test

Elastic Modulus (Mpa)	Poisson ratio	g1	Shear relaxation time $\tau 1$ (s)
2.04	0.49	0,32	0.034

2.6.2 Results

The numerical response using the identified parameters of the Prony series is in good agreement with the experimental response of the elastomer without solvent (Figure 3-11).

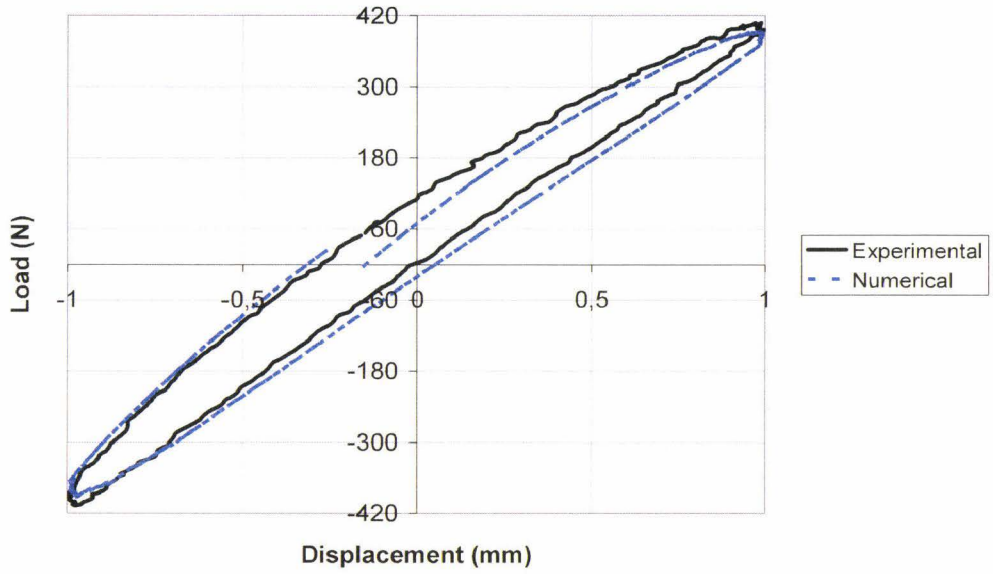

Figure 3-11: Numerical response with the computed parameters and experimental reference response, Polyurethane in dry condition, f=3.8Hz, dh_{max}=2mm

The small gap between curves is due to the numerical optimisation. This operation requires an approximation of the sinus response of the experimental load. This approximated sinus is shifted compared to the initial experimental response. When the computation of the phase angle is done, the obtained final relaxation time can be different from the experimental value. For the comparison presented in Figure 3-11, the average relative error between the numerical and experimental value is 1.5% but we have a standard deviation around 48 for many value. The global numerical response is in good agreement with the experimental load response and then, the behaviour law determination methodology is validated. The model can be used for industrial elastomer in specific environments.

2.6.3 Conclusion

The determination of the elastomer behaviour law associated to a chemical environment has been presented in this previous part. A complete methodology has been developed and used to identify the coefficients of the Prony series. The Prony series will be used to model the real elastomer behaviour in a

numerical simulation of the roll-coating process. The Prony series is a reformulation of the selected generalized Maxwell model. The generalized Maxwell model coefficients have been identified from the experimental results of the cyclic compression test. Finally, the behaviour law has been validated.

The elastomer behaviour evolves in time and is a function of the solvent and paint environment. The next paragraph deals with the cyclic compression results characterizing the selected industrial materials and environments.

2.7 Cyclic compression test on selected industrial materials

On Corus-Myriad production line, the elastomeric roll cover is in contact with different industrial paints, diluent to adjust the viscosity or cleaning solvents. These fluids in contact with elastomer are called environment in the following. During application the wet thickness and ribbing defect evolves for a given roll coater adjustment. In order to understand these observations and problems, we have to determine elastomer behaviour laws for different environments. This step is possible with the specific cyclic compression test: this test permits to analyse the elastomer response according to the time as a function of the environment. The determined behaviour laws will be used to perform an accurate modelling of the roll coating process.

2.7.1 Review of the selected materials

The materials in the roll coating application can be shared in two groups: the deformable roll cover and the fluid. Table 3-2 sums-up the selected roll cover materials and fluids by designation. The used elastomers are PU, EPDM and NITRILE. The used fluids are polyester top coat, polyester diluent and cleaning solvent with Metyl Ethyl Ketone (MEK) and without MEK.

Table 3-2: Materials and designation

Elastomer roll cover	
Description	**Code**
Polyurethane	PU
Ethylen propylen terpolymer	EPDM
Butadiene acrylonitrile	NITRILE
Fluid	
Description	**Code**
White Polyester resin, top coat n°1	TC1
White Polyester resin, top coat n°2	TC2
Polyester diluent to decrease polyester resin viscosity	Pdi
Cleaning solvent with Methyl Ethyl Ketone	CSM
Cleaning solvent without Methyl ethyl ketone	CSWM

The Table 3-3 associates the roll cover materials and fluids in cyclic compression test.

Table 3-3: Roll cover and associated paint during cyclic compression test

	PU	EPDM	NITRILE
TC1	Yes	Yes	Yes
TC2	Yes	No	No
Pdi	Yes	No	No
CSM	Yes	No	No
CSWM	Yes	No	No

The usual elastomeric roll cover used in Myriad is Polyurethane (PU). This material is a reaction between diisocyanate (aromatic and aliphatic types) and a polyol, typically a polyethylene glycol or polyester polyol, in the presence of catalysts and materials for controlling the cell structure. Polyurethane can be made in a variety of densities and hardnesses by varying the type of monomer used and adding other substances to modify their characteristics. Other additives can be used to improve performance and stability in chemical environments (aliphatic hydrocarbons, aromatic hydrocarbons, ketones, esters). Suppliers propose other roll cover material. We will study two of them to increase the knowledge: the EPDM and NITRILE.

Ethylen propylene terpolymer rubber (EPDM) is obtained by a copolymerisation of ethylene and propylene in equal proportion. An added diene inside permits to obtain the necessary double linkage for a good vulcanisation. The properties are closed to the natural rubber but with a glass transition temperature around -55°C.

Butadiene acrylonitrile (NITRILE) is a synthetic rubber copolymer and butadiene. Its physical and chemical properties vary depending on the polymer's composition of acrylonitrile within the polymer. This material is generally resistant to aliphatic hydrocarbons. However, it can be attacked by aromatic hydrocarbons, ketones or esters.

We select two paints usually sensitive to the ribbing defect. The two selected paints are white polyester resins used as top coat (TC1, TC2).

Inline, diluent is used to decrease the viscosity and improve the paint application quality. To understand this quality improvement and influence on the elastomer, an aromatic diluent is selected (Pdi).

At last, two cleaning solvents are selected (CSM, CSWM). The first is the initial formulation with Methyl Ethyl Ketone. The second is the modified formulation without Methyl Ethyl Ketone to reduce the environment and toxicity impact. These two solvents are used to clean the roll coater.

2.7.2 Cyclic compression test results

The cyclic compression test has been performed on the PU and two other materials EPDM, Nitrile in the different presented environments TC1, TC2, PDi, CSM and CSWM. The load response according to the time is proposed in Figure 3-12. The load response is the direct measurement for the imposed 2mm on the workpiece coupled to the cyclic solicitation ($dh\max, f$). Before each cyclic compression test 100 cycles are performed to ensure an initial accommodation and to limit error of measurement in the first cycles. In order to complete analysis, a load variation compared to the first load response is established in Figure 3-13. The elastomer response evolves as a function of the chemical environment. The presented values in this analysis come from the equilibrium state around 6500-7000 cycles.

- **Global load response analysis**

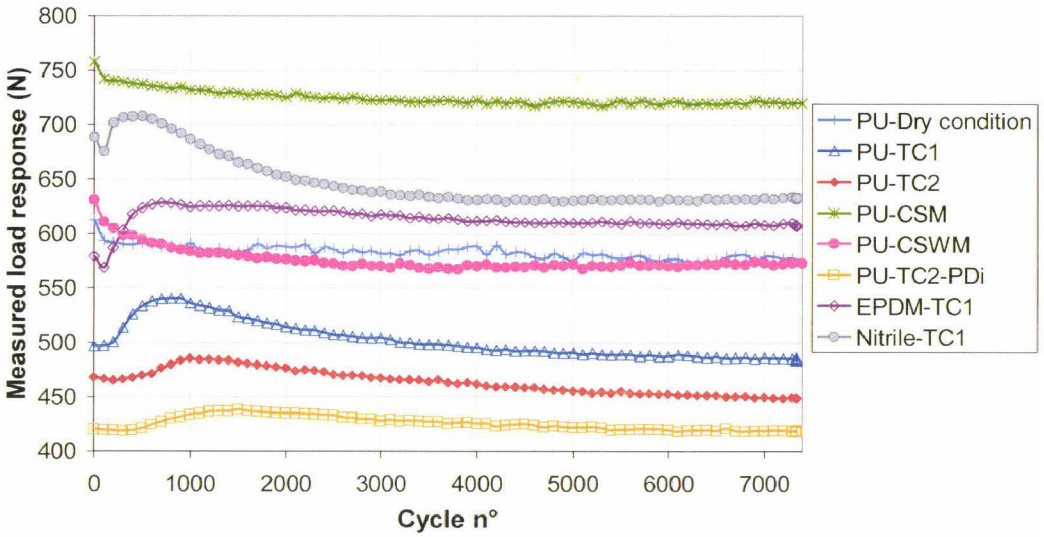

Figure 3-12: Elastomer load response in different environments as a function of the solicitation cycle, f=3.8Hz, dhmax=1.5mm, Ng=2mm

The first observation is the influence of the environment on the PU. We can show an offset around 300N for the same PU with two different environments (PU-CSM and PU-TC2-PDi). The PU is chemically modified by environment. This modification is highlighted by its behaviour evolution. The maximum is 720N for (PU-CSM). The CSM increases the PU stiffness. The minimum load response is 420N for (PU-TC2-PDi). The PDi decreases the PU stiffness. In addition, we can show the less influence of the CSWM on the PU. The curve with this cleaning solvent (PU-CSWM) is the same that the one obtained with (PU-dry condition).

EPDM and Nitrile have been tested in TC1 (EPDM-TC1 and Nitrile-TC1) environment. The load response of each one of them is compared to the PU in the same environment (PU-TC1). The load response for (PU-TC1) is the lowest with 470N. The load response for (Nitrile-TC1) is the highest with 640N. We have an offset of 170N between (PU-TC1) and (Nitrile-TC1) for the same chemical environment (TC1). EPDM response is closer from the Nitrile response than the PU response.

The Young Modulus modification as a function of the environment explains this load variation response. The Young modulus for PU-CSM is the highest with 2.8MPa. The Young Modulus for PU-TC2-PDi is the lowest with 1.6MPa. These Young modulus are found to be in good agreement with the load response measurement during test.

The second observation is the material behaviour accommodation to the imposed solicitation. In fact, the elastomer behaviour is a function of the temperature, the frequency of solicitation, the amplitude of solicitation and the chemical environment. Figure 3-13 allows to better understand the different elastomer accommodation states as a function of chemical industrial environments.

- **Elastomer accommodation states: load variation analysis**

This figure shows the load variation face to the first cycle as a function of solicitation cycles for different elastomer and environment.

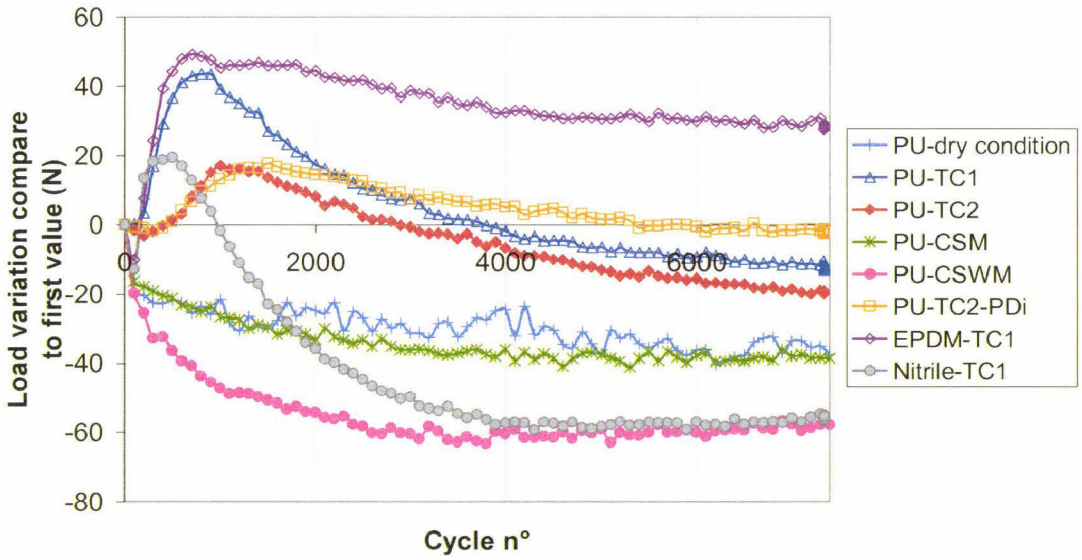

Figure 3-13: Elastomer load variation to the first cycle response as a function of the solicitation cycle, f=3.8Hz, dhmax=1.5mm, Ng=2mm

An important observation is the difference between the responses in polyester resin TC1, TC2 and the response in solvent CSM, CSWM, PDi. We can share in two groups the load responses.

- ***Group 1: TC1 and TC2***

The load variation can be divided in two parts. A high load increasing to reach a maximum corresponding to 1200 cycles. A slow decreasing to reach an equilibrium state around 6000 cycles.

The polyester resins seem to increases the load response of the PU, NITRILE and EPDM. Inline, this load variation in two phases will involve a wet thickness decreasing followed by a wet thickness increasing in a second time for a same roll coater adjustment.

The EPDM has a load increasing and a slow load decreasing to reach an equilibrium state. This material seems the best to have a fast and constant roll coater adjustment. In opposite way, Nitrile has a load increasing followed by an important load decreasing. In this case, it is very difficult to anticipate the roll coater adjustment.

- ***Group 2: CSM, CSWM and PDi***

The load variation corresponds to a slow decreasing to reach an equilibrium state around 6000 cycles.

PU in the cleaning solvent with MEK (PU-CSM) has the same behaviour that in dry condition (PU-dry condition). The load decreases and reaches an equilibrium state. Inline, these solvent is used between colour resin modifications on the roll coater to clean it. It is difficult to establish a relation with the inline behaviour, but we have shown an increase of the load response with this type of solvent on the global response.

For a same roll coater configuration obtained different inline wet thickness and application quality one. The cyclic compression test observations confirm the chemical environment influence on the elastomer behaviour. In the next point, the computed Prony series corresponding to cyclic compression test are exposed with analysis of these coefficients in relation with the load response.

2.8 Sum-up of materials properties for the F.E.M simulations

A set of elastomer and fluid have been used and characterized with the cyclic compression test in association with the identification methodology. In order to perform the F.E.M simulation and correlate with the experimental part, a sum-up

of the experimental results material is presented. Table 3-4 sums-up the Prony series results of the elastomer behaviour law.

Table 3-4: Prony series coefficient for different Elastomeric roll cover and associated environment of the cyclic compression test

Elastomer material beahviour coefficents for FEM simulation				
Designation	**Young Modulus E(Mpa)**	**g1**	**Shear relaxation time $\tau 1(s)$**	**Poisson ratio ν**
PU	2,04	0,32	0,034	0,49
PU--CSM	2,8	0,32	0,034	0,49
PU--CSWM	1,96	0,32	0,044	0,49
PU--TC1	1,78	0,32	0,146	0,49
PU--TC2	1,71	0,32	0,034	0,49
PU--TC2--Pdi	1,6	0,32	0,002	0,49
EPDM--TC1	2,55	0,32	0,036	0,49
NITRILE--TC1	2,57	0,32	0,059	0,49

In these results, g1=0.32 and ν=0.49 are constant for each selected case. The two coefficients E the Young Modulus and τ_1 the relaxation time evolves as a function of the material and environment. The coefficients proposed in this table are the results corresponding to 7000th cycle.

In the previous analysis, (PU-CSM) gives the higher load response and (PU-TC2-PDi) the lower one. In the Prony series result, the Young Modulus agrees with these observations. (PU-CSM) gives 2.8MPa when (PU-TC2-PDi) is 1.6MPa. (PU- dry condition) is between these two values with E=2.04MPa so as the load response.

The relaxation time is also very different. (PU-CSM) has τ_1=0.034 when (PU-TC2-PDi) has τ_1=0.002. In the load variation response, (PU-CSM) has a loss of (40N) when (PU-TC2-PDi) has no load variation compared to the first cycle. We can show a similarity between PU-dry condition and (PU-CSM) with τ_1=0.034. The load variation is the same in the Figure 3-13 with (-40N) for both cases. The relaxation time correlates the load/time variation of the elastomer as a function of the chemical environment. The relaxation time influence will be discussed in the numerical simulation plan.

A numerical simulation of the process is performed to better understand the load variation influence in the gap and its influence on the flow rate. The goal is to analyse for the same roll coater adjustment the influence of the load variation on the ribbing wavelength and final wet thickness.

3. Numerical simulation strategy by an example

The F.E.M simulations of the roll coating process will be done in two steps. The first is the simulation of the deformable contact between applicator roll and pick-

up roll without fluid. The goal is to obtain the mechanical pressure in the contact for a selected behaviour law of the elastomer and a set of adjustment parameters.

Second, we perform a F.E.M simulation of the flow rate between these two rolls without deformable part. An imposed pressure field as boundary condition computed in the deformable simulation models the elastomer impact on the fluid. The goal is to obtain the free surface position and associated wet thicknesses on each roll.

This numerical simulation plan is presented through a complete example. This example is detailed in the following part.

3.1 Deformable F.E.M simulation between applicator and pick-up rolls

3.1.1 Geometry and boundary condition

Figure 3-14 presents the numerical simulation of the deformable contact without fluid (A) and the associated real contact on the industrial roll coater (B).

This contact is studied for a real line speed of 85m/min. Two rigid bodies model the pick-up and the core of the applicator rolls. Their centre of rotation drives these two rolls. The applicator and pick-up roll speeds are respectively 110% and 30% of the line speed. The elastomeric applicator cover is polyurethane composed of 17500 plane strain linear elements with 4 integration points. The elastomer thickness is 37.5mm. The behaviour law used in the simulation is the Prony series computed in the previous part for the polyurethane in polyester top coat 1 (PU-TC1). In a first step, the pick-up roll penetrates the applicator to reach an initial compression of 2mm. Then, the centres of the applicator and pick-up rolls begin their rotation. To reproduce the influence of the fluid in the contact a friction coefficient of 0.03 is applied between these two rolls [49].

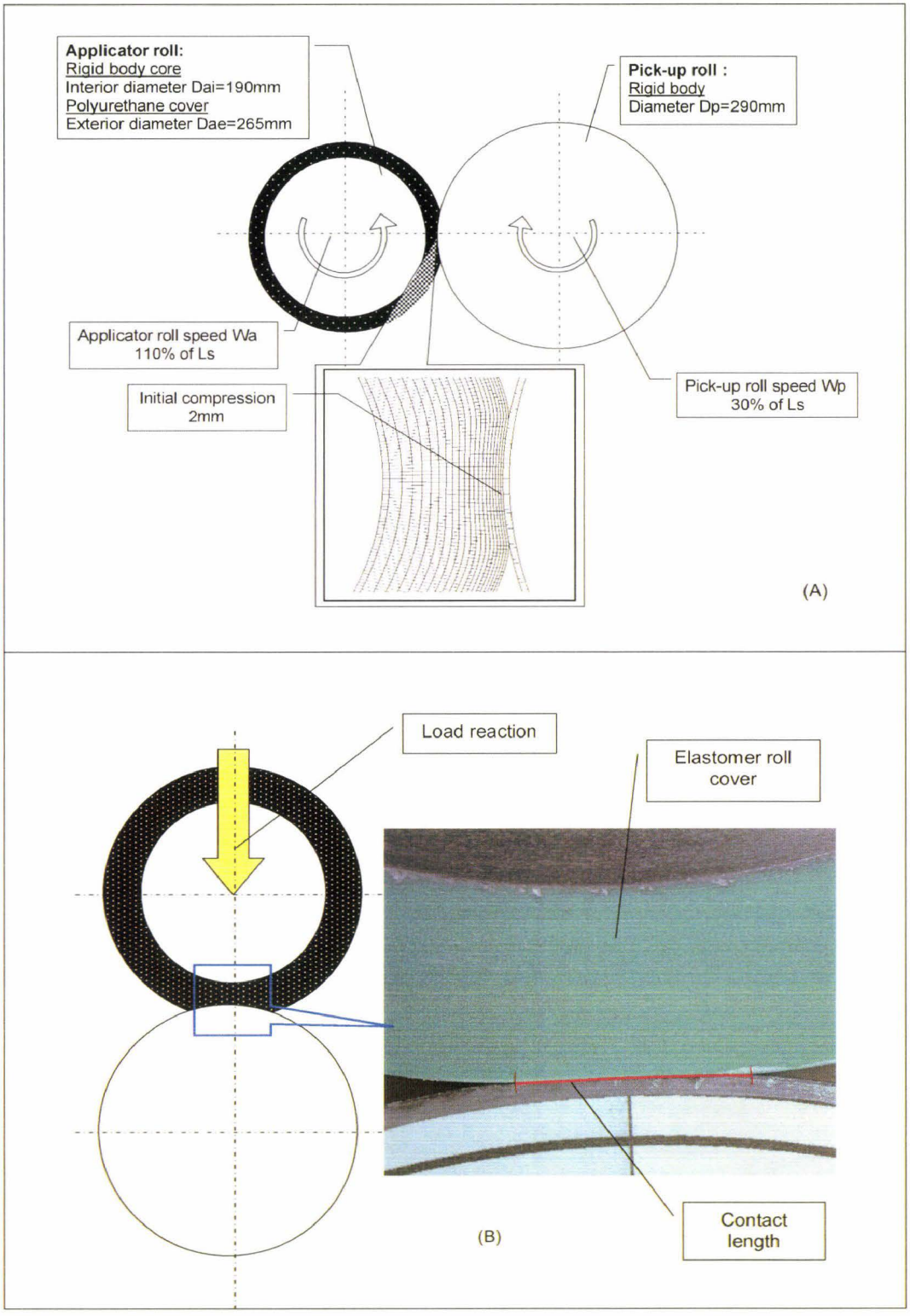

Figure 3-14: Deformable F.E.M simulation between applicator and pick-up rolls(A) and associated real contact (B)

3.1.2 Results of the structural numerical simulation

➢ **Load reaction**

The first result is the load reaction for the imposed 2mm initial compression. The layer thickness is 37.5mm with a PU-TC1 behaviour law for the elastomer. The experimental measurement of the chapter 2 gives one load measurement for the same roll coater adjustment. This experimental load is compared to the numerical one in order to correlate the F.E.M simulation result with the experimental data. We can show a good agreement. The Figure 3-15 shows the load reaction comparison. The load reaction is given on 0.1s. This is the time of the rotation in the simulation after the initial compression. The load reaction reaches a constant value of 7333N after an initial increase.

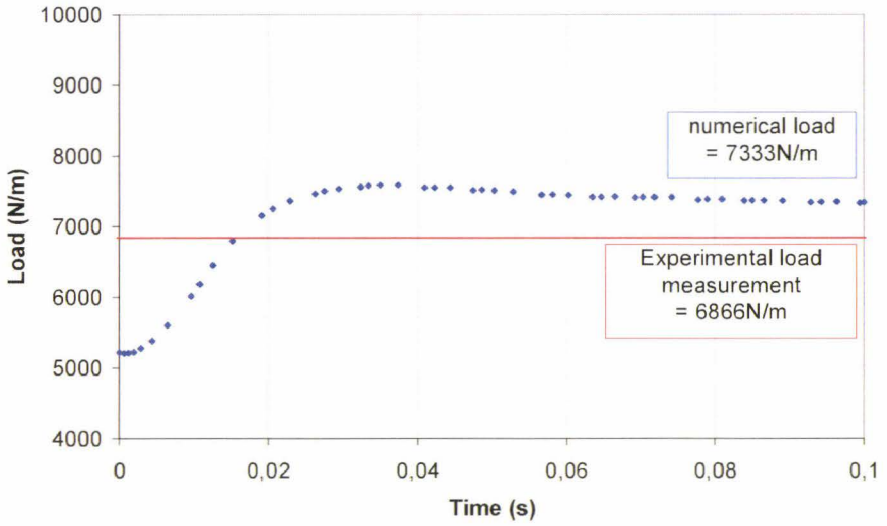

Figure 3-15: Load reaction in the centre of applicator roll during simulation, PU-TC1, Ls=85m/min, Va=110%, Vp=30%, initial compression=2mm, Layer thickness=37,5mm

➢ **Stress field in the elastomer layer**

The imposed external load implies a material response. In our case, the elastomeric roll cover is a viscoelastic material defined by a Young Modulus, a Poisson ratio and a relaxation time. Figure 3-16 shows the Von Mises stress in the elastomer thickness. Figure 3-17 illustrates the shear stress localisation in the layer thickness.

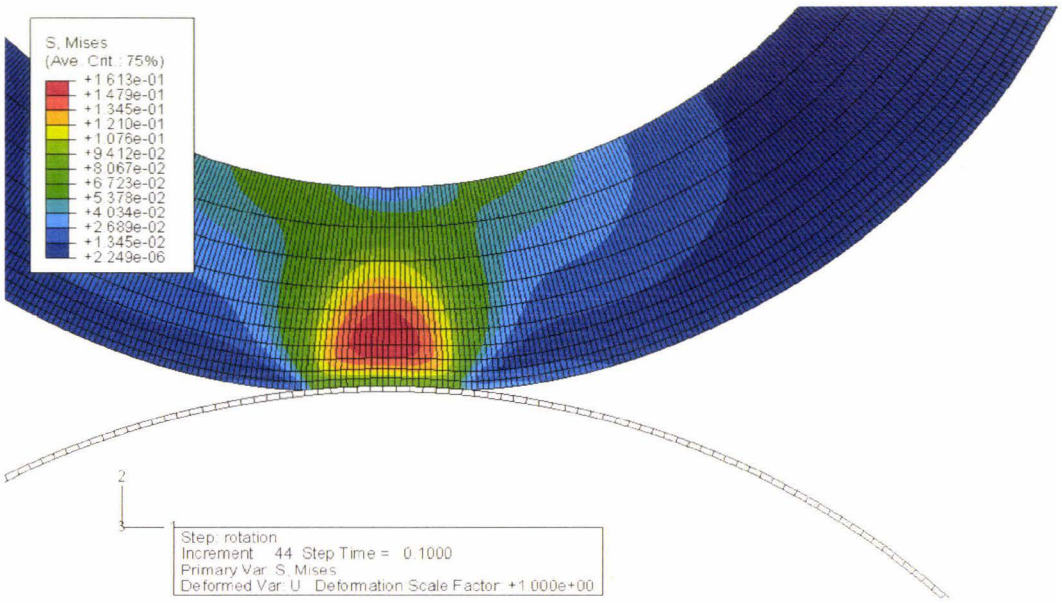

Figure 3-16: Von Mises equivalent stress in the elastomer layer, PU-TC1, Ls=85m/min, Va=110%, Vp=30%, initial compression=2mm

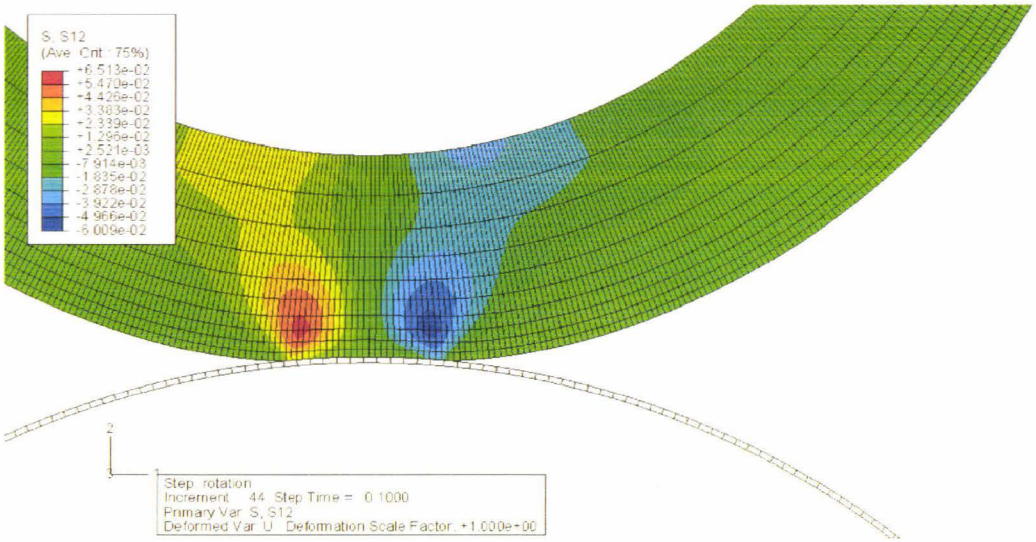

Figure 3-17: Shear stress in the elastomer layer, PU-TC1, Ls=85m/min, Va=110%, Vp=30%, initial compression=2mm

The maximum equivalent stress is σ=0.16MPa at 7.3mm deep. The absolute maximum shear stress is τ = 0.065MPa at 5.7mm deep. Two zones of maximum shear exist: one near the contact inlet and one near the contact exit.

➢ **Mechanical pressure at the pick-up/applicator interface**

The last important information used in the numerical plan is the mechanical pressure obtained in the contact for a set of adjustments. Figure 3-18 illustrates the mechanical pressure result obtained for this example.

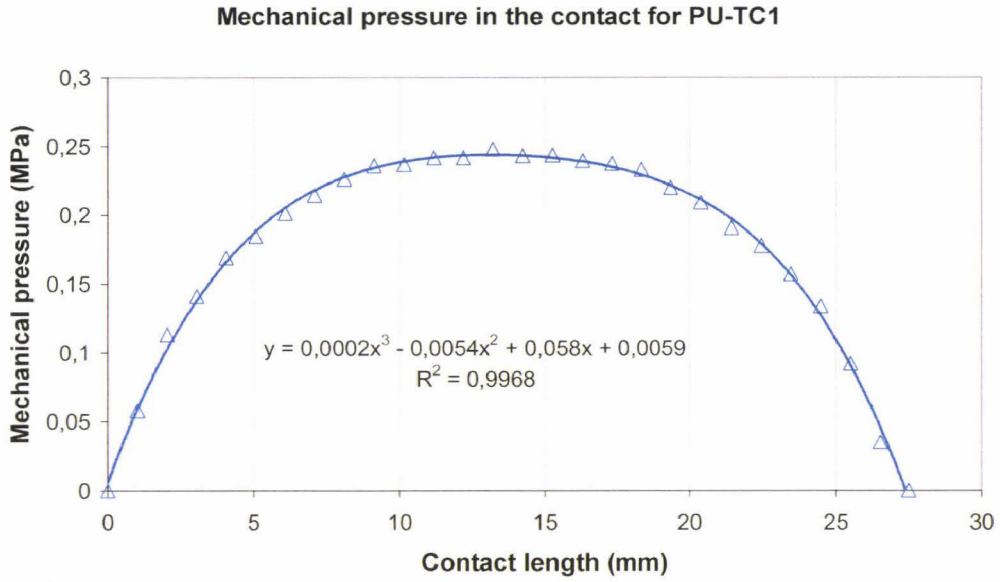

Figure 3-18: Mechanical pressure in the contact for the PU-TC1 studied case

The maximum mechanical pressure is P=0.25 MPa near the centre of the contact. The contact length L is around 28 mm. From this result, a third order polynomial approximation is fitted to obtain a coefficient of determination at least 99%. In this example the approximation gives equation (3-21).

$$P_{def}(x) = 0.0059 + 0.058x - 0.0054x^2 + 0.0002x^3 \quad (3\text{-}21)$$

This result will be implemented in the flow rate simulation to represent boundary condition. The next paragraph deals with the dynamic fluid simulation.

3.2 Fluid dynamic F.E.M simulation

3.2.1 Geometry and boundary conditions

Figure 3-19 presents the simulation of the flow rate with free surface between applicator and pick-up rolls. Table 3-5 sums-up the properties of the used fluid in the free surface simulation.

Table 3-5: Experimental paint properties of the selected fluid

Fluid properties for FEM simulation			
Designation	**Density(kg/m3)**	**Viscosity(Pa.s)**	**Surface tension(N/m)**
TC1	1390	0,51	0,035

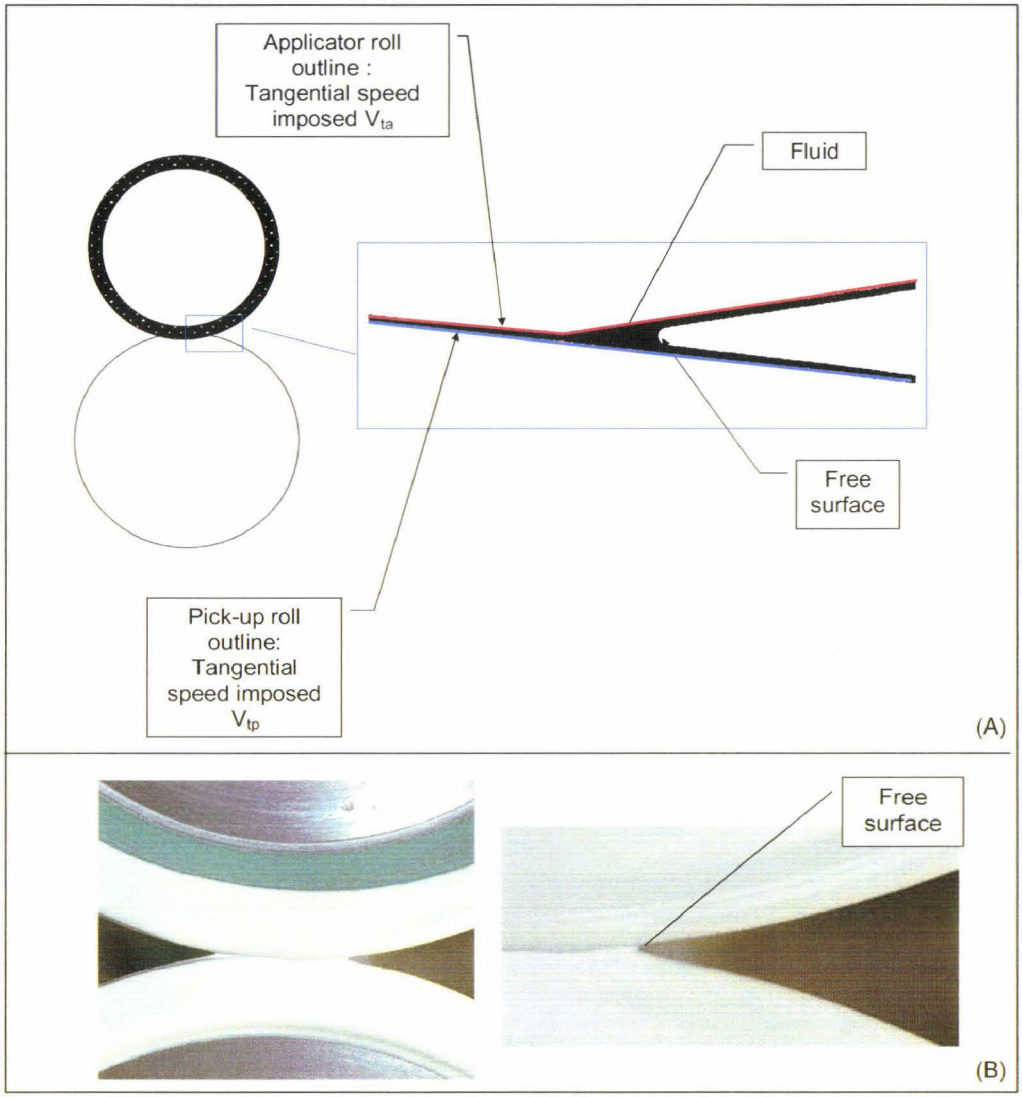

Figure 3-19: Dynamic fluid F.E.M simulation (A) and associated real contact (B)

The fluid numerical simulation is defined by the outline of the applicator and pick-up rolls. It is composed of 1500 quadrangle elements with 4 integration points. The output of the contact is a free surface governed by its surface tension. The inlet is modelled by a speed flooded condition. A tangential speed is applied to the fluid located on the applicator and pick-up rolls outline.

3.2.2 Specific pressure boundary condition determination

The numerical plan is based on a mechanical pressure transfer from the deformable simulation to the free surface fluid simulation. This transfer is performed by an imposed pressure field as boundary condition illustrated in Figure 3-20. This imposed pressure field is the sum of the mechanical pressure result (3-21) (deformable F.E.M simulation) and the pressure resulting (3-22) from an initial free surface F.E.M (without imposed pressure field).

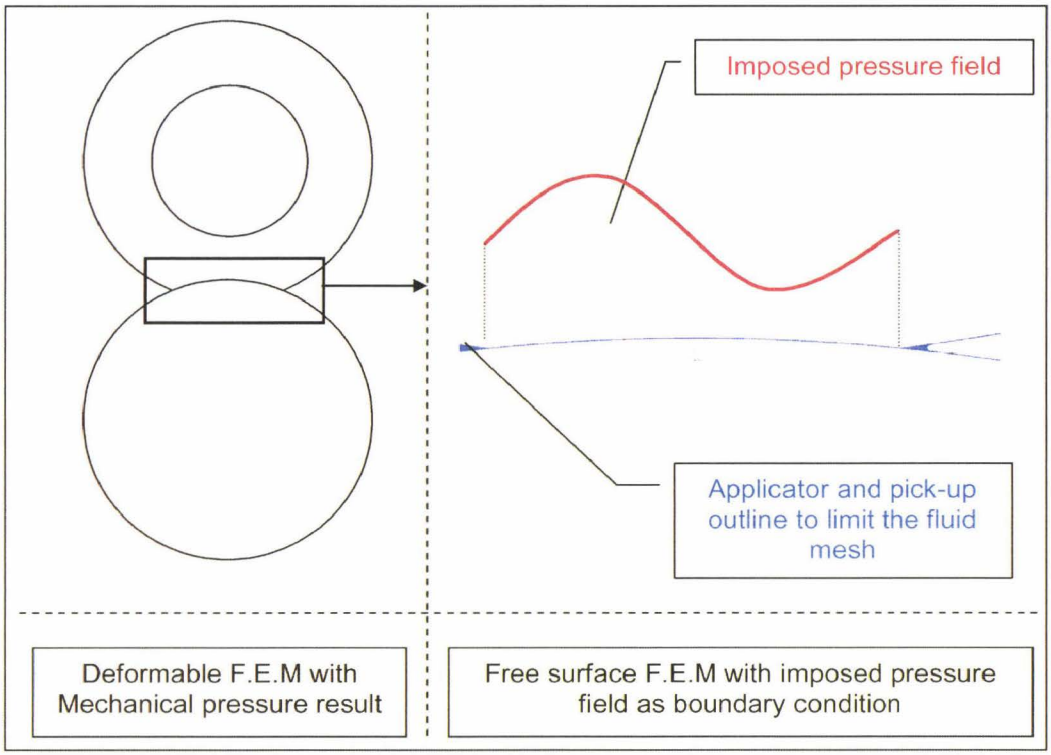

Figure 3-20: Pressure field transfer in the free surface F.E.M simulation

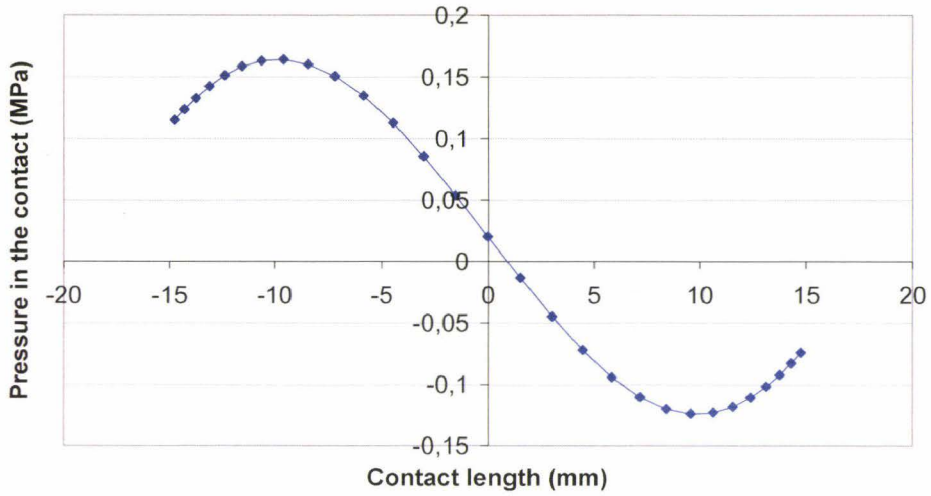

Figure 3-21: Pressure result in the contact from the fluid dynamic simulation without imposed pressure field of the deformable F.E.M; TC1, Ls=85m/min, Va=110%, Vp=30%

Figure 3-21 illustrates the initial fluid dynamic simulation. The result is a classical curve for this converging-diverging flow rate [40]. The curve is not symmetric to the x-axis. The pressure amplitude is in the range [-0.12MPa; 0.16MPa].

A third order polynomial approximation of the pressure result is done (3-22) as the deformable F.E.M simulation.

$$P_{fluid}(x) = 0.0724 + 0.0324x - 0.0032x^2 + 7.10^{-5}x^3 \quad (3\text{-}22)$$

The final imposed pressure as boundary condition is the sum of (3-21) and (3-22). The result is equation (3-23):

$$P_{sum}(x) = 0.363 - 0.0248x - 0.001x^2 + 7.10^{-5}x^3 \quad (3\text{-}23)$$

Figure 3-22 illustrates the pressure result (3-23) that will be used as boundary condition in the free surface F.EM simulation (Figure 3-20). This pressure reproduces the elastomer impact on the flow rate. The meniscus position and associated wet thickness will be obtained by this simulation.

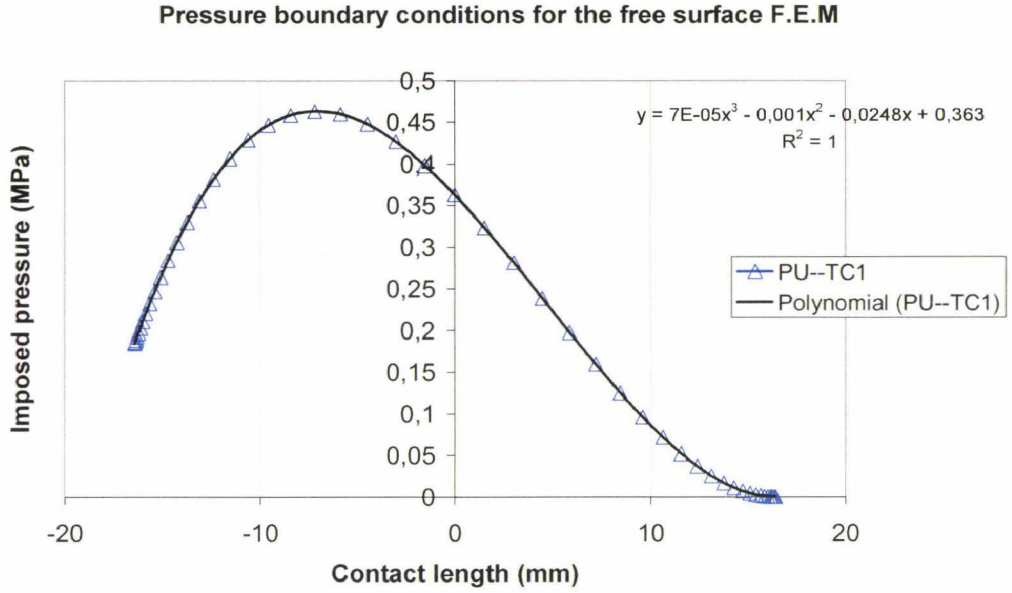

Figure 3-22: Pressure field as boundary condition in the free surface F.E.M simulation

The pressure transfer between the deformable F.E.M simulation and the free surface F.E.M simulation has been presented. The next paragraph gives the obtained results in terms of free surface position, wet thickness and velocity vectors field.

- **Velocity vector**

Figure 3-23 presents the velocity vector near the free surface. The velocity in the numerical simulation is in (mm/s). The applicator roll speed is 1560mm/s (110% of the 85m/min line speed). The pick-up roll is 425mm/s (30% of the 85m/min line speed).

We can show a low speed zone in blue with V=70mm/s when the applicator roll speed is 1560mm/s. This is the film split area where the film separates in two unequal wet thicknesses. This low speed area measures around 250µm in this example. The free surface position will modify this zone length and then the film split position and stability.

We have seen the influence of the free surface position on the ribbing wavelength through the literature in chapter 1 and experimental investigation in the chapter 2. This numerical approach will lead us to have an accurate analysis of the roll coater parameters on the free surface position.

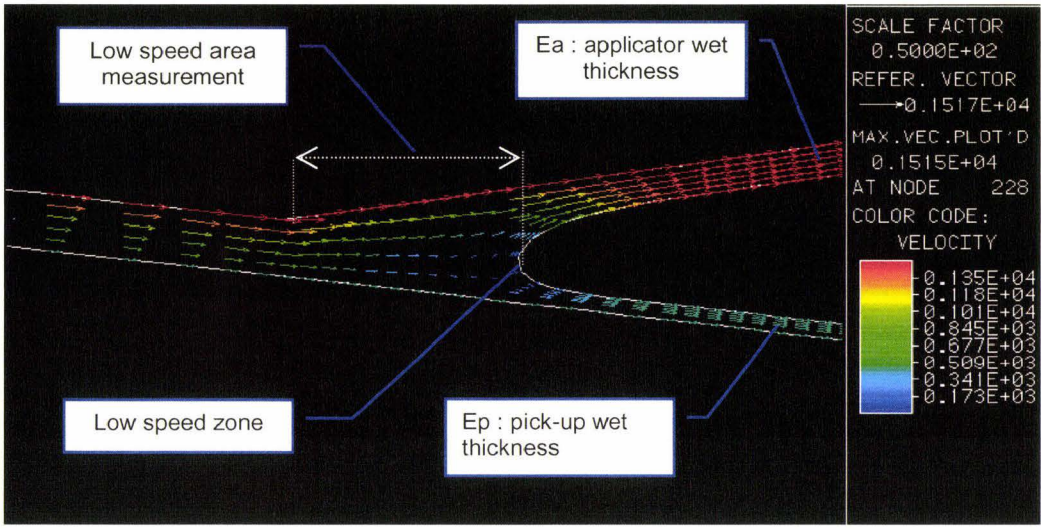

Figure 3-23: Velocity vector to the output of the contact; TC1, Ls=85m/min, Va=110%, Vp=30%

- **Free surface position**

Figure 3-24 illustrates the free surface or meniscus position. In white, this is the initial position of the free surface before computation. In green, this is the final position of the free surface after computation and convergence for the set of input parameters. When the free surface position evolves, the associated wet thickness on each roll evolves in the same time.

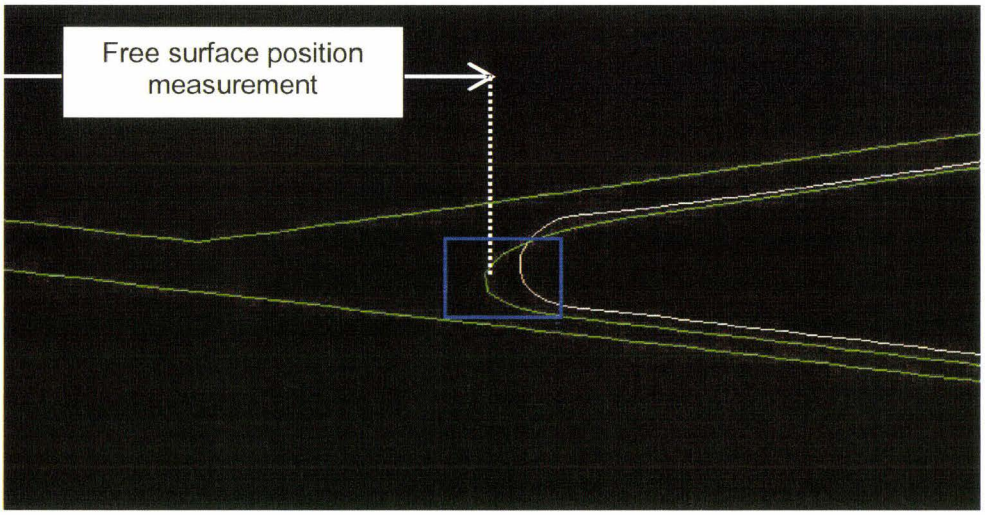

Figure 3-24: free surface position, comparison between initial (white) and final position after computation (green)

The center of meniscus is the measured value to evaluate the position of the free surface. It is 16.87 mm to the centre of the contact in this example. Figure 3-25 illustrates the focus on free surface.

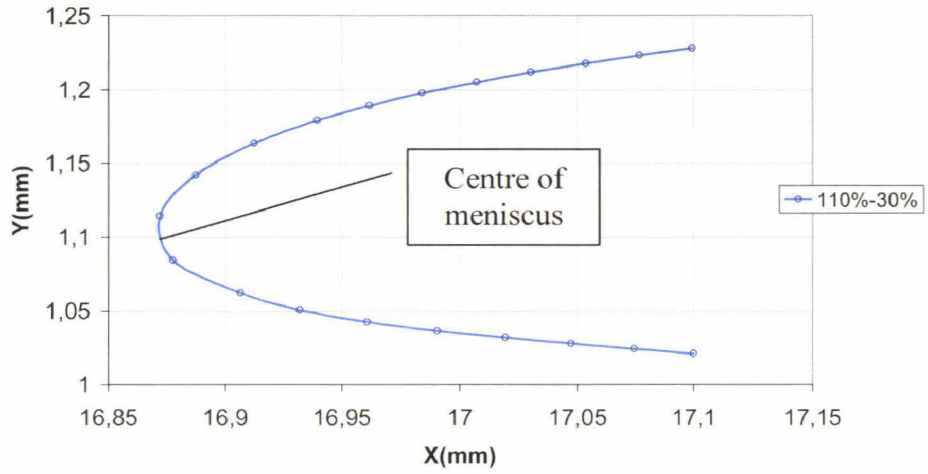

Figure 3-25: focus on the free surface

- **Wet thickness**

In association with the free surface position, we have the wet thicknesses on each roll. These wet thicknesses are function of the pressure in the contact, roll speeds and fluid properties. The obtained results are:

- Applicator roll wet thickness ea_{num}=81µm

- Pick-up roll wet thickness ep_{num}=37µm

We can compare these numerical wet thicknesses to the experimental one. In the numerical simulation F.E.M, we have the pick-up roll wet thickness and the applicator roll wet thickness. In our experimental investigation of the chapter 2, the associated result is the pick-up wet thickness since no applicator wet thickness is available. The experimental pick-up wet thickness is ep_{exp}=44µm.

The agreement is found to be good between experimental and numerical pick-up wet thickness with a difference of 15%.

As comparison, Cohu experimentally studied a three deformable roll coater. He compared his experimental wet thickness measurement to a predictive wet thickness power law. He evaluated the relative error between experimental and model around 25% [28].

The global numerical simulation strategy has been presented. The classical FSI framework has been simplified. First, a deformable F.E.M simulation gives mechanical parameters at the "pick-up/applicator" rolls interface.

Second, these parameters are implemented in a F.E.M fluid model to compute their impact on the paint behaviour, in term of free surface position and wet thickness at the exit. An example (Ls=85m/min, Va=110%, Vp=30%, PU-TC1, initial compression of 2mm, layer thickness=37.5mm) has been used to present the strategy.

3.3 Numerical simulation plan

The goal of the following simulation plan is to investigate with accuracy the influence of all the parameter on numerical results. Two numerical modelling are available to study the deformable roll coating process. The first is the deformable F.E.M simulation. This one permits to analyse the elastomer behaviour in the contact and its influence on the geometry response. The next paragraph deals with the obtained results

3.3.1 Contact pressure at pick-up/applicator interface : influence of elastomer behaviour and layer thickness

- **Elastomer behaviour law influence on the deformable contact**

Different elastomeric roll covers in different industrial chemical environments have been studied. Their behaviour has been analysed through Prony series. Figure 3-26 presents the obtained mechanical pressure in the contact for the different behaviour laws. The mechanical pressure in the contact is a function of the elastomer properties since the other parameters are constant in this case (Ls=85m/min, Va=110%, Vp=30%, Poisson ratio=0.49, applicator diameter=265mm, pick-up diameter=290mm, layer thickness=37.5mm, initial compression=2mm). The mechanical pressure fields correlate the loads response coming from the cyclic compression test. The relaxation time could explain the difference. The curves are parabolic with a maximum mechanical pressure near the centre of the contact. The maximum mechanical pressure in the contact is 0.38MPa for the Polyurethane in cleaning solvent with MEC (PU-CSM). The minimum is 0.15MPA for the Polyurethane in polyester topcoat 2 with diluent added (PU-TC2-Pdi). The difference between both pressure values is 0.23MPa. We will show the influence of this difference on the free surface position and wet thickness in the free surface simulation results.

The contact length is around 28mm. The contact length variation between the maximum and the minimum is 1mm.

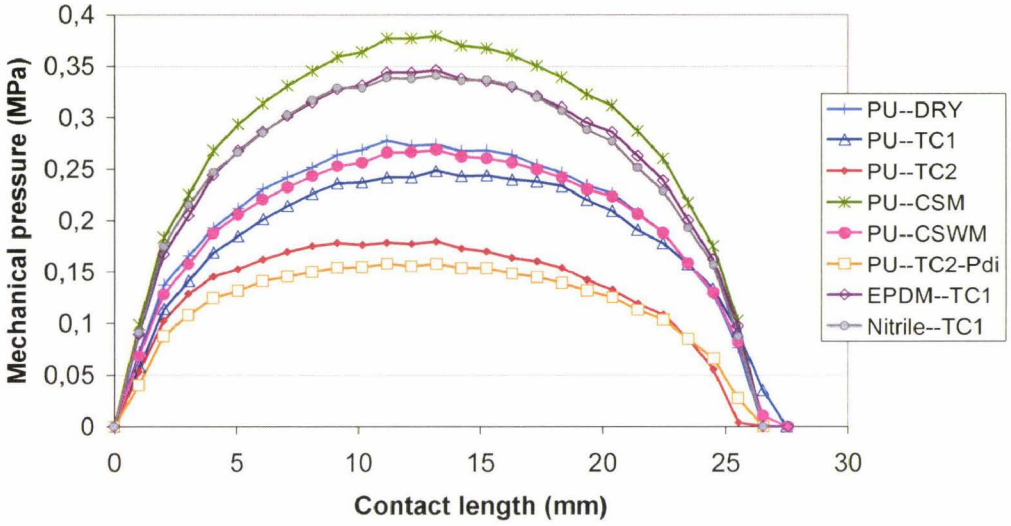

Figure 3-26: Mechanical pressure in the contact for the different behaviour laws, initial compression 2mm, Ls=85m/min, Va=110%, Vp=30%, Layer thickness=37,5mm

The chemical environments imply different mechanical pressure response in the contact for the same material (PU). The mechanical pressure in the contact can be at least the double of the minimum value for two different used solvent (PDi and CSM). These chemical environments act on the elastomer structure. This modification is directly indicative to a different mechanical response.

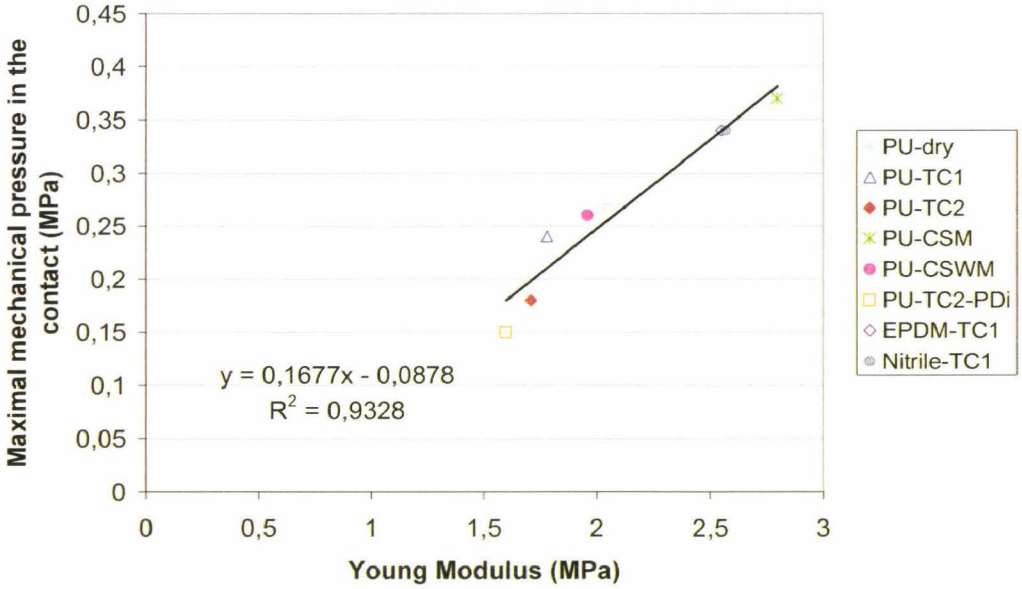

Figure 3-27: Maximum mechanical pressure in the contact as a function of the corresponding Young modulus for the different behaviour law

Chemical environments modify dynamic Young modulus and relaxation time of the elastomer(Table 3-4). In Figure 3-27, we can see the maximal mechanical pressure in the contact and the associated computed Young modulus. The higher is the Young Modulus, the higher is the maximum pressure in the contact. The mechanical pressure in the contact agrees with the value of their Young Modulus.

The relaxation time modify the mechanical pressure response. We use an additional study to show the relaxation time influence on the mechanical pressure in the contact. The PU-CSM case is selected for this study.

Its initial relaxation time result is τ_1=0.034. Two numerical simulations are performed with the same roll coater configuration and behaviour law. The difference is the relaxation time modification in these simulations to evaluate the influence of this parameter on the mechanical pressure and contact length. The two values are τ_1=0.0034 and 0.34. Figure 3-28 exposes the mechanical pressure response and contact length for these two added simulations.

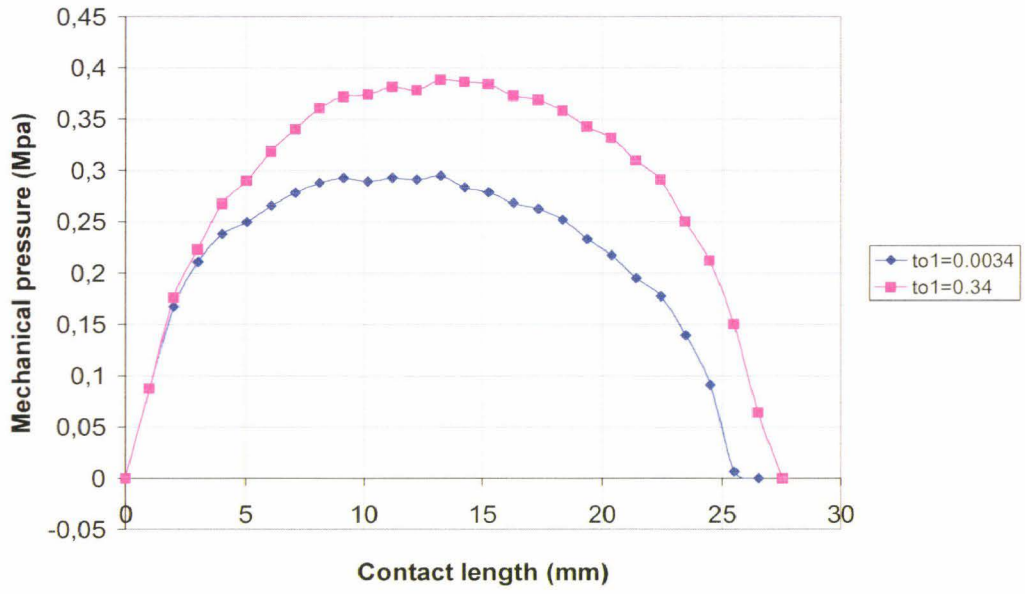

Figure 3-28: Mechanical pressure in the contact for PU-CSM, initial compression 2mm, Ls=85m/min, Va=110%, Vp=30%, Layer thickness=37.5mm, two different relaxation time to1=0.0034 and 0.34

The dynamic Young modulus is E=2.8MPa for the two curves. The mechanical pressure and contact length difference are observed as a function of the relaxation time.

The mechanical pressure in the contact is 0.38MPa for τ_1=0.34. The contact length is 28mm. These values are equal of the initial PU-CSM case.

The mechanical pressure in the contact is 0.29MPa when τ_1=0.0034. The contact length is 27mm.

A difference is noted between two relaxation times on the mechanical pressure response and contact length. For the selected roll coater configuration, it seems to exist a limit of relaxation time influence. On one hand, for the PU-CSM example, we obtain equal result for E=2.8MPA with to1=0.034 and τ_1=0.34. On the other hand, a difference is observed when to1=0.0034 with a smaller mechanical pressure and contact length result. In fact, the peripheral roll speed is around 1500mm/s (110% of 85m/min) and then for 28mm, the material is deformed during 0.018s in the contact. This time is lower than 0.034 and 0.34. The elastomer do not has the time to relax the stress inside it and the pressure is maximum.

In fact, a same roll coater adjustment brings different mechanical pressure in the contact as a function of the elastomer behaviour. Moreover, the elastomer layer thickness modifies the pressure response in the contact.

- **Layer thickness influence on the deformable contact pressure**

Inline, the deformable roll undergoes mechanical wear because of the contact with the strip during paint application. Surface finishing is performed to eliminate defects on the roll. This finishing implies a decrease of elastomer layer thickness, leading to a new roll when this thickness is not sufficient. This smaller layer thickness causes a modification of the roll coater adjustment for the same targeted wet thickness. A layer thickness variation is coupled to the mechanical pressure variation in the contact. The goal of this numerical simulation will be to evaluate the mechanical pressure in the contact for the different roll diameter evolution. A standard adjustment is expected to obtain the good wet thickness as a function of the roll coater configuration. The same contact configuration (contact length and mechanical pressure) can be obtained by a different imposed gap or load, for different elastomer layer thicknesses.

Four deformable numerical simulations are performed to illustrate the layer thickness influence on the mechanical pressure and on the roll coater adjustment:

The first is the above deformable simulation (Figure 3-14). The applicator roll diameter is Dae=265mm corresponding to 37.5mm elastomer thickness. The pick-up roll diameter is 290mm. The initial compression is 2mm. The line speed is 85m/min with Va=110% of Ls and Vp= 30% of Ls. The used behaviour law is PU-TC1.

For this first simulation considered as reference, the maximal mechanical pressure in the contact is 0.25MPa with 28mm contact length.

A second simulation is performed with the same parameter but with a smaller applicator roll diameter. In this case, Dae=255mm corresponds to 32.5mm elastomer thickness.

The maximum pressure in the contact is 0.27MPa with 30mm contact length.

A third and a fourth simulation are performed with the same parameters of the second case (smaller diameter). The difference is the initial imposed compression with respectively 1.5mm and 1.8mm.

The maximal pressure is 0.22MPa and the contact length 24mm for 1.5mm initial compression. When, the initial compression is 1.8mm the mechanical pressure in the contact is the same that the reference case, equal to 0.25MPa. The contact length is also the same with 28mm.

Figure 3-29 exposes the mechanical pressure in the contact for the four studied cases.

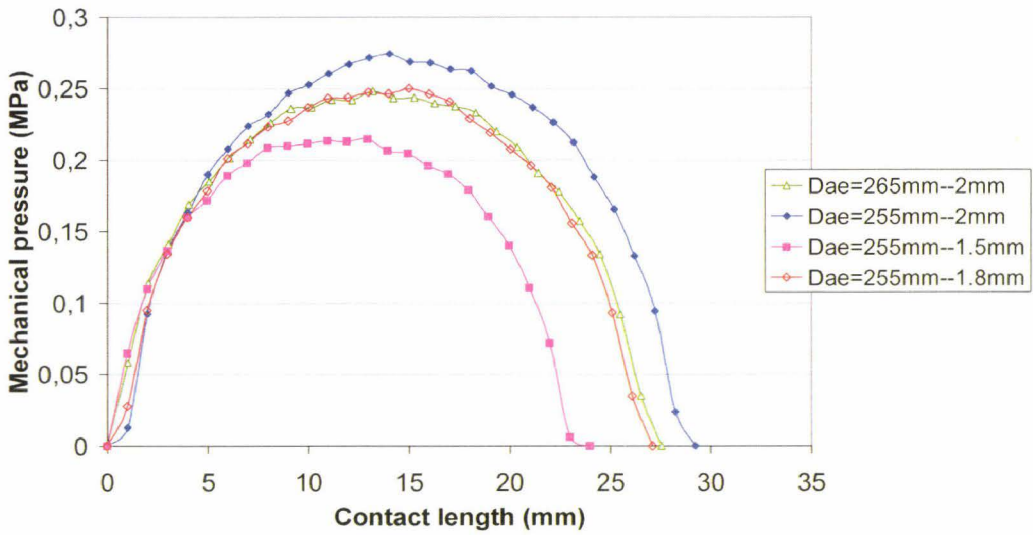

Figure 3-29: Mechanical pressure in the contact, PU-TC1, two deformable roll diameter (255mm,265mm) and different initial compression (1.5mm, 1.8mm and 2mm)

We have shown the elastomer behaviour and layer influence on the mechanical pressure response in the contact. The free surface F.E.M simulation can be introduced to study the mechanical pressure influence on the free surface or meniscus position and on the wet thicknesses.

3.3.2 Free surface F.E.M simulation results : influence of elastomer behaviour and roll speeds

➢ **Elastomer behaviour law influence on the meniscus position**

Elastomer behaviour influence has been studied in the above paragraph. The result was a set of mechanical pressures in the contact. These different mechanical pressures have been implemented in the free surface F.E.M simulation. Figure 3-30 illustrates the different imposed pressure in the free surface F.E.M corresponding to the different elastomer behaviour law.

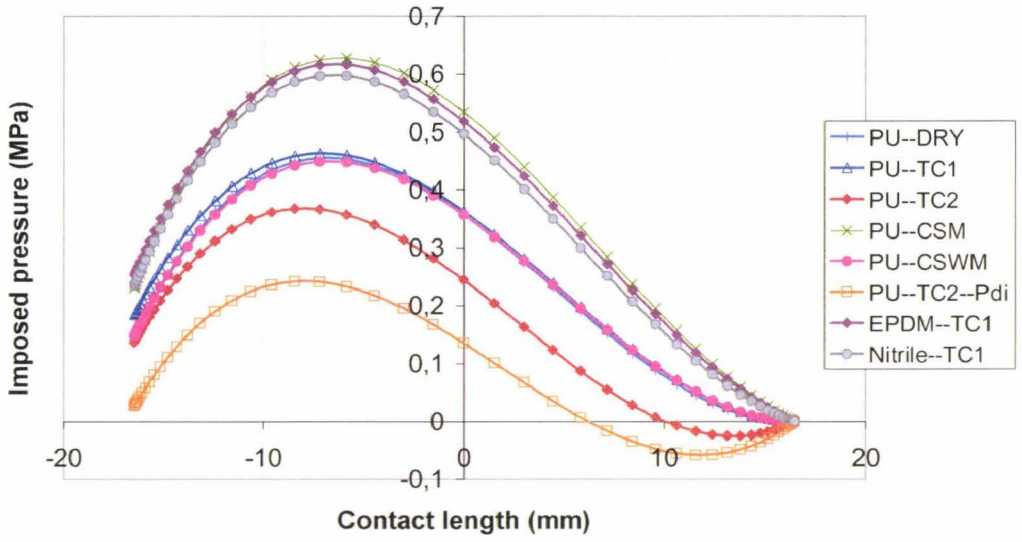

Figure 3-30: Imposed pressure in the free surface F.E.M for the different behaviour laws, initial compression 2mm, Ls=85m/min, Va=110%, Vp=30%, Layer thickness=37,5mm

The maximum pressure is before the centre of the contact. These curves agree with the literature observations [3]. The maximum pressure in the contact is observed for PU-CSM with 0.62MPa. The minimum is 0.25MPa for PU-TC2-PDi.

Three different selected cases: PU-TC1, PU-TC2 and PU-CSM illustrate the results of free surface F.E.M. in the following. TC1 and TC2 are the used paint of the chapter 2 experimental investigation. PU-CSM is the cleaning solvent used during trials.

- **Velocity vector**

Figure 3-31 presents the velocity vector in the meniscus zone for PU-TC1 in negative gap mode. The gap between rolls is around 70µm. The film splits in two unequal wet thicknesses near the meniscus. We only present the PU-TC1 since there are no important differences between PU-CSM, PU-TC1 and PU-TC2 for the speed vector field. We can show a low speed area (70mm/s) near the meniscus. The applicator roll speed is around 1560mm/s (110% of 85m/min

line speed) and the pick-up roll speed is 425mm/s (30% of 85m/min line speed). Moreover, there is no recirculation of fluid near the free surface as exposed in the literature [40], [10].

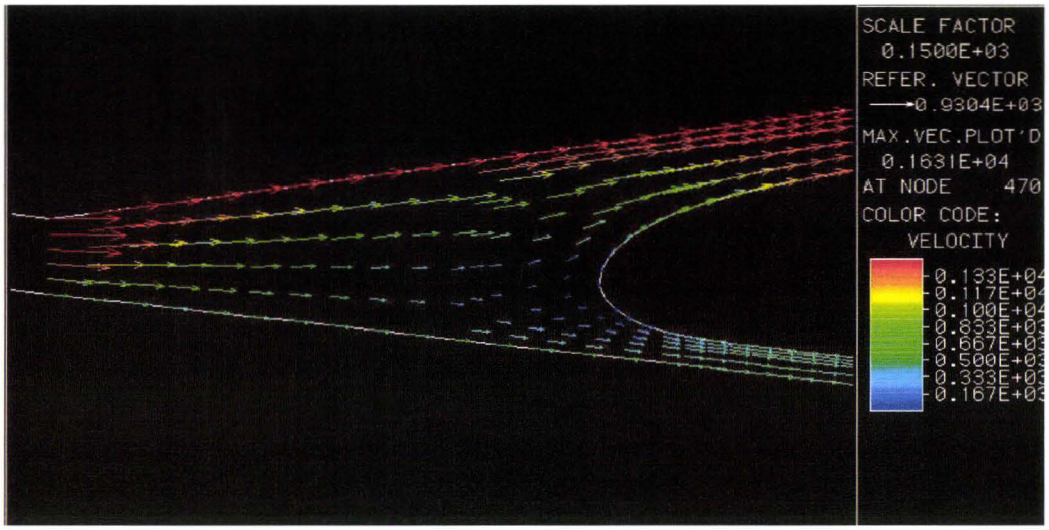

Figure 3-31: Velocity vector for PUTC1 case, initial compression 2mm, Ls=85m/min, Va=110%, Vp=30%, Layer thickness=37,5mm

Figure 3-32 illustrates a case with fluid recirculation near the free surface. The gap between rolls is 2mm and the dynamic viscosity is 1Pa.s. The roll speed is very low around 1mm/s.

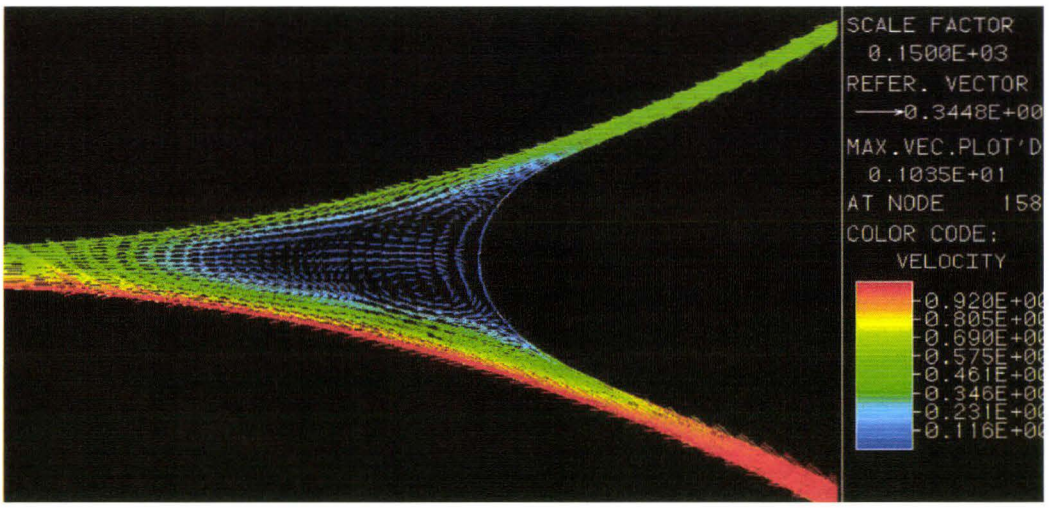

Figure 3-32: Velocity vector for a rigid roll case, positive gap of 2mm

This type of speed vector field never appears in our industrial negative gap mode. The free surface area is smaller than the positive gap mode one. The meniscus is closer to the contact output. In the negative gap mode, the elastomer viscoelasticity is a mainly parameter and affects the pressure in the

contact. A modification of the pressure modifies the free surface position near the contact exit. In the next paragraph, the free surface F.E.M simulation results highlight this pressure influence on the free surface position and then on the ribbing defect wavelength.

- **Free surface position**

Figure 3-33 exposes the free surface position results for the three selected cases. The three-selected behaviour law are PU-CSM, PU-TC1 and PU-TC2. The used fluid properties are the one of Topcoat 1 (TC1) paint. In fact, TC2 properties are very close to the TC1 properties.

The parameters of the simulation are Ls=85m/min, Va=110% of Ls, Vp=30% of Ls, Poisson ratio=0.49, applicator diameter=265mm, pick-up diameter=290mm, layer thickness=37.5mm, initial compression=2mm. The difference is the imposed pressure boundary corresponding to the behaviour law.

We can show a modification of the free surface position as a function of contact pressure. The minimum free surface position is 16.85mm for the PU-CSM case. The maximum free surface position is 17.03mm for the PU-TC2 case. The PU-TC1 is between the PU-CSM and PU-TC2.

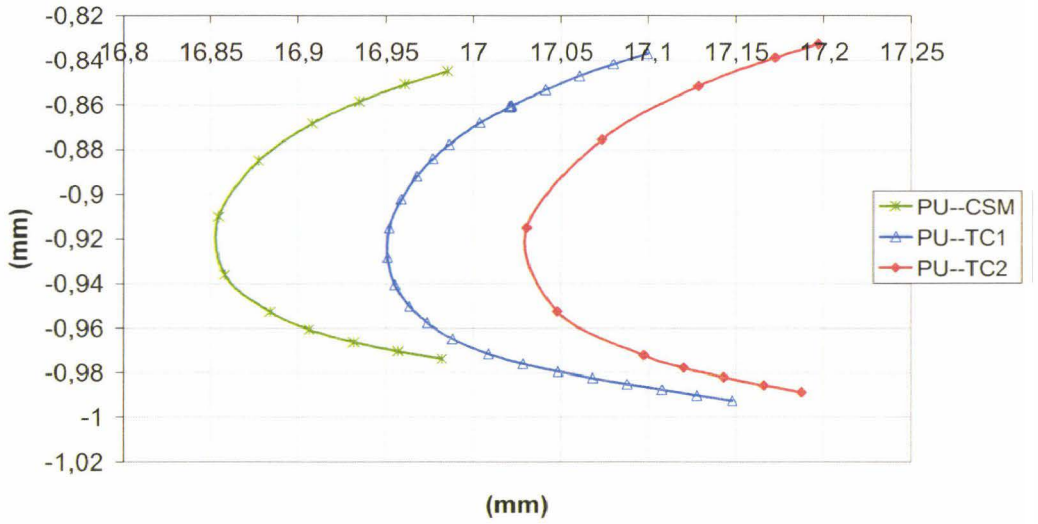

Figure 3-33: Free surface position for three different elastomer and TC1 paint, initial compression 2mm, Ls=85m/min, Va=110%, Vp=30%, Layer thickness=37,5mm, WL

The correlation between this free surface position and the three dimensional ribbing wavelength is essential to use these model in a predictive way to reduce ribbing.

Adachi [32] studied the ribbing instability for a rigid roll-plate apparatus. Figure 3-34 illustrates the link between ribbing wavelength and free surface position. The ribbing amplitude and wavelength increases when the free surface moves far from the contact exit. Inversely, the ribbing wavelength and amplitude decreases when the free surface comes in the contact.

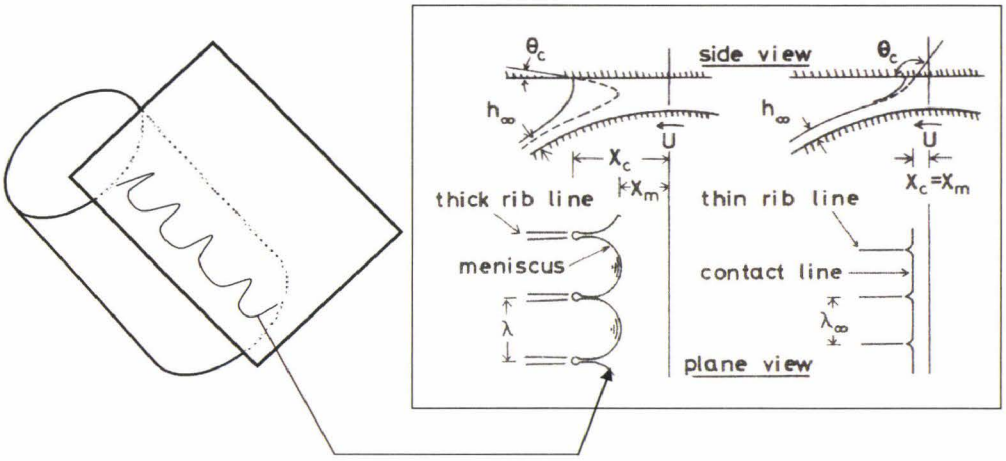

Figure 3-34: Adachi experimental observation between ribbing wavelength and meniscus position

In our experimental investigation, we have performed different ribbing wavelength photography on the deformable roll. Two different paints have been tested TC1 and TC2. Table 3-6 sums-up the experimental results for the corresponding numerical simulation.

Table 3-6: ribbing wavelength and associated wet thickness for TC1, TC2 and WL, Ls=78m/min, Va=110%, Vp=30%

	Low load WL 6866N/m
TC1	
ep(µm)	32
λ(mm)	**1.49**
TC2	
ep(µm)	33
λ(mm)	**1.79**

The experimental observations show a higher ribbing wavelength for TC2 than TC1. The wet thicknesses are the same and have no influence on the result. A comparison with the numerical free surface position for TC1, TC2 is performed. In Figure 3-33, we can show a difference between TC1 and TC2 free surface position. TC2 free surface is far from the contact exit than TC1 free surface. We can consider a relation between the free surface position and the ribbing wavelength. A free surface position far from the contact exit will imply a long

ribbing wavelength. This hypothesis agrees with the literature observation and our experimental investigation. The idea will be to establish a law to determine the ribbing wavelength as a function of the bidimensional free surface position as Figure 3-35.

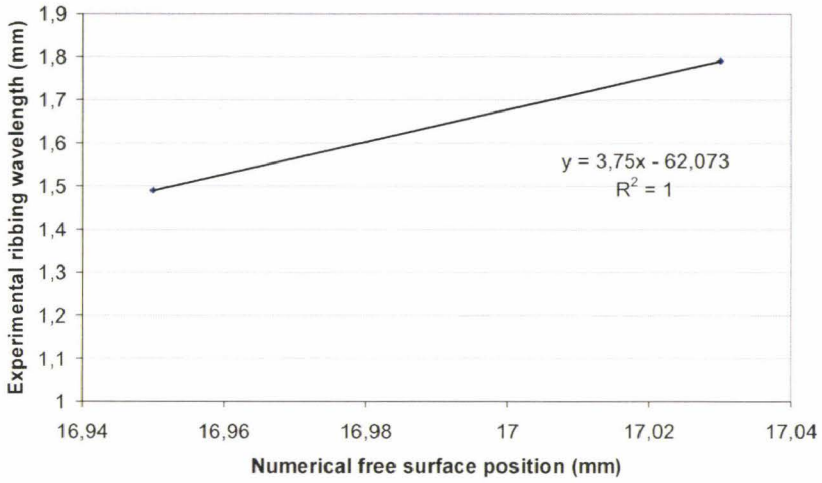

Figure 3-35: experimental ribbing wavelength as a function of the numerical free surface position

In addition, we can add the experimental exterior load influence on the ribbing wavelength. In our experimental investigation, different applied load have been tested to evaluate this parameter influence on the ribbing wavelength. We have shown a ribbing wavelength decreasing when the imposed load increases between rolls (Figure 3-36).

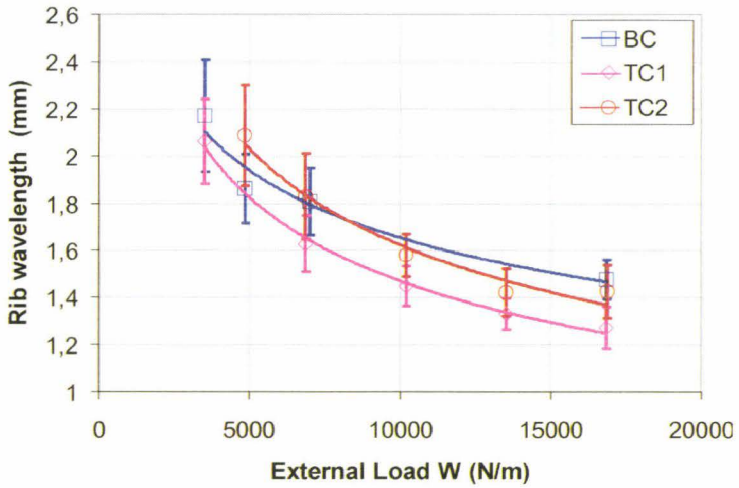

Figure 3-36: Experimental applicator ribbing wavelength as a function of the imposed external load between rolls for the three paints BC, TC1 and TC2

In this experimental approach, the exterior load modifies the ribbing wavelength. This load modification implies a pressure variation in the contact as a function of the elastomer behaviour and chemical environment. Moreover, this pressure in the contact variation can be assimilated to an elastomer behaviour modification. The ribbing wavelength during application is a function of the elastomer behaviour in chemical environment and imposed exterior load.

The elastomer behaviour and exterior load modify the ribbing wavelength and the wet thickness. An analysis of this influence is proposed in the next paragraph.

➢ **Elastomer behaviour law influence on the wet thickness**

The numerical simulation for the three different behaviour law PU-TC1, PU-TC2, PU-CSM permits to obtain the pick-up and applicator roll wet thicknesses. On one hand, the numerical pick-up wet thickness for the three cases is 33µm. On the other hand, the applicator wet thickness is different in the three simulation:

- Ea_{num} = 58µm for PU-CSM
- Ea_{num} = 65µm for PU-TC1
- Ea_{num} = 80µm for PU-TC2

We can show for a same pick-up wet thickness an increasing of the applicator wet thickness when the pressure in the contact decreases. In opposite way, the free surface is far from the contact exit and the ribbing wavelength increases when the pressure in the contact decreases(Figure 3-33, Table 3-6). A goal in relation with the production line is to target a wet thickness on the strip. In fact, we consider the wet thickness on the strip equals to the applicator wet thickness. This wet thickness will be obtained by a modification of the exterior load or by roll speed compensation.

➢ **Roll speed influence on the meniscus position**

The experimental approach in the chapter 2 has shown the roll speed influence on the final wet thickness. Experimentally, it was impossible to define its influence on the ribbing wavelength. The free surface F.E.M simulation could permit to obtain the roll speeds influence on the ribbing wavelength and especially on the free surface position. The PU-TC1 is selected for this study and Figure 3-37 illustrates the results. The pick-up roll speed increases from 35% to 60% of Line speed for a constant applicator roll speed at 101% of Line speed. This speed increasing involves a free surface shifting to the output contact. The minimum free surface position is 16.93mm for (Va=101%,

Vp=35%). The maximum is 17.01mm for (Va=101%, Vp=60%). A set of computation are performed with Vp constant to complete these results.

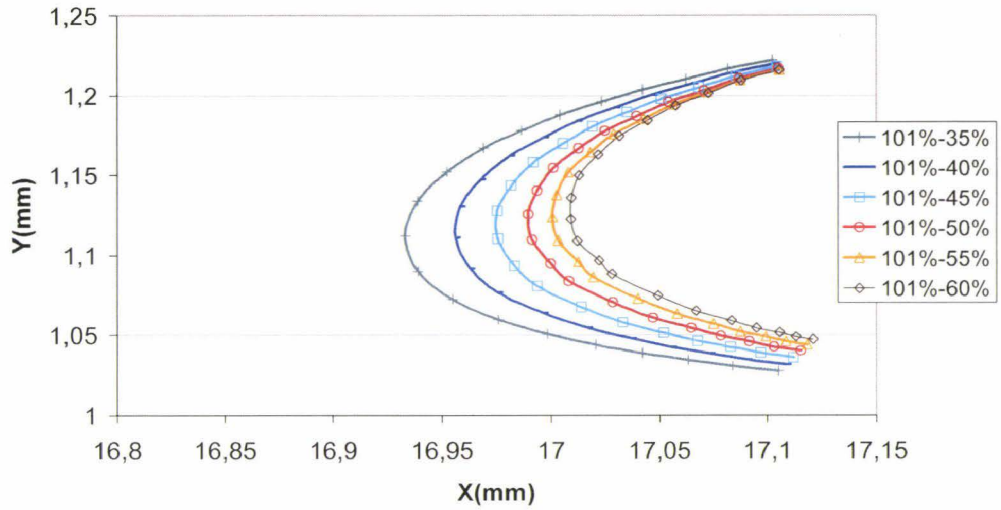

Figure 3-37: free surface position, Vl=85m/min, Va=101%, viscosity=0,51Pa.s, surface tension=0,035N/m, Vp variation from 35% to 60%

Figure 3-38 shows the applicator roll speed increasing influence on the free surface. The applicator roll speed increases from 100% to 120% of Ls for a constant pick-up roll speed at 30% of Ls.

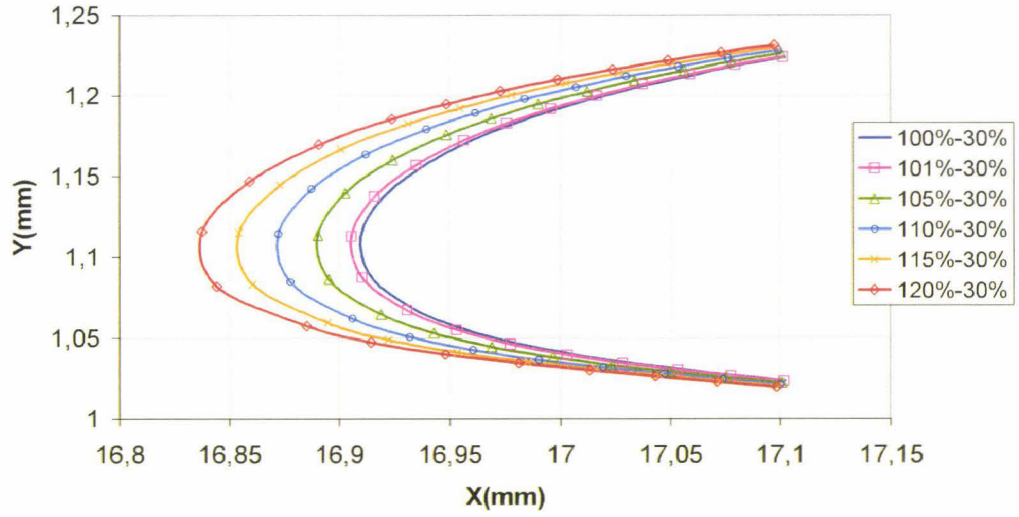

Figure 3-38: free surface position, Vl=85m/min, Vp=101%, Vp=30%, viscosity=0,51Pa.s, surface tension=0,035N/m, Va variation from 100% to 120%

This speed increasing involves a free surface shifting in the contact. The minimum free surface position is 16.83mm for (Va=120%, Vp=30%). The maximum is 16.92mm for (Va=100%, Vp=30%).

On one hand, the accurate numerical results permit to show the rolls speeds influence on the free surface position. The applicator roll speed increasing seems to improve the application quality by a decreasing of the ribbing wavelength through the free surface position. In opposite way, the pick-up roll speed seems to damage the application quality by a increasing of the ribbing wavelength.

On the other hand, the experimental investigation does not permit to have the same observations. In fact, the used image analysis tool is not enough accurate to feel the roll speed influence face to the imposed external load impact on the ribbing defect. An improvement of the data processing would be interesting to complete this study.

The roll speed influence has been exposed above. These rolls speeds modification improve or degrade the film quality during application. In parallel, this roll speed modification involves a modification of the wet thickness. The next paragraph deals with this wet thickness variation as a function of the roll speeds.

- **Roll speed influence on the wet thickness**

Figure 3-39 sums-up the numerical wet thickness results. The applicator roll speed is constant at 101% of Line speed and the pick-up speed increases from 15% to 60% of Line speed.

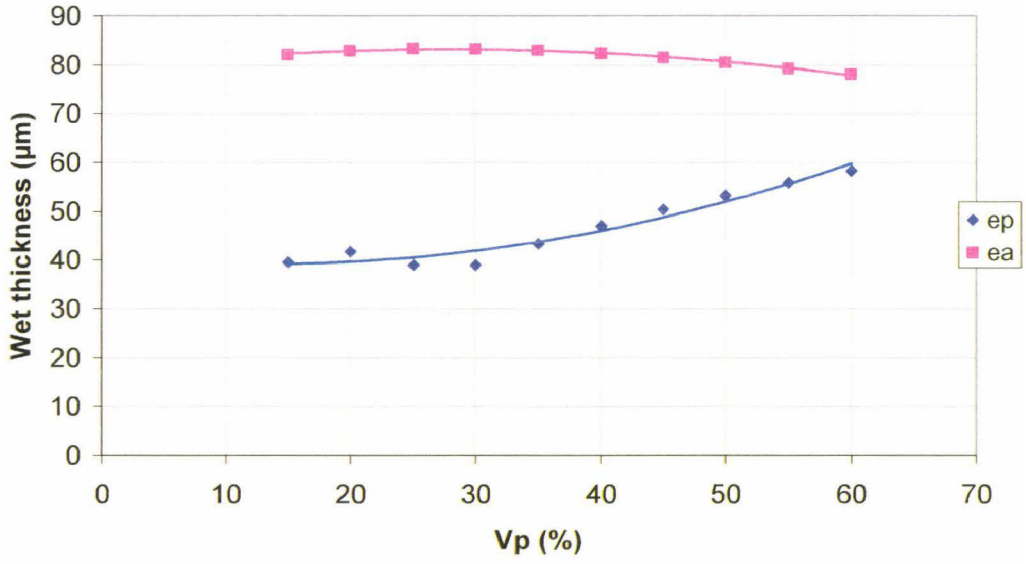

Figure 3-39: numerical wet thickness, Va=constant, Vp increases, Ls=85m/min, initial compression=2mm, paint: TC1

First, we can show a pick-up wet thickness increasing with the pick-up roll speed. The minimum pick-up wet thickness is ep=40µm and the maximum pick-up wet thickness is ep=60µm.

Second, the applicator roll wet thickness seems to be constant. The maximum applicator roll wet thickness is ea=82µm and the minimum is ea=78µm.

The pick-up roll speed has an influence on the pick-up wet thickness. The applicator roll wet thickness does not evolve.

Figure 3-40 sums-up the numerical wet thickness result. The pick-up roll speed is constant 30% of Ls and the applicator roll speed increases from 100% to 120% of Ls.

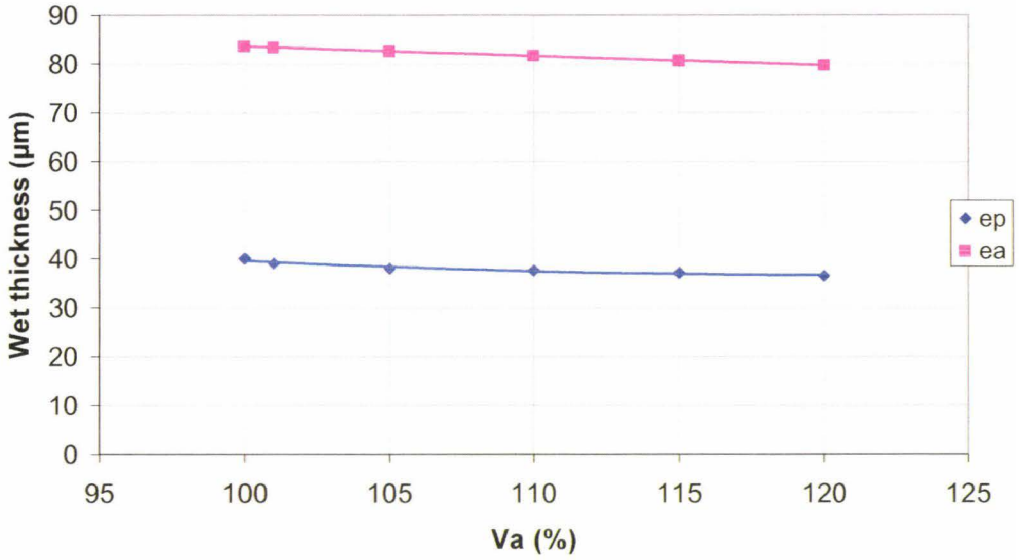

Figure 3-40: numerical wet thickness, Vp=constant, Va increases, Ls=85m/min, initial compression=2mm, paint: TC1

The applicator roll speed has less influence than pick-up roll speed on the pick-up wet thickness and applicator one. The applicator and pick-up rolls wet thickness are respectively 80µm and 40µm.

The applicator roll speed increasing seems to reduce the ribbing wavelength by a shifting of the free surface position in the contact exit. In opposite way, we can show that the pick-up roll speed increasing damages the paint application with a shifting of the meniscus far from the contact exit. In addition, this pick-up roll speed variation implies an increasing of the wet thickness on it.

Experimentally, we have shown a pick-up wet thickness increasing with its roll speeds increasing. This observation agrees with the numerical study. We do not have experimental data for the applicator wet thickness and then no correlation with the numerical results observation.

For the ribbing wavelength defect, we do not observe a decreasing when the applicator roll speed increases. This remark must be linked to the image analysis accuracy. In fact, the ribbing wavelength variations to the roll speed are too small to be detected by this technique.

➢ **Wet thickness : numerical prediction and experimental data comparison**

To complete and validate the different above observations, Figure 3-41 compares experimental wet thickness measurements, numerical model predictions and Cohu power law results [28]. The comparison is proposed for two load cases (WL=6866N/m and WH=16866N/m).

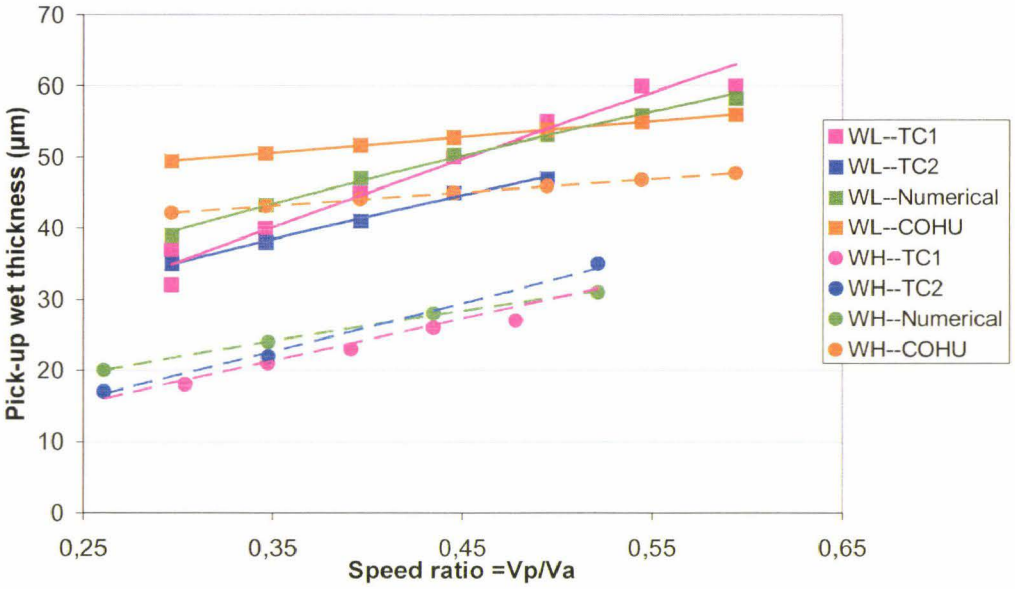

Figure 3-41: Numerical prediction and experimental measurement comparison

On one hand, we can observe a good approximation between numerical model prediction and experimental data. This agreement is found to be good for the two load cases WL, WH.

On the other hand, the results with the power law of Cohu are less accurate than finite element model prediction. Table 3-7 sums-up some results from the curves presented above.

Table 3-7: Relative error between experimental wet thickness, numerical simulation and Cohu power law for two roll speeds couple (101%-30%), (101%-60%) and two exterior load (WL, WH)

	TC1	Numerical	Error(%)	Cohu	Error(%)
101%-30%					
WL	37,00	39,00	5,41	49,00	32,43
WH	23,00	20,00	-13,04	42,00	82,61
115%-30%					
WL	55,00	53,00	-3,64	53,00	-3,64
WH	35,00	28,00	-20,00	45,00	28,57
Average					
WL			**0,88**		**14,40**
WH			**-16,52**		**55,59**

A relative error in (%) notes the accuracy of the F.E.M model and Cohu results to the experimental data. There are two speed couples and two load cases in this table.

- (WL): The numerical model predicts a wet thickness 0.88% higher than the experimental measurement. Cohu predictions are 14.4% higher than the experimental wet thickness in average.
- (WH): The numerical model predicts a wet thickness 16.5% lower than the experimental measurement. Cohu predictions are 55.6% higher than the experimental wet thickness in average.

The wet thickness predictions of the developed F.E.M model are accurate. The relative error is in the range [-3%; 5%] for WL and [-13%; 20%] for WH to the experimental measurement.

4. Conclusion

In this chapter, the roll coating process has been studied through a numerical strategy. This numerical approach permits us to understand the physical mechanisms acting on the flow in the gap. The studied parameters are the elastomer behaviour, imposed load between rolls, elastomer layer thickness and rolls speeds. A specific cyclic compression tests with chemical environment are performed to study the elastomer behaviour. An identification methodology is used to determine elastomer behaviour law from these tests. The identified behaviour law will feed the numerical simulation of the roll coating process.

The numerical simulation was performed in two steps to understand roll coater parameters influence on the final application. The first is a deformable simulation of the contact between the applicator and the pick-up roll. The goal is to obtain the mechanical pressure in the contact and associated load reaction

as a function of the elastomer behaviour law and layer thickness. The next step was the free surface flow simulation with the mechanical pressure of the deformable simulation as boundary condition. The goal was to have the free surface position and associated wet thickness on each rolls.

First, we have shown the chemical environment impact on the elastomer behaviour through the cyclic compression test. The different determined behaviour laws bring different mechanical pressures in the contact for the same roll coater configuration. The Young modulus and relaxation time of elastomer evolves as a function of the paint or used solvent. The relaxation time can be lower or higher than the solicitation time in the contact. The relaxation time has two influences on the application:

- A flow rate modification in the contact (wet thickness)
- A free surface position modification (ribbing defect)

The flow rate increases for a lower relaxation time to the solicitation time. The contact shape evolves by an increasing of the gap and the pressure in the contact decreases. The result is a free surface variation as a function of the pressure in the contact. An high pressure in the contact involves a meniscus closes to the gap exit and inversely. Inline, the increasing of the external load between rolls i.e., a pressure increasing in the contact, involves a ribbing wavelength and amplitude decreasing. Adachi [32] observes the same phenomenon in his experimental study.

In opposite way, the flow rate is constant for a relaxation time higher to the solicitation time. The gap shape does not evolve and the pressure in the contact is maximum. The difficulty is to define the relation between the pressure in the contact and the ribbing wavelength. For a same roll coater and contact geometry, the result can be different for two chemical environments and the same elastomer.

The second result is the influence of the elastomer layer thickness on the roll coater adjustment. In fact, the layer decreasing involves an higher mechanical pressure in the contact for a same roll coater configuration. This pressure increasing involves a flow rate decreasing. The goal will be to create abacus of adjustment as a function of the diameter for the inline operator.

We have shown the pressure impact on the flow rate by the modification of the elastomer behaviour law and layer thickness. Carvalho analysed the layer thickness and viscoelasticity influence on the flow rate. The conclusions on the flow rate are the same [42]. Inline, the roll speed seems to have an importance on the wet thickness and application quality. The experimental investigation has shown a real influence of the pick-up roll speed on the wet thickness but no

influence on the ribbing wavelength. The ribbing wavelength variation to the roll speed seems too sensible for the used measurement technique.

The numerical roll speed study shows wet thickness modification and free surface position variation for a single behaviour law. The free surface position is near the contact exit when the applicator roll speed increases and for a constant pick-up roll speed. The free surface position is far from the contact exit when the pick-up roll speed increases and for a constant applicator roll speed. The numerical wet thickness increases with the roll speed as the inline observations.

A free surface position modification has been observed as a function of elastomer behaviour and roll speed. This free surface position is the link with the ribbing defect problem. In fact, the numerical study is based on bidimensional analysis and the defect is a three dimensional instability. To face this problem, an hypothesis of work has been proposed. The literature and inline observation show a variation of the ribbing wavelength as a function of the meniscus position. We have linked our inline ribbing wavelength measurement to the corresponding free surface F.E.M simulation. The results was a long ribbing wavelength for a long distance free surface position and inversely. From this result, we consider our hypothesis validate. It is possible to evaluate the ribbing wavelength as a function of the bidimensional approach and with its associated parameters.

The link between pressure in the contact (behaviour law, fluid properties, elastomer layer thickness and imposed load) and the roll speed (Ls, Va, Vp) is essential to improve and standardise the roll coater adjustment. In this chapter, we have studied the inline adjustment parameters with the chemical environments influence on the elastomer response. This bidimensional numerical study is based on some work hypothesis to correlate the three dimensional experimental data. A new research way is proposed to complete knowledge. This is a three dimensional approach. These new ways are based on the surface finishing impact on the pressure in the contact and three-dimensional F.E.M simulation of the ribbing. A complementary non-Newtonian model for the fluid is also proposed and face to the present bidimensional model.

Conclusion

In this work, a three deformable roll coater in industrial context has been studied. This study was axed towards the negative gap mode as usually used in MYRIAD and other CORUS plants. This negative gap mode permits to depose thinner wet thickness on the strip than in the positive mode. The goal was to highlight key adjustments and material parameters acting on the paint application control and flow stability. In order to analyze, to understand and to optimize this process both experimental and numerical approaches have been proposed. Moreover, a specific test has been developed to analyse the elastomer roll cover behaviour in the process environment.

A literature review on this topic allowed us to understand the different roll coating applications. We have shown many works and differences on the flow between rolls defined by rigid gap, deformable gap, forward mode and reverse one. The different authors have studied the film splits and the ribbing defect occurrences in both experimental and theoretical approaches. One of the most important problems is the observed differences between testing stand and industrial roll coater results. These differences are very important in term of wet thickness prediction and ribbing wavelength evaluation. In our study, an experimental investigation on industrial roll coater is proposed. The main goal is to understand application and ribbing defect evolution during the process. The hypothesis to transfer results on industrial plant is decreased in this case.

The first research axis in this work was the experimental investigation on the industrial roll coater. The goal was to reproduce exact industrial conditions (dimensions, speeds, imposed external load, elastomeric roll cover properties and thickness, coil coating paints, temperature, and vibrations) to study the ribbing defect and the wet thickness. Different parameters measurements have been done to create a complete database. Moreover, a specific image analysis tool has been developed to evaluate the ribbing wavelength on the applicator roll. This "experimental-industrial investigation" has highlighted the key parameters acting on the ribbing defect and the wet thickness.

The experimental observations and measurements have mainly shown an external load impact on both ribbing wavelength and wet thickness. The higher is the external load between applicator roll and pick-up roll, the lower are the ribbing wavelength and wet thickness. Moreover, we have shown the pick-up roll speed influence on the wet thickness. For an imposed external load, increasing the pick-up roll speed increases the wet thickness on it. For high negative gap, we have observed a decreasing of the external load influence on the ribbing wavelength and wet thickness. In this case, the elastomeric roll

cover and its viscoelastic properties are dominant to control the flow rate and the film stability. Moreover, the operator inline experiences show a variation of the wet thickness and ribbing wavelength along the production and for a same roll coater adjustment. This variation has been explained by the paint and solvent influence on the elastomer behaviour.

This elastomer behaviour modification has been studied by a specific compression test. The upsetting and relaxation undergone by the elastomer during paint application are reproduced in laboratory in chemical environment. We have shown an evolution of the elastomer load response according to the time. In fact, this load modification can be directly linked to the inline wet thickness increasing or decreasing. The solvent influence on the elastomer is clearly highlighted but more analysis with different paints and for other elastomers are needed to increase the knowledge. This knowledge will be help us to predict the wet thickness variation according to the time during paint application.

In order to understand these experimental observations, the second research axis is the numerical modelling of the process. Two finite element simulations have been used to perform these numerical analysis.

The first is the deformable simulation with a solver of mechanics of solids. It has been used to study the roll coater geometry and elastomer viscoelastic properties influence on the mechanical pressure in the gap between rolls. The behaviour law to feed the deformable simulation comes from the specific cyclic compression test in chemical environment and a coupled identification methodology. The result is a Prony series to model with accuracy viscoelastic behaviour of the elastomer in the simulation. This deformable numerical simulation has shown the elastomer properties and layer thickness influence on the mechanical pressure in the gap. For different chemical environment, the same elastomer has different behaviour and the response in the contact is modified. In fact, the elastomer Young modulus and relaxation time evolves with the solvent or paint. We have shown the relaxation time influence on the mechanical pressure in the gap. As a function of the roll frequency of rotation, the relaxation time can modify the flow rate in the gap and then the stability of the film. This influence is observed for relaxation time lower than the solicitation time in the gap. The next simulation helps us to analyse the elastomer behaviour impact on the flow rate.

The second simulation has been used to understand the influence of the elastomer and roll coater geometry on the wet thickness and ribbing defect. This free surface finite element simulation uses a solver of mechanic of fluid. It is performed with the mechanical pressure of the deformable simulation as boundary condition to reproduce the elastomer influence on the flow rate. This simulation has permitted to analyse elastomer properties and roll speed ratio

influence on the wet thickness and free surface position. The wet thicknesses and ribbing wavelength can be different for a same roll coater adjustment. This difference is explained by the elastomer behaviour as a function of the paint or solvent. The mechanical pressure in the contact evolves and then, the free surface position and wet thickness are modified. The roll coater mastering is a function of standard adjustment parameters and elastomer behaviour prediction for the associated chemical environment. An accurate knowledge of the elastomer behaviour is essential to prevent wet thickness variation during application and then, ribbing wavelength modification.

To complete understanding, the film split ratio study is performed. Experimentally, the increasing of the external load decreases the ribbing wavelength but in the same time, the wet thickness decreases on the pick-up roll. To face this problem, the pick-up roll speed increasing is a part of the solution to obtain the targeted wet thickness with a minimum of ribbing. We can show a modification of the free surface position with the pick-up roll speed increasing in the numerical simulation. This acceleration seems to increase the ribbing wavelength but the imposed external load has more influence than speed on the defect wavelength. Experimentally, this pick-up roll increasing influence on the ribbing is not seen since the measurement technique is not accurate enough for high external load.

The coupled experimental and numerical studies have highlighted different direct parameters influence:

External load and speed are the two direct parameters to control the flow rate and the ribbing wavelength. To limit the external load on the roll coater and increase the mechanical pressure in the contact, a lower elastomeric layer thickness can be used. In parallel, we have shown the importance of the elastomer behaviour modification as a function of the chemical environment. Moreover, this parameter is dominant in high negative gap when the ribbing wavelength is very low. A work on the elastomer to obtain a neutral behaviour in the time is essential to master the roll coater. As a function of the different paints, solvent and elastomer, a maximum knowledge on their interactions is essential to predict the roll coater behaviour during application.

Outline studies

1. Outline

In the two previous chapters, the basis of work was an optimization of the usual application on the Myriad plant. From the different inline adjustment parameters (geometry, roll speed, external load and materials properties), a complete analysis by experimental and numerical approach has been performed. This analysis allowed to highlight the key parameters acting on the ribbing wavelength and wet thicknesses. From the different observations and investigations, it is possible to improve the liquid paint application. In order to get better the understanding of the ribbing defect occurrence, new research axes are proposed. The new goal is to identify the ribbing defect origin. The different research axes are defined as follows:

- The first approach is the applicator roll surface finishing influence on the paint application quality. During its service-life, the applicator roll undergoes surface finishing to recover both mechanical properties and surface aspect. This surface finishing involves diameter decreasing and new surface roughness. From the surface roughness measurement on industrial applicator roll, a three dimensional numerical simulation will be performed to obtain the corresponding contact pressure in the contact. Using the same methodology as in chapter 3, a free surface F.E.M simulation with the pressure result as boundary condition will permit us to obtain the free surface shape and position. The goal is to have the numerical ribbing wavelength for a specific roll coater adjustment.

- The second approach is the inline vibration influence on the liquid paint application. The roll coater undergoes vibration by its contact with the strip, the roll rotations and others machine on the plant. Moreover, the roll coater has no vibration insulating. A three dimensional simulation of the applicator roll is proposed and allows us to extract the eigenvalues. These extractions will get the different critical natural frequencies of vibration and the associated mode shapes.

2. Roll roughness influence on the paint application

This part deals with the three dimensional modelling of the contact between applicator and pick-up rolls to evaluate the applicator roll roughness influence on the paint application. A three dimensional deformable F.E.M simulation is performed with a roughness profile on the deformable roll. The pressure results will be introduced in the free surface FEM simulation to study the free surface stability. The elastomer layer thickness (30mm) in this simulation is lower than the case proposed in the chapter 3 (37.5mm). It is a simple approach to evaluate the possibility of the 3D roughness modelling with other roll coater geometry.

2.1 Inline roughness measurement

The first step is the roughness measurement. The different roughness measurements are performed with a mechanical profilometer. The sampling length is 50mm at 2mm/s by zone. The measurement is performed on three different zones along the roll length. Two values define the surface finishing quality. The wavelength P(mm) and the amplitude Wm(µm). Figure 4-1 illustrates the three measurement zones on the roll.

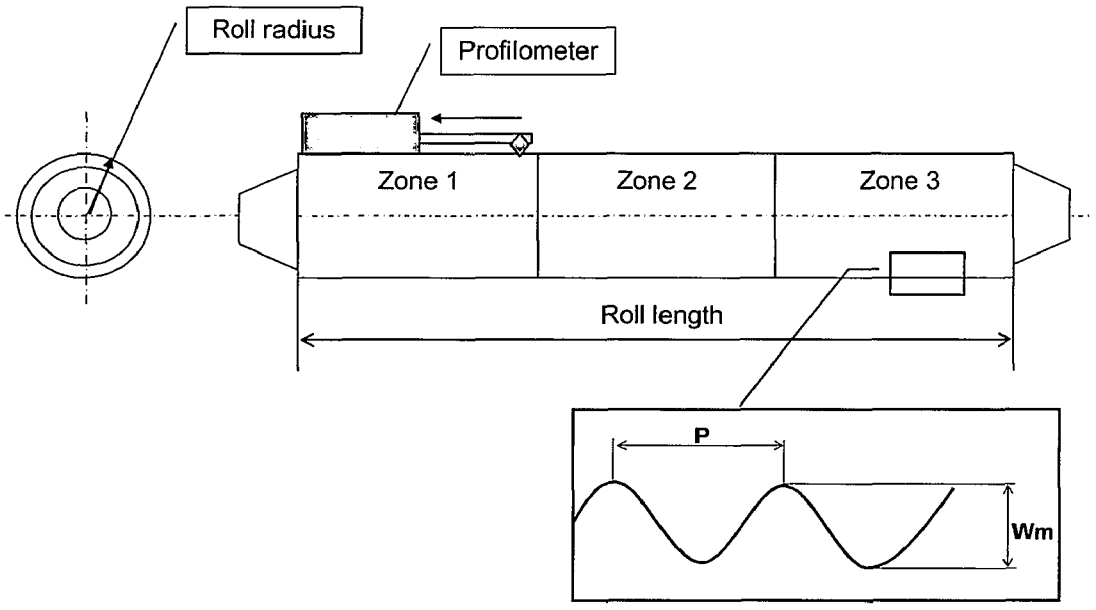

Figure 4-1: measurement zone on the applicator roll

Table 4-1 sums-up the obtained results for each zone and the average roughness.

Table 4-1: Roughness measurements on the applicator roll

Zone1		Zone2		Zone3		Average	
P(mm)	Wm(µm)	P(mm)	Wm(µm)	P(mm)	Wm(µm)	P(mm)	Wm(µm)
0,59	10,61	0,74	7,92	0,67	9,6	0,67	9,38

The roughness evolves along the roll. A maximum Wm=9.6µm is observed in the zone 3 and a minimum Wm=7.92µm in the zone 2. In a complete analysis the influence of roll grinder accuracy and operator practice on the roll roughness should be experienced. In the following part, we will use the average value with P=0.67mm and Wm=9.38µm.

2.2 Roughness modelling in the deformable contact

2.2.1 Deformable contact details

Figure 4-2 presents the three-dimensional numerical simulation of the deformable contact with roughness modelling on the deformable roll. This simulation is without fluid. To reproduce the influence of the fluid in the contact a friction coefficient of 0.03 is applied between these two rolls [49]. The model is extruded on a 5mm width. Two rigid bodies model the pick-up roll and the core of the applicator roll. The applicator roll exterior diameter is 240mm and the pick-up roll diameter equals 290mm. The elastomer thickness of the applicator roll is 30mm. These two rolls are driven in rotation around their revolution axis. 20592 tetrahedral elements compose the elastomeric roll cover. In our simple analysis, the used behaviour law follows a simple elastic model of (PU) to decrease the computation time and convergence problem encountered with a viscoelastic law. We define a sinusoid with the average value P=0.67mm and Wm=9.38µm to model the roughness on the applicator roll in the three dimensional F.E.M simulation. A 2 mm height initial compression is applied between rolls.

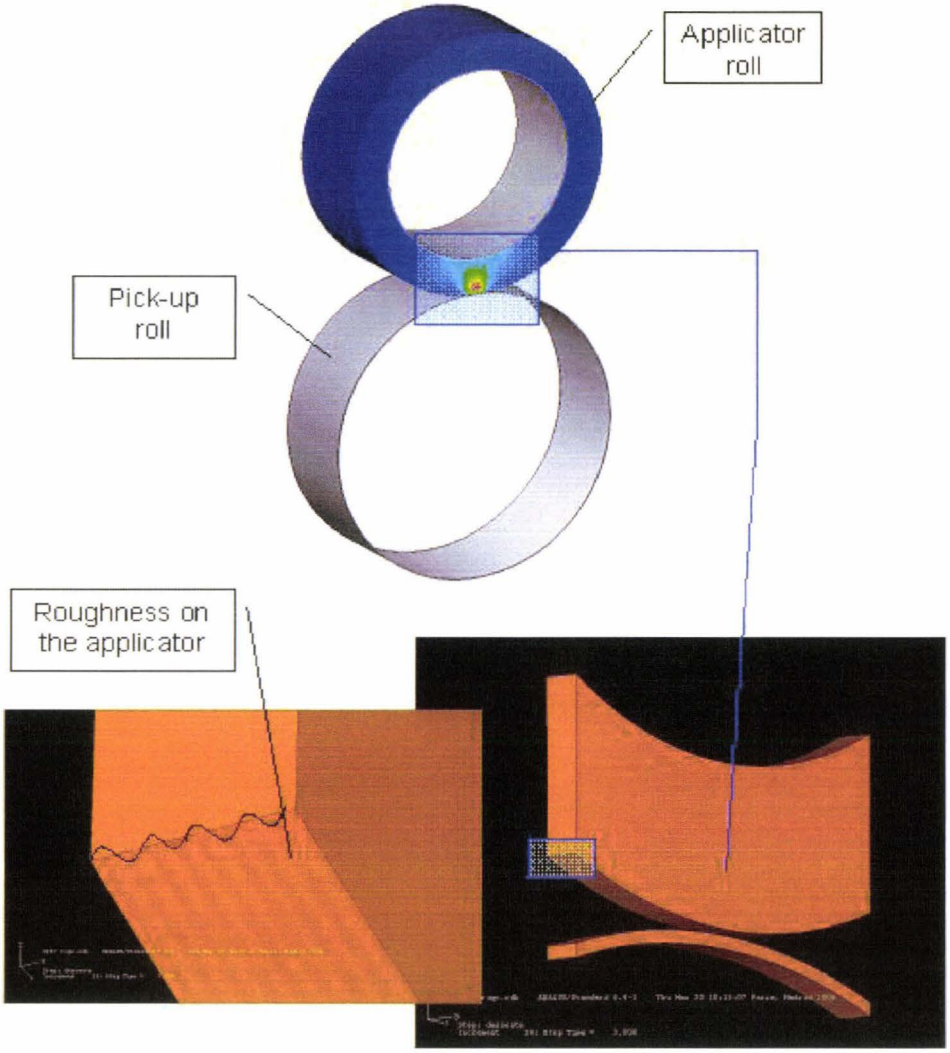

Figure 4-2: deformable F.E.M simulation, roughness modelling on the applicator roll

2.2.2 Deformable model result

Figure 4-3 illustrates the contact pressure print result. Figure 4-4 presents the contact pressure in the contact along the path. The contact pressure along the path is in the range [0.6MPa; 2.1MPa]. Its influence on the free surface position has been discussed in the numerical chapter 3. The free surface (i.e., the fluid meniscus) moves towards the contact with the pressure increasing and then, the ribbing wavelength decreases. Inversely, the free surface moves outwards the contact exit with the pressure decreasing and the ribbing wavelength increases.

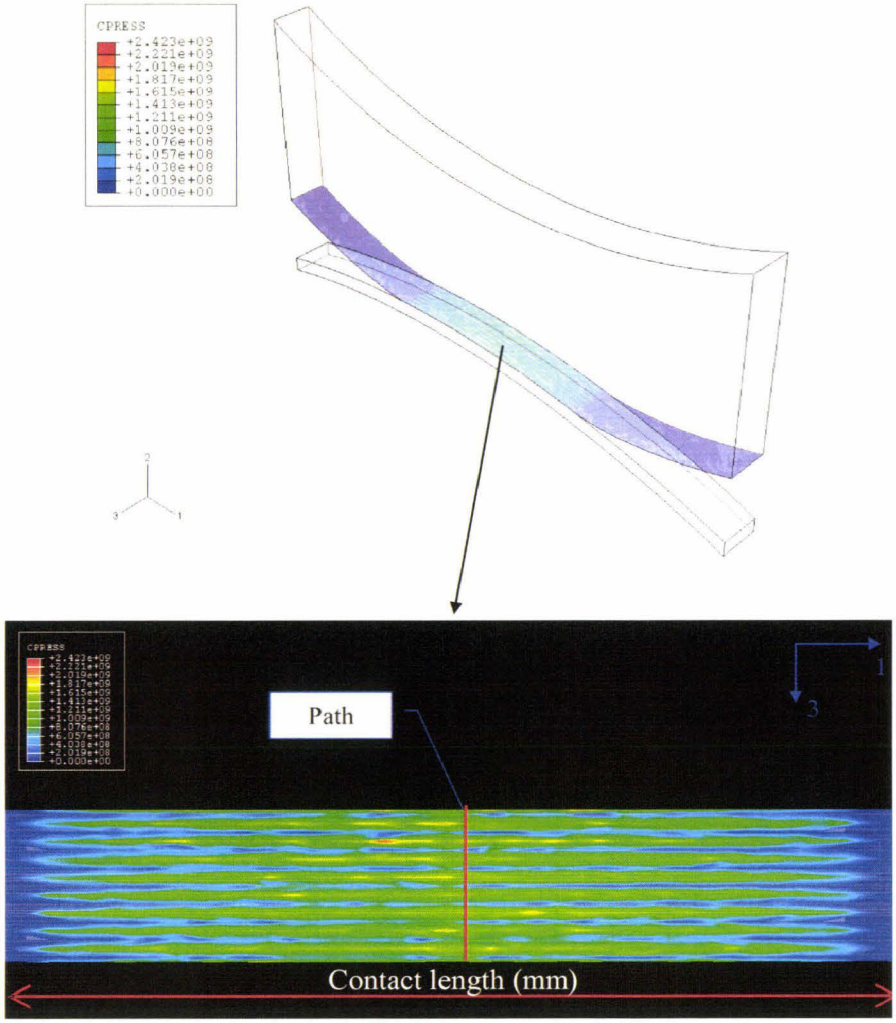

Figure 4-3: Contact pressure print in the contact between rolls

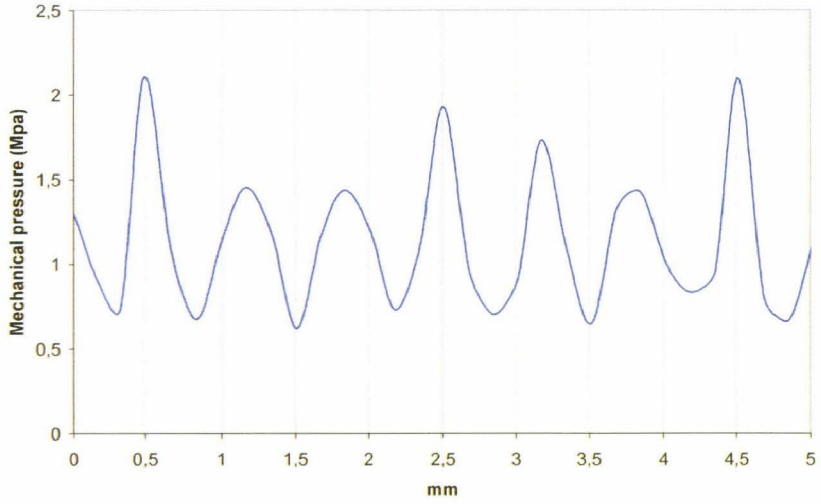

Figure 4-4: Contact pressure along the path in the contact

The contact pressure profile along the path is a function of the surface finishing. The roughness profile acts on the local pressure and the ribbing wavelength will be directly modified as we can see in the chapter 3. The modification of the pressure in the contact involves a variation of the free surface position and then, the wet ribbing wavelength. As an example, a measurement on a dry prepainted workpiece is performed. We can see a sinusoidal profile on the final product with an amplitude in the range [-4µm; 3µm]. This observation leads us to analyze the surface finishing influence on the ribbing wavelength by a numerical fluid approach. An initial perturbation approach is used in the three dimensional F.E.M simulation. This perturbation is evaluated from two-bidimensional simulations. The methodology is exposed in the following part.

2.3 3D free surface F.E.M simulation

2.3.1 Initial perturbation approach

➢ **Methodology**

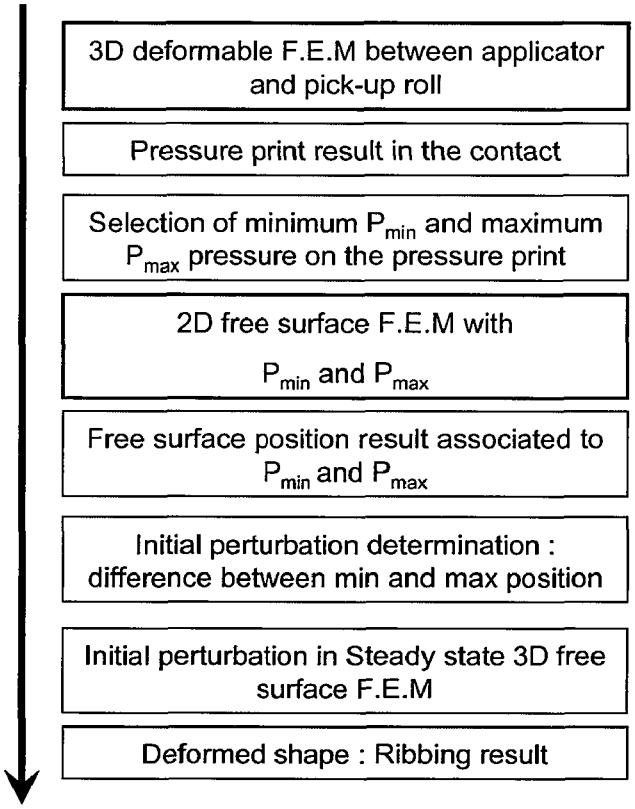

Figure 4-5: Detail of the numerical methodology

This paragraph deals with an initial perturbation approach of the 3D free surface F.E.M to obtain the numerical ribbing defect. The basis of this new approach is the minimum and maximum pressure in the contact using. Figure 4-5 sums-up the different steps of the methodology from the 3D deformable simulation to the ribbing result.

→ The start point of the methodology is the 3D deformable F.E.M simulation (solid) and its contact pressure print result (Figure 4-6).

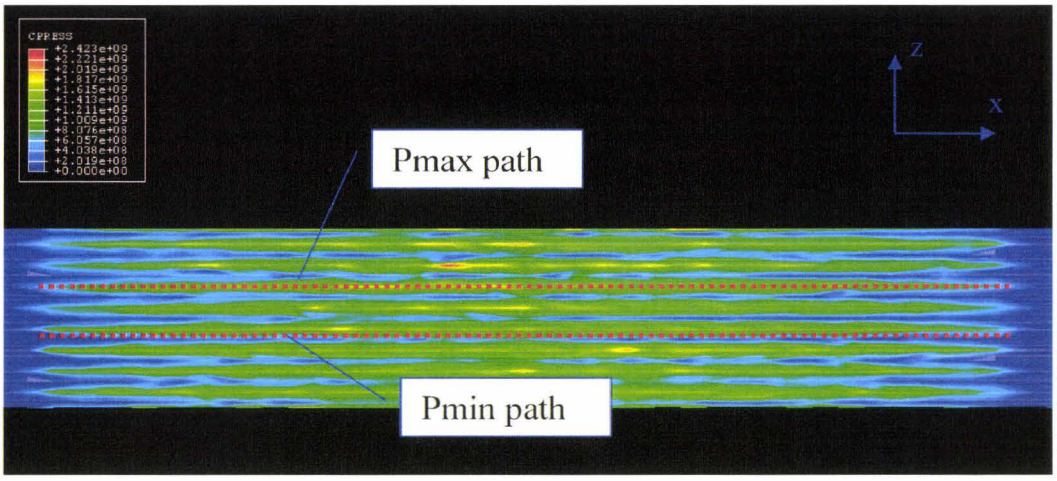

Figure 4-6: Contact pressure print and selected path for P_{max} and P_{min}

→ On the pressure print, we define two paths to obtain a maximum contact pressure and a minimal one in the contact. Figure 4-7 illustrates the two selected pressure curves. These curves are third order polynomial approximations. The maximum contact pressure is 1.6MPa and the minimum is 0.4MPa.

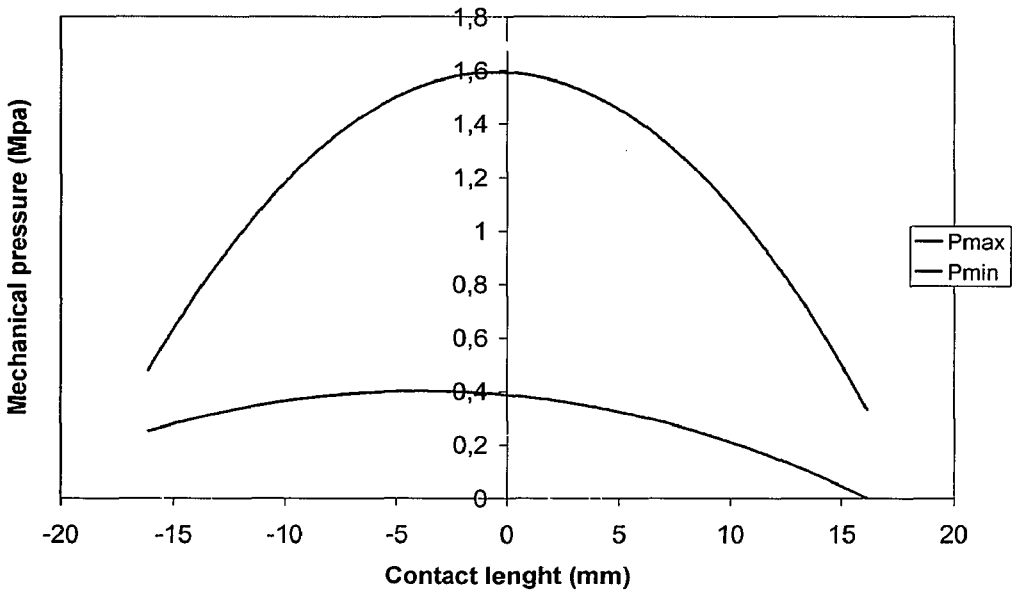

Figure 4-7: Polynomial approximation of the contact pressure in the contact

→ These polynomial approximations are used as boundary conditions in the bidimensional free surface F.E.M (fluid) of chapter 3. The results are two free surface positions. The free surface positions are 16.7mm for the simulation with P_{max} and 17.2mm for P_{min}.

→ The difference between the maximal free surface position and the minimal free surface position gives the initial perturbation. In this case, the initial perturbation is 0.5mm.

→ A first 3D free surface F.E.M simulation is performed to obtain a steady state flow rate. Figure 4-8 shows the result focus on the meniscus.

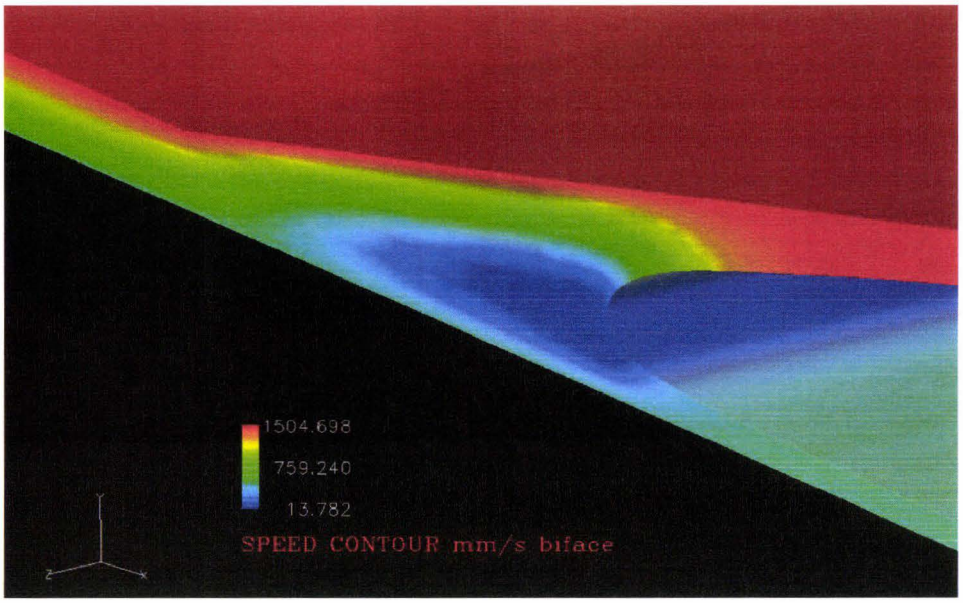

Figure 4-8, Speed contour : 3D free surface F.E.M, steady state flow rate

→ The evaluated initial perturbation of 0.5mm is introduced in the steady state simulation. The goal of this perturbation is to modify the equilibrium of the steady state flow rate to obtain a numerical ribbing. The initial perturbation will be the initial displacement imposed to a free surface node. After convergence of the 3D free surface F.E.M with initial perturbation, a rib between rolls occurs.

➢ Results

Figure 4-9 shows the obtained rib between applicator and pick-up rolls in the 3D free surface F.E.M. The result of the 3D free surface simulation with initial perturbation is the free surface shape. This result is not sufficient to evaluate the ribbing wavelength because there is only one rib. A simulation on 5mm extrusion width with a fine meshing will give best results on the ribbing wavelength evaluation.

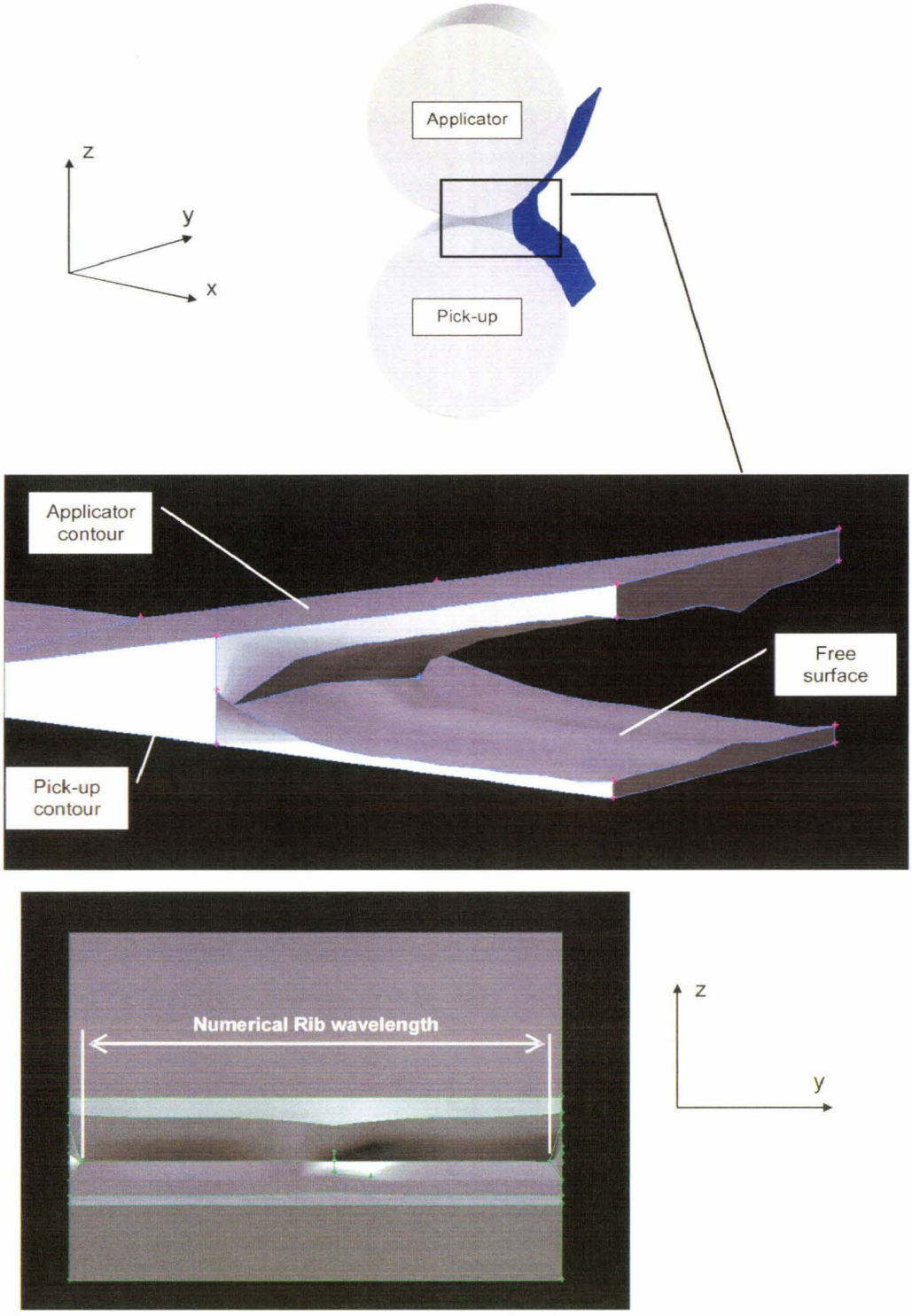

Figure 4-9: Rib result of the 3D free surface F.E.M simulation

In this paragraph, we have exposed the first future work; a new numerical approach to increase the understanding on the ribbing defect occurrence has

been exposed. This 3D numerical approach allows ribbing occurrence for a specific roll coater adjustment. The 3D simulation F.E.M is a step development and could be used in future works. The roll coater parameters influence on the 3D instability could be a research axis to correlate with the inline data. The model requires a larger extrusion in the third dimension to obtain more rib between rolls and to evaluate the defect wavelength.

Inline, different phenomena can disturb the paint application and especially the vibration. The next paragraph will introduce this second research axe.

2.4 Vibration influence on the applicator roll

2.4.1 Model details

This is a three-dimensional approach with free rotation conditions (Figure 4-10). The applicator roll is defined by a deformable part following an elastic (PU) law. This deformable part is composed of 6800 plane strain elements with 4 integration points. The core of the roll is a rigid body since the steel Young modulus of this part is at least 100000 higher than (PU). An eigenvalues extraction is performed with a Lanczos eigensolver to determine the natural frequencies of vibration.

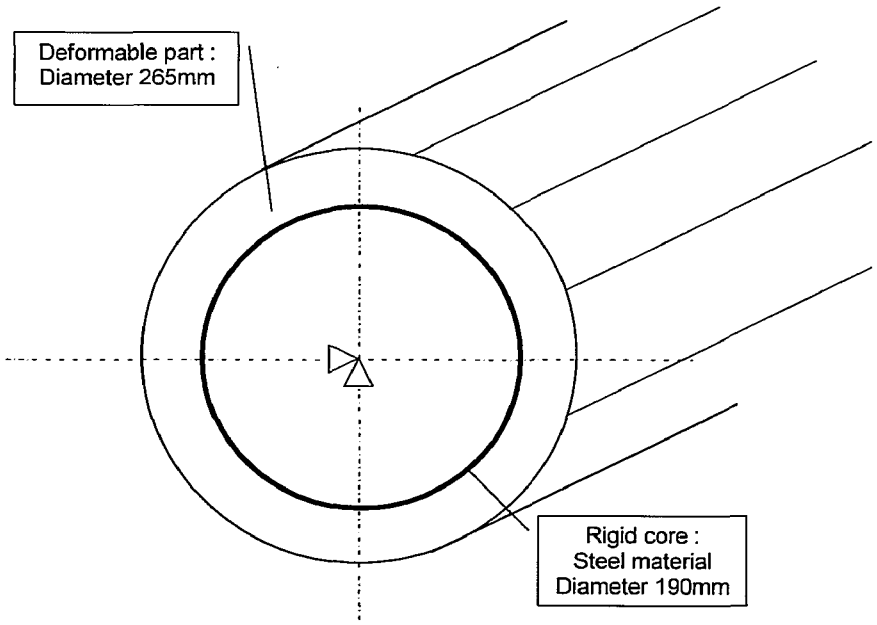

Figure 4-10: bidimensional vibration model

2.4.2 Results

Figure 4-11 and Figure 4-12 show two obtained natural frequencies of vibration. The frequencies are 4.9Hz and 5.2Hz. We apply a scale factor of 100 on the displacement amplitude to highlight the different modes shapes.

These natural frequencies of vibration are the double of the roll frequency of rotation during paint application (applicator roll frequency f≈2-2.5Hz). Inline, there are many rotating machine with different roll frequencies and the roll coater has no vibration insulating. An important observation is the deformed shape. It has a sinusoidal shape like the ribbing instabilities.

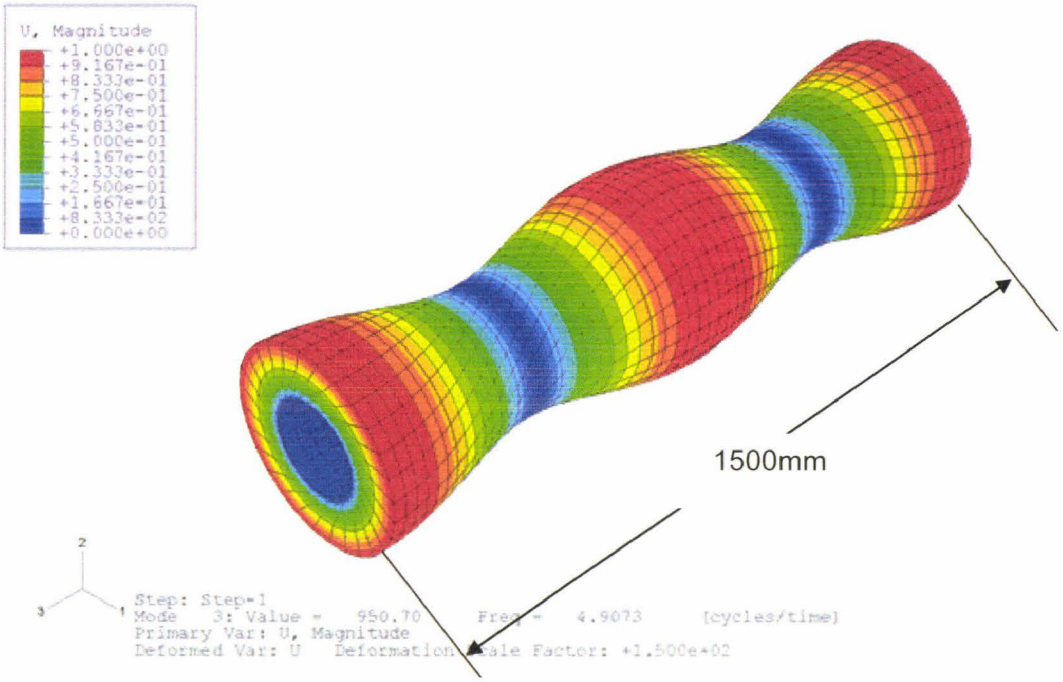

Figure 4-11: Natural frequencies of vibration for the applicator roll, elastic behaviour law PU, f=4.9Hz

The defect along the roll is much higher than the ribbing defect during application. For f=4.9Hz, the roll length is 1500mm and we can see two approximated periods on the sinusoid wave. In the second case illustrated in Figure 4-12, the number of period equals seven. In this case, the wavelength (214mm) decreases but it is still higher than the liquid ribbing wavelength (around 1mm).

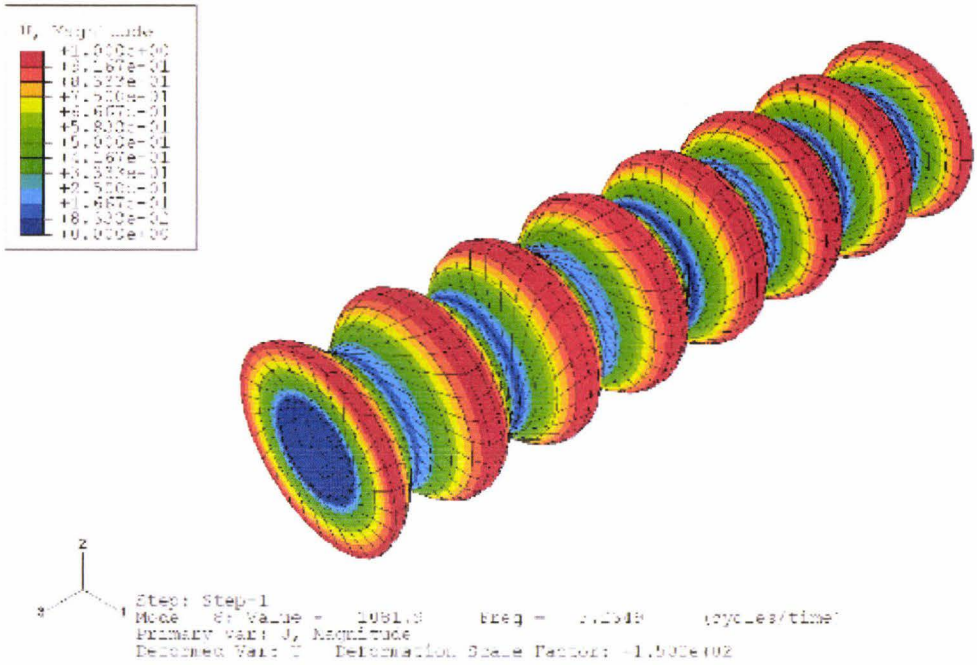

Figure 4-12: Natural frequencies of vibration for the applicator roll, elastic behaviour law PU, f=5.2Hz

The frequency of vibration gives different deformed shape closer to the ribbing defect shape. The wavelengths are very different from the one occurring during the liquid application but the impact on the flow rate is certainly present. A more complex study and modelling are necessary to improve the understanding of the vibration influence on the flow rate. The management of the contact between rolls will lead to improve the accuracy and reality of the vibration impact on the flow rate.

2.5 Conclusion

Different additional works to understand the ribbing defect origin have been proposed above. These works are just outlined and require more analyses to bring scientific added value.

The first research axis has been the numerical modelling of the ribbing defect. The advantage of the three dimensional approach is the hypothesis elimination of the bidimensional approach. The result is a three dimensional flow rate as a function of the fluid properties and roll coater adjustments. We can measure the numerical ribbing defect wavelength and will correlate the result with the inline measurement in a near future. The current model is not sufficient to perform this

correlation because it requires a more width extrusion to obtain two or three wavelengths. The disadvantages of the extrusion increasing in the three dimensional modelling are the computation time and the meshing time between restart to obtain the final free surface position. As an example, the current model needs of two or three remeshing to converge. The total computation time is around 140h on a 2.1 GHz processor.

The second axis proposed is the vibration analysis. It is just a simple elastic three-dimensional modelling. This simulation has permitted to extract the natural frequencies of vibrations for the deformable roll. To improve the modelling, a three-dimensional approach with different viscoelastic behaviour law and layer thickness can be performed to complete this first analysis. The contact between roll will be added to have an accurate and realist result.

These outline studies leads us to new research ways. In future works, we can increase the experimental measurement and numerical modelling accuracy.

Experimentally, the applicator roll wet thickness measurement seems important to have an accurate correlation with the numerical simulation. Moreover, this parameter is essential to control the targeted wet thickness on the strip during application. An upsetting roll measurement during application will be interesting to have a good correlation with the external load. This instrumentation will allow to accurately master the wet thickness and ribbing wavelength on the roll coater. Moreover, the image analysis tool used and developed can be improve by a Fourier transform using to evaluate the ribbing wavelength. This last one will permit to have an accurate ribbing wavelength measurement on the roll coater.

Numerically, we can consider new research axis. The using of non-newtonian fluid to accurately model the coil coating paint in the free surface finite element simulation. The aim will be to analyse the fluid viscoelasticity influence on the wet thickness and ribbing wavelength. The coil coating paint are not Newtonian except in the gap. After the high shear rate in the gap, the paint recover is initial viscosity. This time to recover its initial properties is very important for the surface tension before curing. This parameter acts directly on the final product aspect. This Non newtonian model will be also used in the three dimensional approach for the ribbing wavelength evaluation.

The second numerical axis can be the modelling of the contact between applicator roll and the strip. During this last contact, a paint transfer is performed and new defect can occur. Besides, for a same roll coater adjustment, the wet thickness on the strip can be different as a function of this new gap geometry. This understanding of the last contact in association with the current work will get an accurate mastering of the roll coater during application.

References

[1] Deltombe R., Dubar M., Dubois A. and Dubar L. , A new methodology to analyse iron fines during steel cold rolling processes, Wear, 2003, 254(3-4): 211-221.

[2] Huart S., Dubar M., Deltombe R., Dubois A., Dubar L., Asperity deformation lubricant trapping and iron fines formation mechanism in cold rolling processes, Wear, 2004, 257: 471-480.

[3] Carvalho M.S., Scriven L.E., Flows in forward deformable roll coating gaps: comparison between spring and plane strain models of roll cover, Journal of computational physics, 1997, 138: 449-479.

[4] Greener J., Middleman S., A theory of roll coating of viscous and viscoelastic fluids, Polymer Engineering and science, 1975, 15(1): 1-10.

[5] Hooke C.J., O'Donoghue J.P., Elastohydrodynamic lubrication of soft, highly deformed contacts, Journal Mechanical Engineering Science, 1972, 14(1): 34-48.

[6] Cohu O., Magnin A., The levelling of thixotropic coatings, Progress in organic coatings, 1996, 28: 89-96.

[7] Greener J., Middleman S., Theoretical and experimental studies of the fluid dynamics of a two roll coater, Ind. Eng. Chem. Fundam., 1979, 18: 35-41.

[8] Greener J., Sullivan T., Turner B., Middleman S., Ribbing instability of a two-roll coater: Newtonian fluids, Chem. Eng. Commun., 1980, 5: 73-83.

[9] Babchin A.J., Clish R.J., Wahren D., Stability and disturbance of coating films, Advance in colloid and interface Science, 1981, 14: 251-280.

[10] Benkreira H., Dynamic wetting in metering and pre-metered forward roll coating, Chemical Engineering Science, 2002, 57: 3025-3032.

[11] Benkreira H., An experimental study of dynamic wetting in reverse roll coating, 2001, AIChE Journal, 48(2), 226.

[12] Benkreira H., Edwards M.F., Wilkinson W.L., Ribbing instability in the roll coating of Newtonian fluids, Plastics and rubber processing and application, 1982, 2: 137-144.

[13] Thompson H.M., Kapur N., Gaskell P.H., Summers J.L., Abbott S.J., A theoretical and experimental investigation of reservoir-fed, rigid-roll coating, Chemical Engineering Science, 2001, 56: 4627-4641.

[14] Savage M.D., Mathematical model for the onset of ribbing, AIChE Journal, 1984, 30(6): 999-1002.

[15] Savage M.D., Mathematical models for coating processes, J. Fluid Mech., 1982, 117: 443-455.

[16] Savage M.D., Cavitation in lubrication. Part 1. On boundary conditions and cavity-fluid interfaces, J. Fluid Mech., 1977, 80(4): 743-755.

[17] Savage M.D., Cavitation in lubrication. Part 2. Analysis of wavy interfaces, J. Fluid Mech., 1977, 80(4): 757-767.

[18] Pearson J.R.A., The instability of uniform viscous flow under rollers and spreaders, J. Fluid Mech., 1959, 31: 481-500.

[19] Pitts E., Greiller J., The flow of thin liquid films between rollers, J. Fluid Mech., 1961, 11 : 33-50.

[20] Mill C.C., South G.R., Formation of ribs on rotating rollers, J. Fluid Mech., 1967, 28(3): 523-529.

[21] Ruschak K.J., Coating flows, Ann. Rev. Fluid Mech., 1985, 17: 65-89.

[22] Herrebrugh K., Solving the incompressible and isothermal problem in elastohydrodynamics trough an integral equation, ASME J. Lub. Technol., 1968, 90 : 262.

[23] Hall R.W., Savage M.D., Two-dimensional elastohydrodynamic lubrication-Part2, Solution of the line contact problem, Proc. Inst. Mech. Eng., 1988, 202: 354.

[24] Coyle D.J., Macosko C.W., Scriven L.E., The fluid dynamics of reverse roll coating, AIChE Journal, 1990, 36(2): 161-174.

[25] Coyle D.J., Forward roll coating with deformable rolls: A simple one-dimensional elastohydrodynamic model, Chemical Engineering Science, 1988, 43(10): 2673-2684.

[26] Hooke C.J., The elastohydrodynamic lubrication of a cylinder on an elastomeric layer, Wear, 1986, 111: 83-99.

[27] Carvalho M.S., Elastohydrodynamics of tensioned web roll coating process, Int. J. Numer. Meth. Fluids, 2003, 41: 561-576.

[28] Cohu O., Magnin A., Forward roll coating of newtonian fluids with deformable rolls: an experimental investigation, Chemical Engineering Science, 1997, 52: 1339-1347.

[29] Carvalho M.S., Scriven L.E., Three dimensional stability of free surface flows: Application to forward deformable roll coating, Journal of Computational Physics, 1999, 151: 534-562.

[30] Gostling M.J., Savage M. D., Young A.E., Gaskell P.H., A model for deformable roll coating with negative gaps and incompressible compliant layers, J. Fluid Mech., 2003, 489: 155-184.

[31] Smith J., Maloney J.D., Flow of fluids between rotating rollers, Tappi J., 1966, 49 : 63.

[32] Adachi K., Tamura T., Nakamura R., Coating flows in a nip region and various critical phenomena, AIChE Journal, 1988, 34(3): 456-464.

[33] Carvalho M.S., Scriven L.E., Deformable roll coating flows: steady state and linear perturbation analysis, J. Fluid Mech., 1997, 339: 143-172.

[34] Chong Y.H., The Onset of Ribbing in Forward-mode Deformable Roll Coating, University of leeds.

[35] Tiu C., Wang L., Liu T.J., Non newtonian effects on pre-metered reverse roll coating, J. Non newtonian Fluid Mech., 1999, 87: 247-261.

[36] Zevallos G.A., Carvalho M.S., Pasquali M., Forward roll coating flows of viscoelastic liquids, Journal of Non-Newtonian Fluid Mechanics, 2005, 130: 96-109.

[37] Chandio M.S., Webster M.F., Numerical study of transient instabilities in reverse-roller coating flows, 2001, University of Wales, Swansea.

[38] Orchard S.E., Appl. Sci. Res. A, 1962, 2, 451.

[39] Jones E.R., The fluid mechanics of deformable roll coating, 2000, PhD Thesis, University of Bradford.

[40] Gaskell P.H., Innes G.E., Savage M.D., An experimental investigation of meniscus roll coating, J. Fluid Mech., 1998, 355: 17-44.

[41] Coyle D.J., Macosko C.W, Scriven L.E., Reverse roll coating of non newtonian liquids, J. Rheology, 1990, 34(5): 615-636.

[42] Carvalho M.S., Effect of thickness and viscoelastic properties of roll cover on deformable roll coating flows, Chemical Engineering Science, 2003, 58: 4323-4333.

[43] Alonso S., Bertrand F., Tanguy P.A., A torque based analysis of the reverse roll coating process, Chemical Engineering Science, 2003, 58: 1831-1837.

[44] Carvalho M.S., Huelsman G.L., Kolb W.B., Elastohydrodynamics of a moving substrate over a curved plate, AIChE Journal, 2002, 48;4: 739-751.

[45] Koishi M., K. Kabe, and M. Shiratori, Tire Cornering Simulation using Explicit Finite Element Analysis Code, 16th annual conference of the Tire Society at the University of Akron, 1997.

[46] Matlab help files, Optimization toolbox, trust-region.

[47] Gieck K. Formulaire Technique. In : Dunod, 1997.

[48] Martinon P., Caractéristiques des élastomères. In : Techniques de l'ingénieur, REF K380-1.

[49] Zambelli G, Vincent L. Matériaux et contacts : une approche tribologique. In : Presses Polytechniques et universitaires Romandes, 1998.

[50] Fourcade E., Bertrand F., Réglat O., Tanguy P.A., Finite element analysis of fluid solid interaction in the metering nip of a metering size press, Computer methods in applied mechanics and engineering, 1999, 174: 235-245.

[51] Grillet A.M., Lee A.G., Shaqfeh E.S.G, Observation of ribbing instabilities in elastic fluid flows with gravity stabilization, J. Fluid Mech., 1999, 399: 49-83.

[52] Gokhale V.V., Exact solution to the ribbing instability problem in lubrication flow by invariant imbedding, Chem. Eng. Commun., 1983, 21: 81-87.

[53] Ruschak K.J., Boundary conditions at a liquid/air interface in lubrication flows, J. Fluid Mech., 1982, 119: 107-120.

[54] Bauman T., Sullivan T., Middleman S., Ribbing instability in coating flows: effect of polymer additives, Chem. Eng. Commun., 1982, 14: 35-46.

[55] Middleman S., Reverse roll coating of viscous and viscoelastic liquids, Ind. Eng. Chem. Fundam., 1981, 20: 63-66.

Appendix 1 : inline measurements

Date	27/07/2006
Code	1SG410
Viscosity	105s
Applicator diameter	265 mm
Layer thickness	22,5mm
Elastomer	PUV550

External load W(N/m)	LS(m/min)	Va(%)	Vp(%)	Ep(µm)	S=Vp/Va	Ribbing wavelength(mm)
2417	75	101	30	100	0,30	2,49
2417	75	101	35	100	0,35	2,24
2417	75	101	40	100	0,40	2,80
2417	75	101	45	100	0,45	2,80
2417	75	101	50	100	0,50	2,80
2417	75	105	30	100	0,29	3,73
2417	75	105	35	100	0,33	2,80
2417	75	105	40	100	0,38	2,80
2417	75	105	45	100	0,43	2,49
2417	75	105	50	100	0,48	2,80
2417	75	110	30	100	0,27	2,49
2417	75	110	35	100	0,32	3,20
2417	75	110	40	100	0,36	3,20
2417	75	110	45	100	0,41	2,80
2417	75	110	50	100	0,45	4,48
2417	75	115	30	100	0,26	2,49
2417	75	115	35	100	0,30	3,20
2417	75	115	40	100	0,35	2,24
2417	75	120	30	100	0,25	3,20
2417	75	120	35	100	0,29	2,80
2417	75	120	40	100	0,33	2,80
2867	75	101	30	62	0,30	1,82
2867	75	101	35	67	0,35	2,15
2867	75	101	40	75	0,40	1,97
2867	75	101	45	77	0,45	2,36
2867	75	101	50	80	0,50	2,36
2867	75	105	30	62	0,29	2,15
2867	75	105	35	67	0,33	2,36
2867	75	105	40	70	0,38	2,36
2867	75	105	45	77	0,43	2,15
2867	75	105	50	80	0,48	2,15
2867	75	110	30	57	0,27	2,15
2867	75	110	35	65	0,32	2,15
2867	75	110	40	77	0,36	2,36
2867	75	110	45	80	0,41	2,36
2867	75	110	50	87	0,45	2,36
2867	75	115	30	62	0,26	2,36
2867	75	115	35	67	0,30	2,36
2867	75	115	40	77	0,35	2,15
2867	75	120	30	62	0,25	2,15
2867	75	120	35	65	0,29	2,63
2867	75	120	40	75	0,33	2,63
2867	75	120	45	82	0,38	2,36
3533	75	101	30	52	0,30	2,66
3533	75	101	35	60	0,35	2,18
3533	75	101	40	67	0,40	2,66
3533	75	101	45	67	0,45	1,99
3533	75	101	50	77	0,50	1,84
3533	75	105	30	57	0,29	1,99
3533	75	105	35	65	0,33	1,99
3533	75	105	40	67	0,38	1,99
3533	75	105	45	72	0,43	2,18

3533	75	105	50	75	0,48	2,39
3533	75	110	30	50	0,27	1,84
3533	75	110	35	57	0,32	2,18
3533	75	110	40	65	0,36	2,39
3533	75	115	30	50	0,26	2,18
3533	75	115	35	57	0,30	2,18
3533	75	115	40	62	0,35	2,39
3533	80	120	30	52	0,25	2,18
3533	80	120	35	60	0,29	1,84
3533	80	120	40	67	0,33	2,18
4867	80	101	30	47	0,30	1,94
4867	80	101	35	50	0,35	1,94
4867	80	101	40	57	0,40	2,12
4867	80	101	45	62	0,45	1,79
4867	80	101	50	67	0,50	1,79
4867	80	105	30	45	0,29	1,66
4867	80	105	35	47	0,33	1,79
4867	80	105	40	60	0,38	1,94
4867	80	105	45	62	0,43	2,12
4867	80	105	50	65	0,48	1,94
4867	80	110	30	47	0,27	1,94
4867	80	110	35	50	0,32	1,66
4867	80	110	40	57	0,36	1,94
4867	80	110	45	60	0,41	1,66
4867	75	115	30	45	0,26	1,66
4867	75	115	35	50	0,30	1,94
4867	75	115	40	55	0,35	1,94
4867	75	115	45	62	0,39	1,79
4867	75	120	30	42	0,25	1,79
4867	75	120	35	50	0,29	1,79
4867	75	120	40	55	0,33	1,66
4867	75	120	45	62	0,38	2,12
6883	75	101	30	45	0,30	1,86
6883	75	101	35	47	0,35	1,73
6883	75	101	40	55	0,40	1,61
6883	75	101	45	57	0,45	1,73
6883	75	101	50	60	0,50	1,61
6883	75	101	55	65	0,54	1,86
6883	75	101	60	70	0,59	1,86
6883	75	105	30	40	0,29	1,73
6883	75	105	35	47	0,33	2,02
6883	75	105	40	55	0,38	1,73
6883	75	105	45	57	0,43	1,73
6883	75	105	50	60	0,48	1,73
6883	75	105	55	65	0,52	1,86
6883	75	105	60	70	0,57	1,73
6883	75	110	30	45	0,27	2,20
6947	75	110	35	47	0,32	2,02
6947	75	110	40	50	0,36	1,73
6947	75	110	45	55	0,41	1,86
6947	75	110	50	60	0,45	1,73
6947	75	110	55	62	0,50	1,73
6947	75	110	60	67	0,55	1,73
6947	75	115	30	42	0,26	1,73
6947	75	115	35	47	0,30	1,73
6947	75	115	40	50	0,35	1,61
6947	75	115	45	60	0,39	2,02
6947	75	115	50	62	0,43	1,61
6947	75	115	55	62	0,48	1,73
6947	75	115	60	65	0,52	1,86
7000	75	120	30	42	0,25	1,86
7000	75	120	35	47	0,29	2,20
7000	75	120	40	52	0,33	1,86
7000	75	120	45	57	0,38	1,86
7000	75	120	50	62	0,42	1,73
7000	75	120	55	65	0,46	1,86
7000	75	120	60	67	0,50	1,73
16867	75	101	30	35	0,30	1,41
16867	75	101	35	40	0,35	1,41
16867	75	101	40	42	0,40	1,49

16867	75	101	45	50	0,45	1,49
16867	75	101	50	52	0,50	1,59
16867	75	101	55	52	0,54	1,49
16867	75	101	60	55	0,59	1,41
16867	75	105	30	35	0,29	1,49
16867	75	105	35	40	0,33	1,41
16867	75	105	40	42	0,38	1,33
16867	75	105	45	45	0,43	1,41
16867	75	105	50	47	0,48	1,59
16867	75	105	55	50	0,52	1,59
16867	75	105	60	57	0,57	1,49
16867	75	110	30	32	0,27	1,49
16867	75	110	35	37	0,32	1,59
16867	75	110	40	47	0,36	1,49
16867	75	110	45	47	0,41	1,49
16867	75	110	50	50	0,45	1,59
16867	75	110	55	50	0,50	1,33
16867	75	110	60	55	0,55	1,41
16867	75	115	30	35	0,26	1,33
16867	75	115	35	37	0,30	1,41
16867	75	115	40	42	0,35	1,49
16867	75	115	45	47	0,39	1,59
16867	75	115	50	47	0,43	1,49
16867	75	115	55	52	0,48	1,41
16867	75	120	30	32	0,25	1,59
16867	75	120	35	37	0,29	1,59
16867	75	120	40	40	0,33	1,41
16867	75	120	45	47	0,38	1,41
16867	75	120	50	47	0,42	1,49
16867	75	120	55	50	0,46	1,41
16867	75	120	60	52	0,50	1,59

Date	03/08/2006
Code	2BW830
Visosity	105s
Applicator diameter	265mm
Layer thickness	22,5mm
Elastomer	PUV550

External load W(N/m)	LS (m/min)	Va(%)	Vp(%)	Ep(µm)	S=Vp/Va	Ribbing wavelength(mm)
3533	82	101	30	50	0,30	2,08
3533	82	101	35	60	0,35	2,27
3533	82	101	40	65	0,40	1,92
3533	82	101	45	75	0,45	2,08
3533	82	101	50	80	0,50	2,08
3533	82	101	55	85	0,54	2,08
3533	82	101	60	90	0,59	2,08
3533	82	105	30	50	0,29	1,92
3533	82	105	35	60	0,33	2,08
3533	82	105	40	65	0,38	2,08
3533	82	105	45	70	0,43	1,78
3533	82	105	50	75	0,48	1,92
3533	82	105	55	85	0,52	2,27
3533	82	105	60	95	0,57	1,66
3533	82	110	30	52	0,27	1,92
3533	82	110	35	57	0,32	1,92
3533	82	110	40	62	0,36	2,27
3533	82	110	45	67	0,41	1,92
3533	82	110	50	75	0,45	2,27
3533	82	110	55	82	0,50	1,78
3533	82	110	60	90	0,55	2,50
3533	82	115	30	47	0,26	1,92
3533	82	115	35	60	0,30	1,92
3533	82	115	40	60	0,35	2,08
3533	82	115	45	67	0,39	2,08
3533	82	115	50	75	0,43	1,92
3533	82	115	55	80	0,48	2,27
3533	82	115	60	87	0,52	2,08
3533	82	120	30	52	0,25	2,27
3533	82	120	35	60	0,29	2,27
3533	82	120	40	67	0,33	2,08
3533	82	120	45	70	0,38	1,92
3533	82	120	50	75	0,42	2,27
3533	82	120	55	77	0,46	2,27
3533	82	120	60	90	0,50	1,92
6867	82	101	30	37	0,30	1,49
6867	82	101	35	40	0,35	1,41
6867	82	101	40	45	0,40	1,68
6867	82	101	45	50	0,45	1,58
6867	82	101	50	55	0,50	1,79
6867	82	101	55	60	0,54	1,79
6867	82	101	60	60	0,59	1,68
6867	82	105	30	35	0,29	1,58
6867	82	105	35	37	0,33	1,79
6867	82	105	40	40	0,38	1,58
6867	82	105	45	47	0,43	1,49
6867	82	105	50	50	0,48	1,68
6867	82	105	55	55	0,52	1,49
6867	82	105	60	60	0,57	1,79
6867	82	110	30	32	0,27	1,49
6867	82	110	35	37	0,32	1,68
6867	82	110	40	45	0,36	1,58

6867	82	110	45	47	0,41	1,58
6867	82	110	50	52	0,45	1,58
6867	82	110	55	55	0,50	1,79
6867	82	110	60	57	0,55	1,92
6867	82	115	30	32	0,26	1,49
6867	82	115	35	40	0,30	1,49
6867	82	115	40	42	0,35	1,41
6867	82	115	45	45	0,39	1,68
6867	82	115	50	50	0,43	1,68
6867	82	115	55	52	0,48	1,58
6867	82	115	60	57	0,52	1,68
6867	82	120	30	35	0,25	1,68
6867	82	120	35	37	0,29	1,58
6867	82	120	40	40	0,33	1,68
6867	82	120	45	45	0,38	1,68
6867	82	120	50	50	0,42	1,58
6867	82	120	55	52	0,46	1,79
6867	82	120	60	60	0,50	1,68
6867	82	101	30	32	0,30	1,49
10200	82	101	30	25	0,30	1,49
10200	82	101	35	26	0,35	1,41
10200	82	101	40	31	0,40	1,41
10200	82	101	45	32	0,45	1,58
10200	82	101	50	37	0,50	1,58
10200	82	101	55	41	0,54	1,41
10200	82	101	60	47	0,59	1,41
10200	82	105	30	22	0,29	1,28
10200	82	105	35	26	0,33	1,41
10200	82	105	40	30	0,38	1,34
10200	82	105	45	33	0,43	1,41
10200	82	105	50	36	0,48	1,58
10200	82	105	55	37	0,52	1,49
10200	82	105	60	43	0,57	1,58
10200	82	110	30	20	0,27	1,41
10200	82	110	35	23	0,32	1,49
10200	82	110	40	30	0,36	1,41
10200	82	110	45	32	0,41	1,34
10200	82	110	50	36	0,45	1,41
10200	82	110	55	38	0,50	1,49
10200	82	110	60	43	0,55	1,34
10200	82	115	30	20	0,26	1,49
10200	82	115	35	25	0,30	1,34
10200	82	115	40	30	0,35	1,49
10200	82	115	45	33	0,39	1,41
10200	82	115	50	37	0,43	1,49
10200	82	115	55	42	0,48	1,58
10200	82	115	60	43	0,52	1,41
10200	82	120	30	20	0,25	1,34
10200	82	120	35	25	0,29	1,41
10200	82	120	40	27	0,33	1,41
10200	82	120	45	30	0,38	1,49
10200	82	120	50	33	0,42	1,58
10200	82	120	55	36	0,46	1,41
10200	82	120	60	42	0,50	1,58
10200	82	101	30	22	0,30	1,28
13533	82	101	30	21	0,30	1,33
13533	82	101	35	23	0,35	1,33
13533	82	101	40	26	0,40	1,21
13533	82	101	45	30	0,45	1,27
13533	82	101	50	33	0,50	1,39
13533	82	101	55	35	0,54	1,33
13533	82	101	60	40	0,59	1,39
13533	82	105	30	20	0,29	1,27
13533	82	105	35	22	0,33	1,27
13533	82	105	40	27	0,38	1,39
13533	82	105	45	30	0,43	1,21
13533	82	105	50	32	0,48	1,27
13533	82	105	55	35	0,52	1,39
13533	82	105	60	37	0,57	1,33
13533	86	110	30	18	0,27	1,21

13533	78	110	35	20	0,32	1,27
13533	78	110	40	25	0,36	1,27
13533	78	110	45	26	0,41	1,39
13533	78	110	50	31	0,45	1,27
13533	78	110	55	35	0,50	1,47
13533	80	110	60	38	0,55	1,27
13533	80	115	30	17	0,26	1,33
13533	80	115	35	22	0,30	1,27
13533	80	115	40	25	0,35	1,39
13533	80	115	45	28	0,39	1,33
13533	80	115	50	32	0,43	1,33
13533	80	115	55	36	0,48	1,39
13533	80	115	60	37	0,52	1,39
13533	87	120	30	18	0,25	1,47
13533	87	120	35	21	0,29	1,33
13533	87	120	40	25	0,33	1,27
13533	87	120	45	28	0,38	1,39
13533	87	120	50	32	0,42	1,39
13533	87	120	55	35	0,46	1,33
13533	87	120	60	38	0,50	1,39
13533	87	101	30	20	0,30	1,33
16867	87	101	30	17	0,30	1,21
16867	87	101	35	23	0,35	1,33
16867	87	101	40	26	0,40	1,21
16867	87	101	45	27	0,45	1,40
16867	87	101	50	30	0,50	1,26
16867	87	101	55	33	0,54	1,15
16867	87	101	60	37	0,59	1,26
16867	78	105	30	17	0,29	1,21
16867	78	105	35	21	0,33	1,26
16867	78	105	40	23	0,38	1,40
16867	78	105	45	26	0,43	1,47
16867	78	105	50	31	0,48	1,40
16867	78	105	55	32	0,52	1,47
16867	78	105	60	35	0,57	1,33
16867	78	110	30	16	0,27	1,21
16867	78	110	35	20	0,32	1,21
16867	78	110	40	22	0,36	1,26
16867	78	110	45	25	0,41	1,26
16867	78	110	50	27	0,45	1,21
16867	78	110	55	31	0,50	1,26
16867	78	110	60	33	0,55	1,26
16867	78	115	30	17	0,26	1,21
16867	78	115	35	18	0,30	1,33
16867	70	115	40	21	0,35	1,21
16867	70	115	45	23	0,39	1,15
16867	70	115	50	26	0,43	1,15
16867	80	115	55	27	0,48	1,40
16867	85	115	60	35	0,52	1,21
16867	63	120	30	15	0,25	1,21
16867	63	120	35	17	0,29	1,21
16867	62	120	40	20	0,33	1,33

Date	23/08/2006
Code	2RW708
Viscosity	95s
Applicator diameter	262mm
Layer thickness	
Elastomer	PUV550

External load W(N/m)	LS(m/min)	Va(%)	Vp(%)	Ep(µm)	S=Vp/Va	Ribbing wavelength (mm)
4867	77	101	20	31	0,20	2,12
4867	77	101	30	40	0,30	1,94
4867	77	101	40	52	0,40	1,94
4867	77	101	50	62	0,50	1,94
4867	77	101	60	75	0,59	2,33
4867	77	101	30	45	0,30	1,94
4867	77	105	20	30	0,19	2,12
4867	77	105	30	40	0,29	2,12
4867	77	105	40	55	0,38	2,33
4867	77	105	50	62	0,48	1,94
4867	77	105	60	75	0,57	2,33
4867	77	105	30	40	0,29	1,79
4867	77	110	20	30	0,18	1,79
4867	77	110	30	40	0,27	2,33
4867	77	110	40	52	0,36	1,94
4867	77	110	50	67	0,45	2,59
4867	77	110	60	75	0,55	2,12
4867	77	110	30	40	0,27	1,79
4867	77	115	20	25	0,17	1,94
4867	77	115	30	40	0,26	1,79
4867	77	115	40	52	0,35	2,33
4867	77	115	50	63	0,43	2,12
4867	77	115	60	72	0,52	1,94
4867	77	115	30	40	0,26	2,12
4867	77	120	20	27	0,17	2,12
4867	77	120	30	40	0,25	1,94
4867	77	120	40	50	0,33	1,94
4867	77	120	50	62	0,42	2,12
4867	77	120	60	72	0,50	2,59
4867	77	120	30	40	0,25	2,12
6867	77	101	15	17	0,15	1,47
6867	77	101	20	23	0,20	1,79
6867	77	101	25	26	0,25	1,67
6867	77	101	30	35	0,30	1,79
6867	77	101	35	38	0,35	2,09
6867	77	101	40	41	0,40	1,79
6867	77	101	45	45	0,45	1,79
6867	77	101	50	47	0,50	1,67
6867	77	101	30	32	0,30	1,57
6867	77	105	15	17	0,14	1,57
6867	77	105	20	23	0,19	1,79
6867	77	105	25	27	0,24	2,09
6867	77	105	30	32	0,29	1,93
6867	77	105	35	38	0,33	2,09
6867	77	105	40	43	0,38	1,79
6867	77	105	45	47	0,43	1,67
6867	77	105	50	55	0,48	1,93
6867	77	105	55	55	0,52	1,93
6867	77	105	60	60	0,57	2,09
6867	77	105	30	32	0,29	1,79
6867	77	110	15	14	0,14	1,67
6867	77	110	20	20	0,18	1,93

6867	77	110	25	29	0,23	1,67
6867	77	110	30	33	0,27	1,79
6867	77	110	35	37	0,32	1,79
6867	77	110	40	40	0,36	1,67
6867	77	110	45	45	0,41	1,93
6867	77	110	50	52	0,45	1,79
6867	77	110	55	57	0,50	2,09
6867	77	110	60	60	0,55	1,67
6867	77	110	30	32	0,27	1,79
6867	77	115	15	14	0,13	1,67
6867	77	115	20	17	0,17	1,93
6867	77	115	25	25	0,22	1,79
6867	77	115	30	32	0,26	1,79
6867	77	115	35	37	0,30	1,39
6867	77	115	40	40	0,35	1,67
6867	77	115	45	45	0,39	1,93
6867	77	115	50	47	0,43	2,09
6867	77	115	55	55	0,48	2,28
6867	77	115	60	57	0,52	2,09
6867	77	115	30	31	0,26	2,09
6867	77	120	15	14	0,13	1,67
6867	77	120	20	20	0,17	1,79
6867	77	120	25	25	0,21	1,93
6867	77	120	30	30	0,25	1,93
6867	77	120	35	35	0,29	1,93
6867	77	120	40	40	0,33	1,79
6867	77	120	45	45	0,38	2,09
6867	77	120	50	50	0,42	1,67
6867	77	120	55	52	0,46	1,79
6867	77	120	60	55	0,50	1,93
6867	77	120	30	30	0,25	1,57
10200	77	101	20	17	0,20	1,60
10200	77	101	30	25	0,30	1,60
10200	77	101	40	35	0,40	1,51
10200	77	101	50	45	0,50	1,83
10200	77	101	60	50	0,59	1,51
10200	77	101	30	25	0,30	1,51
10200	77	105	20	17	0,19	1,51
10200	77	105	30	29	0,29	1,60
10200	77	105	40	35	0,38	1,42
10200	77	105	50	41	0,48	1,60
10200	77	105	60	50	0,57	1,51
10200	77	105	30	26	0,29	1,60
10200	77	110	20	15	0,18	1,51
10200	77	110	30	25	0,27	1,60
10200	77	110	40	35	0,36	1,60
10200	77	110	50	41	0,45	1,51
10200	77	110	60	45	0,55	1,71
10200	77	110	30	25	0,27	1,42
10200	77	115	20	15	0,17	1,60
10200	77	115	30	25	0,26	1,60
10200	77	115	40	35	0,35	1,51
10200	77	115	50	40	0,43	1,60
10200	77	115	60	47	0,52	1,71
10200	77	115	30	23	0,26	1,51
10200	77	120	20	16	0,17	1,51
10200	77	120	30	22	0,25	1,60
10200	77	120	40	32	0,33	1,71
10200	77	120	50	37	0,42	1,71
10200	77	120	60	47	0,50	1,60
10200	77	120	30	23	0,25	1,60
13533	77	101	20	13	0,20	1,59
13533	77	101	30	21	0,30	1,33
13533	77	101	40	27	0,40	1,33
13533	77	101	50	32	0,50	1,50
13533	77	101	60	37	0,59	1,33
13533	77	101	30	20	0,30	1,33
13533	77	105	20	12	0,19	1,41
13533	77	105	30	21	0,29	1,50
13533	77	105	40	27	0,38	1,41

13533	77	105	50	33	0,48	1,50
13533	77	105	60	40	0,57	1,50
13533	77	105	30	21	0,29	1,33
13533	77	110	20	13	0,18	1,59
13533	77	110	30	21	0,27	1,41
13533	77	110	40	28	0,36	1,41
13533	77	110	50	35	0,45	1,26
13533	77	110	60	39	0,55	1,41
13533	77	110	30	20	0,27	1,50
13533	77	115	20	11	0,17	1,33
13533	77	115	30	20	0,26	1,33
13533	77	115	40	30	0,35	1,33
13533	77	115	50	36	0,43	1,41
13533	77	115	60	41	0,52	1,50
13533	77	115	30	21	0,26	1,41
13533	77	120	20	12	0,17	1,26
13533	77	120	30	18	0,25	1,33
13533	77	120	40	27	0,33	1,50
13533	77	120	50	32	0,42	1,59
13533	77	120	60	37	0,50	1,59
13533	77	120	30	20	0,25	1,50
16927	77	101	20	11	0,20	1,27
16927	77	101	30	17	0,30	1,50
16927	77	101	40	23	0,40	1,50
16927	77	101	50	30	0,50	1,34
16927	77	101	60	35	0,59	1,50
16927	77	101	30	20	0,30	1,41
16927	77	105	30	17	0,29	1,34
16927	77	105	40	23	0,38	1,21
16927	77	105	50	30	0,48	1,41
16927	77	105	60	36	0,57	1,34
16927	77	105	30	20	0,29	1,34
16927	77	110	30	17	0,27	1,21
16927	77	110	40	23	0,36	1,59
16927	77	110	50	30	0,45	1,41
16927	77	110	60	37	0,55	1,34
16927	77	110	30	17	0,27	1,41
16927	77	115	30	17	0,26	1,59
16927	77	115	40	22	0,35	1,41
16927	77	115	50	28	0,43	1,41
16927	77	115	60	35	0,52	1,59
16927	77	115	30	17	0,26	1,34
16927	77	120	30	16	0,25	1,59
16927	77	120	40	21	0,33	1,50
16927	77	120	50	27	0,42	1,50
16927	77	120	60	31	0,50	1,41
16927	77	120	30	17	0,25	1,59